Virginia Commonwealth University
VCU Scholars Compass

Theses and Dissertations | Graduate School

2016

SULFATED DEHYDROPOLYMER OF CAFFEIC ACID FOR REPAIR OF LUNG DAMAGE AND EMPHYSEMA

Tien M. Truong
Virginia Commonwealth University

Follow this and additional works at: https://scholarscompass.vcu.edu/etd

 Part of the Pharmacy and Pharmaceutical Sciences Commons

© The Author

Downloaded from
https://scholarscompass.vcu.edu/etd/4229

This Dissertation is brought to you for free and open access by the Graduate School at VCU Scholars Compass. It has been accepted for inclusion in Theses and Dissertations by an authorized administrator of VCU Scholars Compass. For more information, please contact libcompass@vcu.edu.

© Tien M. Truong 2016
All Rights Reserved

SULFATED DEHYDROPOLYMER OF CAFFEIC ACID FOR REPAIR OF LUNG DAMAGE AND EMPHYSEMA

A dissertation submitted in partial fulfillment of the requirements for the degree of Doctor of Philosophy at Virginia Commonwealth University

by

TIEN M. TRUONG, B.S. BIOLOGY
University of Virginia
2008

Director: MASAHIRO SAKAGAMI, Ph.D.
Associate Professor
Department of Pharmaceutics, School of Pharmacy

Virginia Commonwealth University
Richmond, Virginia
May 2016

ACKNOWLEDGMENTS

First and foremost, I would like to express my sincere gratitude to my advisor, Dr. Masahiro Sakagami, for his support, guidance, and mentorship for the last seven years of my academic career in the Pharm.D./Ph.D. combined degree program. Thank you for setting high expectations for this project, stimulating me to think critically, and encouraging me to grow into an independent scientist. I would also like to greatly thank the other members of my Graduate Advisory Committee for contributing their expert advice towards this project: Dr. Umesh Desai, Dr. Peter Byron, Dr. Judith Voynow, and Dr. Matthew Halquist. I would like to especially thank Dr. Umesh Desai for providing CDSO3 for this dissertation project.

I am extremely grateful to Ms. Hua Li; thank you for patiently training me on how to handle animals as well as to teach me Western blot technique. Her presence, skills, and kindness have been so invaluable and very much appreciated. Thank you to Dr. Phillip Gerk for graciously opening his lab to me and provided so many important resources for this project.

I would like to acknowledge the members of the Aerosol Research Group that I have had the pleasure of working with during the course of my study: Dr. Peter Byron, Dr. Masahiro Sakagami, Dr. Joanne Peart, Dr. Michael Hindle, Dr. Sandro da Rocha, Dr. Bhawana Saluja, Dr. Ruba Darweesh, Dr. Min Li, Dr. Laleh Golshahi, Dr. Anubhav Kaviratna, Dr. Xiangyin Wei, Dr. Qian Zhong, Mandana Azimi, Susan Boc, Sneha

Dhapare, and Anuja Raut. Thank you for all of the stimulating discussions, and especially for making the lab so much more enjoyable.

I am so grateful to the wonderful School of Pharmacy staff for their tremendous help throughout the years: Karen Bryant, Shakim Jackson, Keyetta Tate, and Laura Georgiadis. Thank you for always being there for us graduate students.

I have been so fortunate to have phenomenal professors and mentors these past 7 years: Dean Joseph Dipiro, Dr. Victor Yanchick, Dr. Jurgen Venitz, Dr. Douglas Sweet, Dr. Patricia Slattum, and Dr. Benjamin Van Tassel. Thank you for always being willing to take time out of your busy schedule to guide, mentor, and offer your advice and support. I would like to especially thank Dr. Susanna Wu-Pong for always being such a positive and encouraging role model.

As I reflect on my time here as a graduate student, I am so grateful for the friendships that I have gained. Thank you to all the graduate students from all over the world that I have had the honor of getting to know. Dr. Bassem Mostafa, thank you for always being so kind and generous. Dr. Meghan Thompson, thank you for your friendship throughout the years. Mandana and Susan, you have both been more than just colleagues, you have become my lifelong friends and sisters.

Last but not least, I would like to thank my family for their enduring support throughout this long journey, especially to my parents who have made so many sacrifices so that I could have what they did not: an education. I would also like to specially thank my fiancé for his patience, love, and prayers. Thank you for encouraging me to pursue my dreams.

TABLE OF CONTENTS

LIST OF TABLES

LIST OF FIGURES

ABBREVIATIONS AND SYMBOLS

AT	α_1-antitrypsin
$ABTS^{\bullet+}$	2,2-azinobis(3-ethyl-benzothiazoline-6-sulphonic acid)
ANOVA	analysis of variance
APTT	activated partial thromboplastin time
ATCC	American Type Culture Collection
BAL	bronchoalveolar lavage
BALF	bronchoalveolar lavage fluid
BCA	bicinchoninic acid
BSA	bovine serum albumin
C	concentration
CA	caffeic acid
CBP	creb-binding protein
CD	unsulfated caffeic acid dehydropolymer
CDSO3	sulfated caffeic acid dehydropolymer
$CDSO3_{BH}$	A batch of CDSO3 synthesized by Henry in 2006
$CDSO3_{MT}$	A batch of CDSO3 synthesized by M. Thompson in 2015
CI	confidence interval
COD	coefficient of determination

COPD	chronic obstructive pulmonary disease
CSE	cigarette smoke extract
Da	dalton
DDW	deionized distilled water
DFO	deferoxamine
DHP	dehydropolymer
DI	destructive index
DMF	dimethylformamide
DMSO	dimethyl sulfoxide
DPI	dry powdered inhaler
ε	molar absorption coefficient
Ech	echinomycin
EDTA	ethylenediaminetetraacetic acid
EE	exercise endurance
FBS	fetal bovine serum
FDA	Food and Drug Administration
Fe^{2+}	ferrous ion
Fe^{3+}	ferric ion
HDAC	histone deacetylase
HE	hematoxylin-eosin
HEPES	N-[2-hydroxy-ethyl]piperazine-N'-[2-ethanesulfonic acid]
HIF-1α	hypoxia-inducible factor-1 alpha
HNE	human neutrophil elastase

HRE	hypoxia response element
HRP	horseradish peroxidase
HS	Hill slope coefficient
HSE	human sputum elastase
IC_{50}	half-maximal inhibitory concentration
ICS	inhaled corticosteroids
LDH	lactate dehydrogenase
log D	distribution coefficient
MDI	metered dose inhaler
MLI	mean linear intercept
MSC	model selection criteria
MW	molecular weight
NA	not applicable
NAD	nicotinamide adenine dinucleotide
NADH	nicotinamide adenine dinucleotide + hydrogen
NF-κB	nuclear factor kappa-light-chain enhancer of activated B cells
NHLBI	National Heart, Lung, and Blood Institute
NRT	nicotine replacement therapy
NS	nebulized solution
ODD	oxygen-dependent degradation domain
OT	orotracheal
PBS	phosphate buffered saline
PO	oral formulation

PS	penicillin streptomycin
PHD	prolyl hydroxylase
PRP	pulmonary rehabilitation programs
pNA	para-nitro anilide
PT	prothrombin time
QOL	quality of life
rGSH	reduced glutathione
RH	relative humidity
RNS	reactive nitrogen species
ROS	reactive oxygen species
SAA	sulfosalicylic acid
SC	subcutaneous
SD	standard deviation
SMI	soft mist inhaler
T	absolute temperature
TBE	trypan blue exclusion
TBS	tris buffered saline
TSA	trichostatin A
U	unit
VEGF	vascular endothelial growth factor
VHL	von Hippel-Lindau tumor suppressor protein
WHO	World Health Organization

ABSTRACT

SULFATED DEHYDROPOLYMER OF CAFFEIC ACID FOR REPAIR OF LUNG DAMAGE AND EMPHYSEMA

by Tien M. Truong, B.S., Biology

A dissertation submitted in partial fulfillment of the requirements for the degree of Doctor of Philosophy at Virginia Commonwealth University

Virginia Commonwealth University, 2016

Major Director: Masahiro Sakagami, Ph.D.
Associate Professor
Department of Pharmaceutics, School of Pharmacy

The complex pathobiologic mechanisms of emphysema are not fully understood, leaving this deadly disease without effective pharmacotherapy for a cure. This project hypothesized that the sulfated dehydropolymer of caffeic acid (CDSO3) exhibits Fe^{2+} chelation-based hypoxia inducible factor-1α (HIF-1α) up-regulatory protective activities against *in vitro* emphysematous cell death and for *in vivo* reversal of emphysema induced with SU5416, a vascular endothelial growth factor blocker.

Using *in vitro* chromogenic competitive inhibition assays, CDSO3 was shown to chelate Fe^{2+} (IC_{50} of 23 µM), but not Fe^{3+} ions. The trypan blue exclusion and lactate

dehydrogenase assays were then employed to examine the cytoprotective activities of CDSO3 against inflammatory, oxidative, elastolytic, and apoptotic cell death using alveolar macrophages, epithelial and endothelial cells. CDSO3 at 10 μM produced significant protective activities against these emphysematous cell deaths by 50-154 %. These protective effects were opposed by the addition of the HIF-1α inhibitors, CAY10585 and echinomycin, and excess Fe^{2+}, but not Fe^{3+}, ions.

Emphysema was then induced in rats following a subcutaneous injection of SU5416 at 20 mg/kg, after which CDSO3 at 60 μg/kg was administered to the lungs 3 times/week for two weeks. Treadmill exercise endurance (EE) was measured to assess the functional impairment, while lung tissues were removed for morphological assessments of alveolar airspace enlargement (MLI) and destruction (DI), as well as to measure protein levels using Western blot. SU5416 significantly impaired EE, MLI, and DI by 81 %, 47 %, and 5-fold, compared to the healthy animals, and these were significantly reversed by CDSO3 by 66, 74, and 87 %. CDSO3 treatment did not change the lung cytoplasmic expression of histone deacetylase 2 (HDAC2), HIF-1α, or a pro-apoptotic marker, BAX. However, induction with SU5416 significantly reduced VEGF expression by 52 % and increased cleaved caspase-3 expression by 1.5-fold, compared to the healthy animals, while CDSO3 normalized the expressions of both proteins in these emphysematous animals. However, when CDSO3 was pre-mixed with excess Fe^{2+}, the reversal activities of CDSO3 were diminished. In conclusion, this study has demonstrated the Fe^{2+} chelation-based HIF-1α up-regulatory dependent *in vitro* and *in vivo* lung repairing efficacies for CDSO3 in emphysema.

CHAPTER 1

EMPHYSEMA: BACKGROUND AND SIGNIFICANCE

1.1 BURDEN AND OUTLOOK

Pulmonary emphysema is a life-threatening lung disease that most often develops in chronic cigarette smokers between the ages of 45 and 60 as one of the major manifestations of chronic obstructive pulmonary disease (COPD) [Taraseviciene-Stewart *et al.*, 2008; Koblizek *et al.,* 2016]. Recent studies have estimated the COPD prevalence to be 5-25 % [Rycroft *et al.,* 2012; Buist *et al.,* 2007], while approximately 50.0-98.3% of patients are under-diagnosed worldwide [Koblizek *et al.,* 2016]. Clinical symptoms include chronic cough, excessive sputum production, and dyspnea, leading to physical and functional disability, and eventually death [Andersson *et al.,* 2015; Koblizek *et al.,* 2016; Celli *et al.,* 2004; Stridsman *et al.,* 2014; Karpman *et al.,* 2014; Tuder, 2008]. COPD is currently the third leading cause of death in the United States, affecting 13 million people, and costing nearly $50 billion annually [Tuder *et al.,* 2012; Ford *et al.,* 2015; NHLBI 2012]. Similarly, the World Health Organization (WHO) has predicted a rapidly increasing prevalence of this disease worldwide, so that it would become the third leading cause of worldwide mortality and the fifth leading cause of morbidity by 2020, imposing a burden of $47 trillion by 2030 [Tuder *et al.,* 2012;

Taraseviciene-Stewart *et al.*, 2008; Murray *et al.*, 1996; Sullivan *et al.*, 2000]. Therefore, there is clearly an urgent need to discover and develop novel drug molecules capable of reversing emphysema for cure in order to address this global epidemic.

1.2 RISK FACTORS

Chronic cigarette smoking is the undisputed leading cause of emphysema, although other factors, such as exposure to household indoor biomass fumes, environmental and occupational exposure to dust, chemicals, and asbestos, as well as respiratory infections and aging, all contribute to the overall epidemiology of COPD/emphysema [Yoshida *et al.,* 2007; Stockley *et al.,* 2009; Taraseviciene-Stewart *et al.*, 2008; Koblizek *et al.,* 2016]. Chronic cigarette smoking is responsible for 80-90 % of COPD cases in the United States; hence, quitting smoking would inarguably be the best way to prevent emphysema [Yoshida *et al.,* 2007]. However, the success rate for smoking cessation is as low as 7-10 % [Messer *et al.,* 2008], and it has also been reported that slow and progressive destruction of the lung parenchyma still occurs even after smoking cessation, for which reasons remain unclear [Yoshida *et al.,* 2007; Hodge 2005, Taraseviciene-Stewart *et al.*, 2008]. Furthermore, smokers show considerable variation in their risk of developing airflow destruction, which suggests that there may be genetic factors that contribute to the development of this disease [Sandford *et al*., 2002]. To date, however, the only proven genetic risk factor for COPD thus far is severe deficiency of α_1-antitrypsin (AAT), which accounts for only 1-2 % of patients with COPD [Hersch *et al.* 2008; Hutchison *et al.,* 1971]. Among many candidate genes,

polymorphic variations in surfactant protein B, mannose-binding lectin, SERPINE2 gene, and matrix metalloproteinase-9 promoter have all been associated with exacerbations of COPD, yet their validation has still to be completed [Hansel *et al.,* 2009; Foreman *et al*., 2008; Yang *et al.,* 2003; Demeo *et al*., 2006; Ito *et al*., 2005(b)]. Hence, at present, the pathobiologic mechanisms of emphysema still remain largely unknown, such that clarification of these pathobiological processes is critical for the development of biomarkers and targets of novel therapies.

1.3 TREATMENT

While it is characterized by the destruction and loss of the alveolar septa, resulting in abnormal and irreversible enlargement of the airspaces (Figure 1.1), the cellular and molecular mechanisms of emphysema are complex and not fully understood even today [Snider *et al.,* 1985; Fisher *et al.,* 2011; Voelkel *et al.,* 2011]. As a result, there have been no pharmacologic cure for emphysema, and the present treatment options are limited to non-pharmacological and pharmacological therapies for symptomatic relief and management of complications, to improve quality-of-life (QOL) in patients [Taraseviciene-Stewart *et al.*, 2008; Voelkel *et al.,* 2011; Fisher *et al.,* 2011].

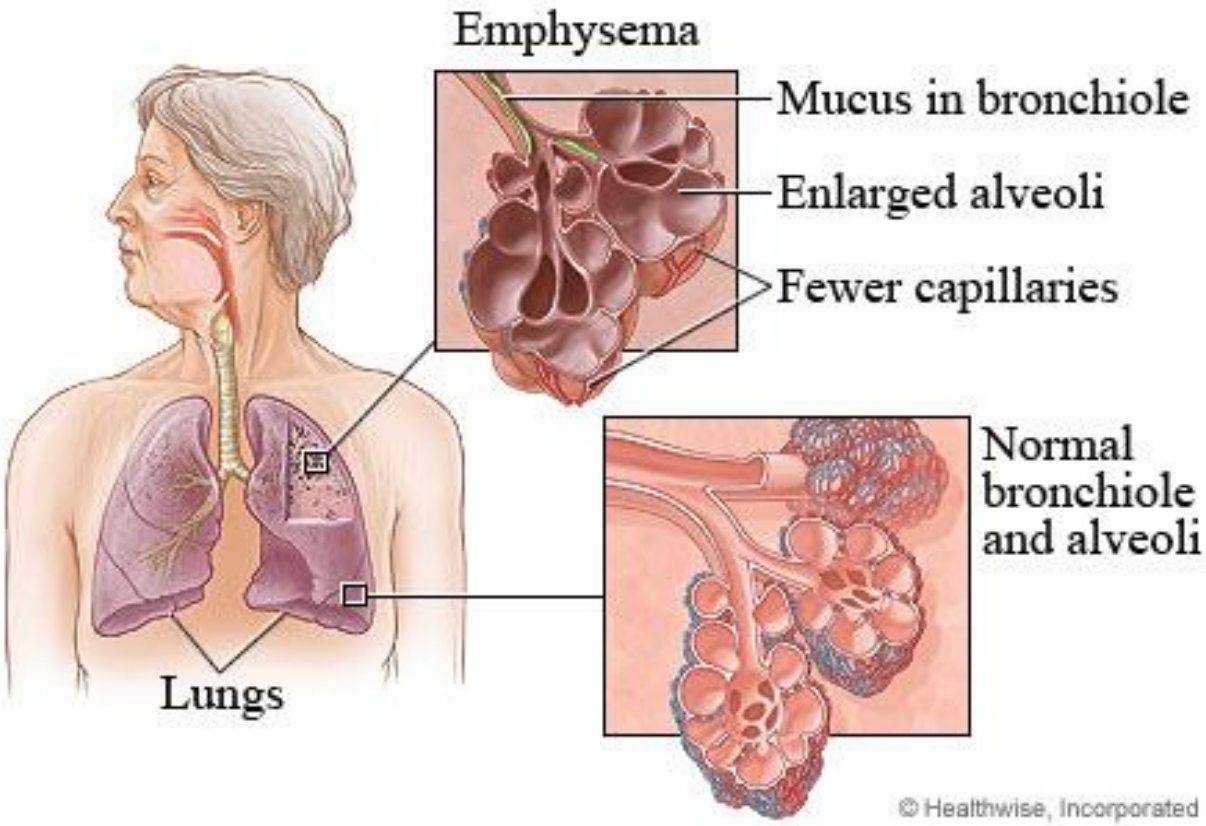

Figure 1.1: Normal versus emphysematous lung alveoli. The image has been taken from WebMD [http://www.webmd.com/lung/emphysema].

1.3.1 Non-pharmacological therapy

Smoking cessation has been attempted together with nicotine replacement therapy (NRT) such as sustained nicotine patches, and medications approved by the Food and Drug Administration (FDA) for smoking cessation, i.e., buproprion (Zyban), varenicline, and cytosine [Piper *et al.,* 2009; Watsky *et al.,* 2006]. While the success rates for NRT and pharmacotherapy alone are similar, their concomitant use has yielded higher success rates as high as 33-37% [Mulhall *et al.,* 2016]. The newest cessation tool is electronic cigarette, a device designed to emit vaporized nicotine

without noxious substances contained in real cigarettes. Although a Cochrane review of e-cigarettes concluded that, while they are effective for cessation and their use over 2 years resulted in no significant adverse effects, additional studies and regulations are necessary before their widespread adoption [McRobbie *et al.,* 2014; McCauley *et al.,* 2012]. By contrast, pulmonary rehabilitation programs (PRP) can recondition patient's non-pulmonary organs to improve exercise tolerance, exertional dyspnea, walk distance, and health-related QOL; however, no study has been shown to improve pulmonary function or mortality [Mulhall *et al.,* 2016]. Long-term oxygen therapy has been used to palliate dyspnea and improve mortality, and non-invasive positive pressure ventilation has also been used to treat acute and chronic respiratory failure [Mullhall *et al*., 2016]. More invasive procedures include lung volume reduction surgery and lung transplantation for end-stage lung disease. However, these non-pharmacological options are expensive, invasive, and produce inconsistent results.

1.3.2 Pharmacological therapy

Currently, pharmacological therapy for COPD/emphysema is available only to reduce its symptoms, reduce the frequency and severity of exacerbations, and improve health status and exercise tolerance. Bronchodilators are the mainstay of COPD/emphysema management and are recommended by national and international guidelines as first-line therapy in symptomatic patients who demonstrate airflow limitation [Hanania *et al*., 2007]. Three classes of bronchodilators – β_2-adrenoreceptor agonists, anticholinergics, and methylxanthines – are currently in use for

COPD/emphysema as summarized in Table 1.1. Inhaled short-acting bronchodilators are recommended for rescue of symptoms in mild disease due to their rapid onset of action, and increased mucociliary clearance [Hanania *et al*., 2007; GOLD 2016]. Inhaled long-acting bronchodilators are the first-line agents for maintenance of daily symptoms in moderate to severe COPD/emphysema [Hanania *et al.,* 2007; GOLD 2016]. When symptoms are not sufficiently controlled with one bronchodilator, it is recommended to combine bronchodilators of different classes [GOLD 2016]. Meanwhile, inhaled corticosteroids (ICS) when used regularly, improve symptoms, lung function and QOL, and reduces the frequency of exacerbations; however, withdrawal from ICS treatment has been shown to lead to exacerbations in some patients [GOLD 2016]. Furthermore, ICS are associated with higher incidences of oral candidiasis, skin bruising, increased risk of reduced bone density and fractures [GOLD 2016]. It should be emphasized that these bronchodilators and ICS only reduce the frequency and severity of exacerbations. To date, none of the existing medications has been shown to modify the long-term decline in lung function [Barnes *et al*., 2005; Wise *et al.,* 2007; Roche *et al.,* 2011].

Table 1.1: Pharmacological therapy for COPD/emphysema [GOLD 2016]

	BRONCHODILATORS	
	Short-acting	**Long-acting**
β_2-agonist	Albuterol (salbutamol) (MDI, DPI, NS, PO) Levalbuterol (MDI, NS) Fenoterol (MDI, NS, PO) Pirbuterol (MDI) Terbutaline (DPI, PO)	Salmeterol (MDI, DPI) Formoterol (MDI, DPI, NS) Arformoterol (NS) Indacaterol (DPI) Olodaterol (SMI)
Anticholinergic	Ipratropium bromide (MDI, NS) Oxitropium bromide (MDI, NS)	Tiotropium bromide (DPI) Umeclidinium (DPI) Aclidinium bromide (DPI) Glycopyrronium bromide (DPI)
Combination	Albuterol/Ipratropium (MDI, NS) Fenoterol/Ipratropium (SMI)	Salmeterol/fluticasone (DPI, MDI) Formoterol/Aclidinium (DPI) Indacaterol/glycopyrronium (DPI) Oladaterol/tiotropium (SMI) Vilanterol/umeclidinium (DPI)
Methylxanthine	Theophylline (PO) Aminophylline (PO)	
	CORTICOSTEROIDS	
	Inhaled	**Systemic**
	Beclomethasone (MDI, DPI, NS) Budesonide (DPI, NS) Fluticasone (MDI, DPI)	Prednisone (PO) Methyl-prednisolone (PO)
Combination	Formoterol/beclometason (MDI, DPI) Formoterol/budesonide (MDI, DPI) Formoterol/mometasone (MDI) Salmeterol/Fluticasone (DPI) Vilanterol/Fluticasone furoate (DPI)	
	PHOSPHODIESTERASE-4 INHIBITORS	
	Roflumilast (PO)	

DPI = dry powder inhaler; MDI =metered dose inhaler; SMI = soft mist inhaler; NS = nebulized solution; PO = oral formulation

1.4 PATHOPHYSIOLOGY

The lack of effective therapy to prevent and/or treat emphysema is largely due to its enigmatic multi-faceted pathobiologic mechanisms that remain not fully understood even today. Several hypotheses have been proposed to explain the pathobiologic mechanisms of emphysema, among which persistent inflammation, oxidative stress, and protease-antiprotease imbalance have been considered to be key components [Suki *et al.,* 2003; Barnes 2009; Stockley *et al*., 2009; Voelkel *et al.,* 2011; Fischer *et al.,* 2011]. However, treatment strategies that target one or more of these mechanisms have been unsuccessful to reverse emphysematous lung damages toward a cure. Thus, a new pathobiologic concept has been recently proposed, based on an imbalance of increased lung cell death and decreased cell proliferation, due to the failure of the homeostatic lung structure maintenance program [Taraseviciene-Stewart *et al.,* 2008; Mizuno *et al.,* 2011; Lee *et al.,* 2012]. In line with this concept, lungs from patients with COPD have been shown to possess apoptotic cells in greater numbers than control lungs or those from smokers without COPD [Demedts *et al.,* 2006; Imai *et al.,* 2005; Kasahara *et al.,* 2000; Yokohori *et al.,* 2004]. This apoptosis has been shown to persist in patients with COPD long after smoking cessation, suggesting that cigarette smoke itself is not the sole agent causing the apoptosis [Henson *et al.,* 2006; Hodge *et al.,* 2005]. These, in addition to other various risks for smokers to develop COPD/emphysema, have shifted research to investigate epigenetic modifications in the lungs of COPD/emphysema patients as a cause for this imbalance.

The failure of the homeostatic lung structure maintenance program has been now attributed to the epigenetically reduced expression of one of the essential lung structure maintenance factors, vascular endothelial growth factor (VEGF), and one of its upstream transcription factors, hypoxia-inducible factor-1α (HIF-1α), as seen in patients with COPD/emphysema [Yasuo *et al.,* 2011; Kasahara *et al.,* 2000; Tuder *et al.,* 2008; Kasahara *et al.,* 2001]. Because VEGF stimulates endothelial cell growth and its removal causes endothelial cell apoptosis, VEGF is considered to be an essential element required for the survival of endothelial cells [Neufeld et. al, 1999; Gerber et al., 1998a; Gerber et al., 1998b]. Indeed, reduced expression of VEGF and HIF-1α has been shown to cause apoptosis and emphysema at cell and animal levels [Yasuo *et al.,* 2011; Lee *et al.,* 2012; Kasahara *et al.,* 2000]. It was therefore hypothesized that this "HIF-1a/VEGF deficiency" is responsible for the failure of the homeostatic lung structure maintenance program, such that recovery of lung's HIF-1α and VEGF levels may be a new strategy to reverse the imbalance of cell death and cell proliferation in emphysema.

By now, it has been shown that this reduced HIF-1α/VEGF expression is likely caused by up-stream inhibition of histone deacetylase (HDAC) [Ellis *et al.,* 2009; Mie Lee *et al.,* 2003; Qian *et al.,* 2006]. Cigarette smoke exposure has been shown to affect chromatin remodeling [Yang *et al.,* 2006], and decreased expression of HDAC, specifically HDAC2, was seen in the lungs from patients with COPD [Ito *et al.,* 2005a; Mizuno *et al.*, 2011], correlated with increased expression of inflammatory genes [Barnes 2009; Ito *et al.,* 2001]. In addition, it was reported that HDAC inhibition increased binding of nuclear factor kappa-light-chain enhancer of activated B cells (NF-κB) to hydrogen peroxide (H_2O_2)-challenged alveolar cells [Rahman 2002], and that

reduced HDAC2 expression resulted from oxidative stress [Ito *et al.,* 2004], with reasonable correlations of HDAC inhibition with oxidative stress and inflammation. These relevant findings have led this research to hypothesize that, while originating from the triple causative features of elastolysis, oxidative stress, and inflammation, the pathobiological mechanism for emphysema involves epigenetic modifications to cause "HIF-1α/VEGF deficiency", leading to increased cell death and emphysema, as shown in Figure 1.1.

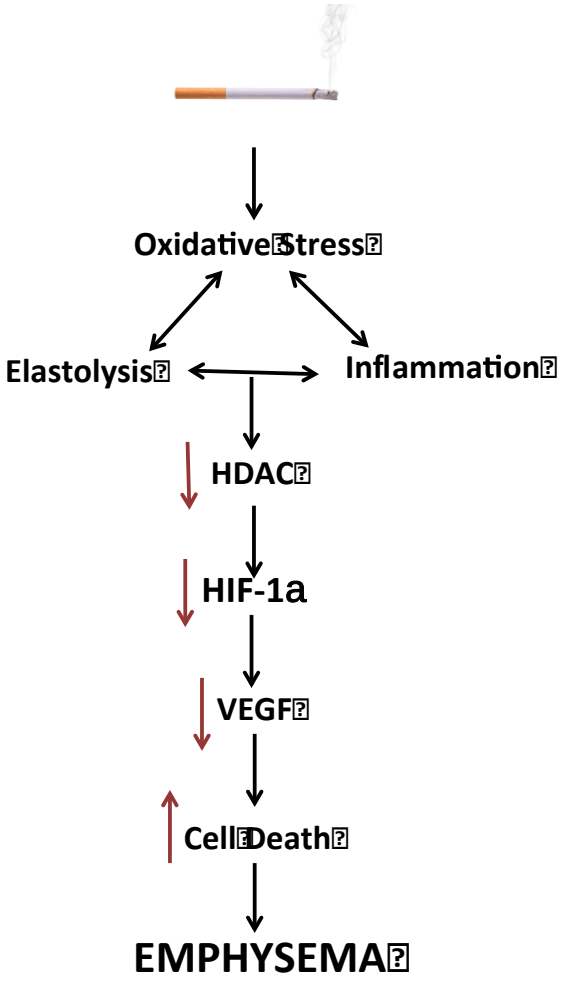

Figure 1.2: Proposed pathobiologic mechanism of pulmonary emphysema.

1.5 HYPOXIA-INDUCIBLE FACTOR-1α

HIF-1α is an oxygen sensitive, ubiquitous transcription factor, which controls many downstream genes for various functions, including cell death and cell proliferation. As described in Figure 1.3, under normoxic conditions and in the presence of Fe^{2+} and 2-oxoglutarate, the conserved proline residues (Pro-402 and Pro-564) of HIF-1α within the oxygen-dependent degradation domain (ODD) are hydroxylated by prolyl hydroxylase (PHD) domain proteins [Ivan *et al.,* 2001; Jaakkola *et al.,* 2001; Masson *et al.,* 2001; Fan *et al.,* 2014]. The hydroxylated HIF-1α then interacts with the β-domain of von Hippel-Lindau tumor suppressor protein (VHL) and is subsequently ubiquitylated by the VHL-E3 ligase complex, thereby marking HIF-1α for degradation by the 26S proteasome [Maxwell *et al*., 1999; Ohh *et al.,* 2000]. In contrast, under hypoxic conditions or in the absence of the essential co-factors, Fe^{2+} and 2-oxoglutarate, the catalytic activity of PHDs is inhibited, and thus, HIF-1α is stabilized and translocates into the nucleus where it dimerizes with the HIF-1β subunit, which is constitutively expressed in the nucleus. The HIF1α/β dimer then interacts with the transcriptional co-activators p300/Creb-binding protein (CBP) and forms a transcriptional complex [Sang *et al.,* 2002; Arany *et al.,* 1996]. This transcriptional complex binds to hypoxia response elements (HREs) of hypoxia-responsive target genes, thereby promoting the expression of genes that regulate angiogenesis and cell survival, such as VEGF. Therefore, pharmacologic inhibition of HIF-PHD by depleting the essential Fe^{2+} could be a means of stabilizing HIF-1α, and thereby overcoming the pathobiologic critical 'HIF-1α

deficiency' in emphysema, as increasing angiogenesis and inhibiting cell death [Sears *et al.,* 2013].

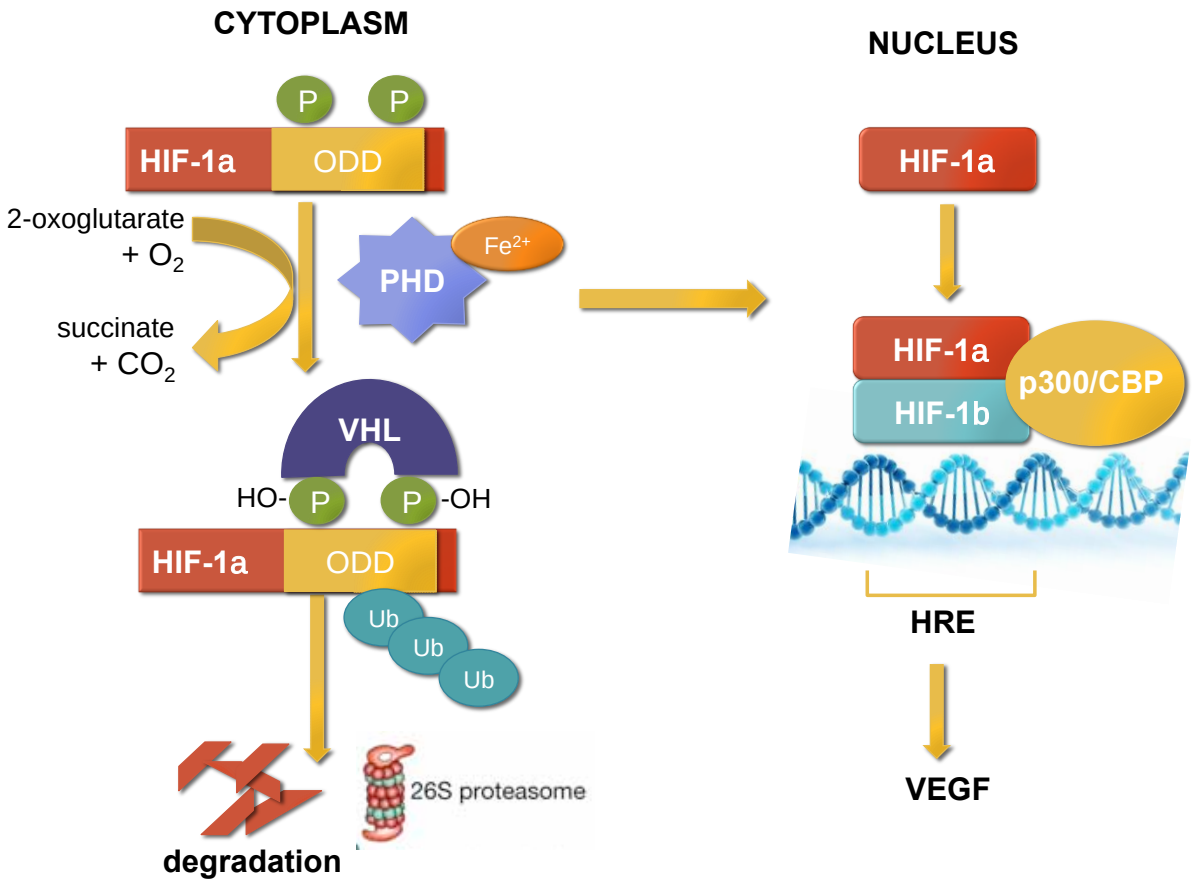

Figure 1.3: HIF-1α regulatory pathway.

1.6 SULFATED DEHYDROPOLYMER OF CAFFEIC ACID (CDSO3)

Recently, dehydropolymers (DHPs) of 4-hydroxy cinnamic acids were discovered as a novel class of anti-coagulants via direct inhibition of thrombin and factor Xa [Monien *et al.,* 2006]. Among them, unsulfated and sulfated caffeic acid (CA) oligomers were chemo-enzymatically synthesized, as described in Figure 1.4 [Monien *et al.,* 2006]. CA monomers were coupled via horseradish peroxidase (HRP)-catalyzed oxidation in the presence of H_2O_2, generating radical intermediates, I_1 and I_2. These radical intermediates were coupled with CA monomers to give β-O-4- and β-5-linked dimeric units, which then underwent further chain extensions with radicals to result in 4-15 units oligomerization to CA-based dehydropolymers (DHPs). These unsulfated DHPs of CA were then reacted with triethylamine-sulfure trioxide (Et_3N/SO_3) complex, yielding sulfated DHP of CA, or CDSO3. The average molecular weight was determined by size exclusion chromatography using their acetylated derivatives, resulting in an average of 3320 Da [Henry *et al.,* 2007]. The elemental analysis revealed that sulfation was added as 0.30-0.40 moles per monomer unit of CDSO3 [Monien *et al.,* 2006]. The prothrombin and activate partial thromboplastin (PT and APTT) were measured with citrated human plasma at six to eight concentrations of CD and CDSO3. In these assays, the anticoagulant activity was defined as the concentration of the DHPs needed for doubling the normal plasma clotting time [Monien *et al.,* 2006]. To assess the effect of CD and CDSO3 on the proteolytic activities of coagulation proteinases, factor Xa and thrombin, the residual enzymatic activity of the two enzymes following incubation for a defined time period with varying concentrations

of DHPs in the presence and absence of antithrombin was measured [Monien *et al.,* 2006]. The proteinase activity was determined under pseudo-first order conditions in a spectrophotometric assay using chromogenic substrates Sepctrozyme fXa and TH for factor Xa and thrombin, respectively. As the concentration of DHP increases, the residual proteinase activity decreases in a sigmoidal manner, which can be fit to a standard dose-dependence equation to derive the IC_{50} values. Their *in vitro* prothrombin and activated partial thromboplastin times (PT and APTT, respectively), and inhibitory binding activities to factor Xa and thrombin, suggested that sulfation substantially potentiated the activities for CDSO3, compared to the unsulfated DHP, or CD. These physiochemical and anti-coagulant activities of CD and CDSO3 are summarized in Table 1.2.

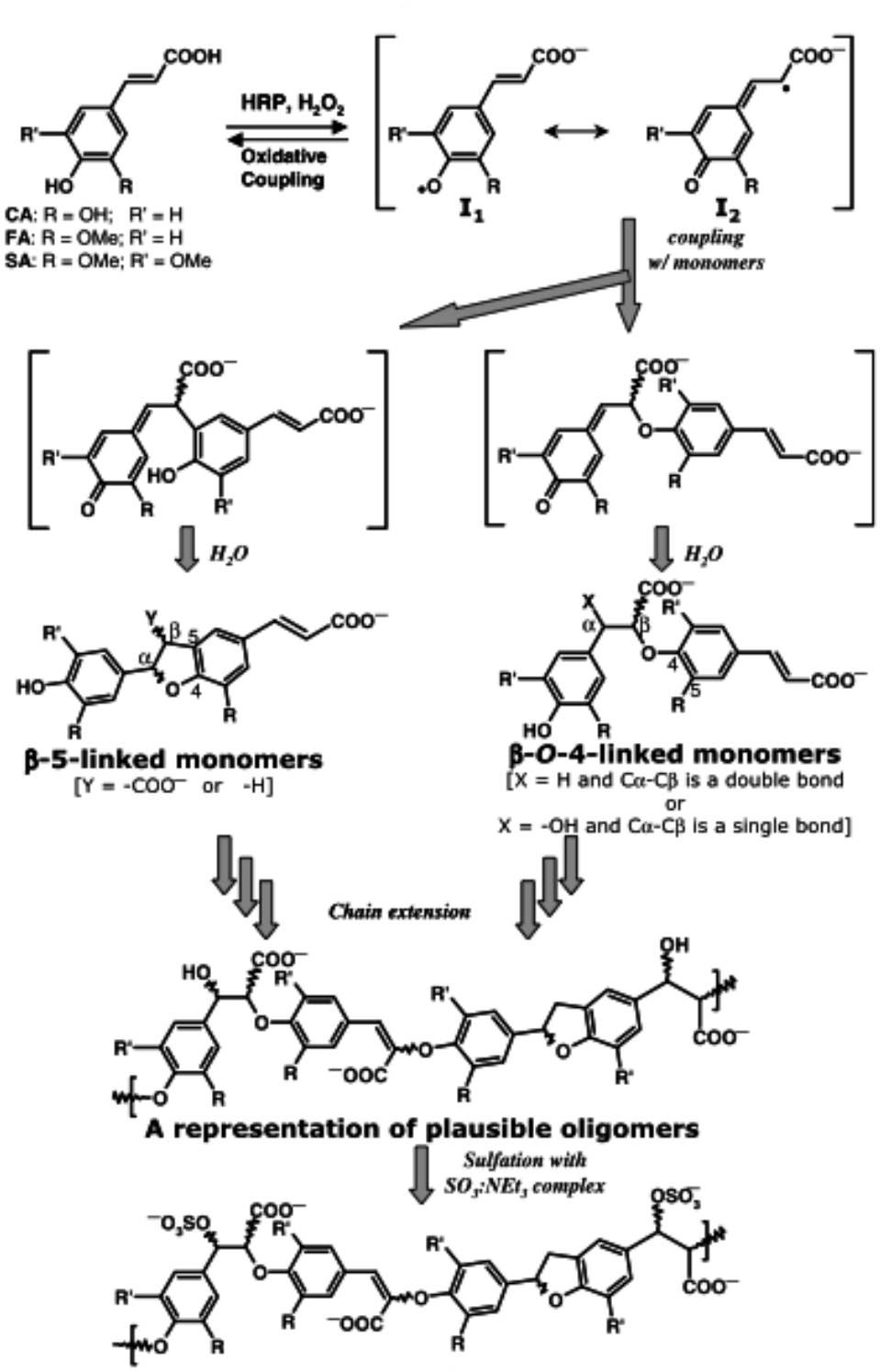

Figure 1.4: Synthetic scheme of the sulfated dehyodropolymer of caffeic acid (CDSO3) [Monien *et al.,* 2006]

Table 1.2: Average molecular weight, sulfate density, and *in vitro* anti-coagulation activities of the unsulfated and sulfated dehydropolymers (DHPs) of caffeic acid, CD and CDSO3, respectively [Monien *et al.,* 2006; Henry *et al.,* 2014]

	MW (Da)[1]	**Sulfates per monomeric unit[2]**	**IC_{50}[3]**		**Clotting assay[4]**	
			Factor Xa	Thrombin	2x PT [µg/mL]	2x APTT [µg/mL]
CD	2,800	NA	0.14	0.07	98.1±0.7	24.9±2.3
CDSO3	3,320	0.40	0.03	0.02	42.1±0.3	13.0±5.0

[1]Weight-averaged molecular weight
[2]Averaged molar number of sulfates per monomeric unit, derived from elemental composition analysis and averaged oligomer size
[3]The half-maximal inhibitory concentration (IC_{50}) obtained from chromogenic substrate hydrolysis assays for each enzyme.
[4]The PT and APTT values were derived *from in vitro* human plasma experiments using thromboplastin or ellagic acid, respectively, as a clotting initiator

1.7 CDSO3 FOR EMPHYSEMA

Many molecules have been examined for the treatment of emphysema in the past few decades. Retinoic acid was shown to inhibit elastase-induced injury in lung epithelial cells [Nakajoh *et al.,* 2003]. Molecules exerting dual inhibitory action, *i.e.,* anti-inflammatory and anti-oxidative activities, such as curcumin and resveratrol, demonstrated improvements in the triple-threat pathogenesis [Biswas *et al.,* 2005; Epstein *et al.,* 2010; Rahman *et al.,* 2006]. Likewise, novel coumarinic derivatives have been shown to be anti-inflammatory and anti-elastase [Bissonnette *et al.,* 2009]. However, no molecule has been discovered to exhibit triple-inhibitory action against elastase, oxidation, and inflammation.

It was intriguing that the complex pathogenesis of emphysema that involves oxidative stress, inflammation, and elastolysis somewhat resembles that seen in blood coagulation. Chronic cigarette smokers have increased blood viscosity due to higher levels of thrombin and fibrinogen and lower levels of anti-factor Xa, all attributed to systemic oxidative stress [Yanbaeva *et al.,* 2007; Hioki *et al.,* 2001; Wannamethee *et al.,* 2005]. Therefore, given CDSO3 as a potent inhibitor of blood serine proteases, e.g., factor Xa and thrombin (Table 1.2), it was hypothesized that CDSO3 could also inhibit the triple-threat pathogenesis of inflammation, elastolysis, and oxidation in emphysema. Table 1.3 summarizes the *in vitro* triple inhibitory activities of CDSO3 along with those for the monomer CA and unsulfated oligomer, CD [Saluja *et al.,* 2013]. CDSO3 was shown to be the most potent, suggesting that oligomerization and sulfation play key roles in their triple inhibitory activities.

Accordingly, the *in vivo* therapeutic efficacy, duration and mode of actions, and the effective route were further tested for CDSO3 in the human sputum elastase and cigarette smoke extract (HSE/CSE) rat model of pulmonary emphysema. CDSO3 was shown to attenuate the development of HSE/CSE-induced emphysema in rats following pulmonary administration, with a dose of 100 µg/kg in both preventive and interventional manners [Saluja *et al.,* 2014]. Preventative treatment showed significant (53-89 %) attenuation in bronchoalveolar lavage fluid (BALF) elastase, lung tissue reduced glutahione (rGSH), and BALF tumor necrosis factor-alpha (TNFα , airway luminal leukocyte infiltration, exercise endurance, and airspace enlargement [Saluja *et a*l., 2014]. Likewise, interventional treatment also attenuated the lung luminal elastolytic and inflammatory inductions, neutrophil infiltration, impaired exercise endurance, and airspace enlargement by 43-82 % [Saluja *et al.,* 2014]. By contrast, systemic subcutaneous injection of CDSO3 was ineffective, in turn suggesting a need for local pulmonary delivery [Saluja *et al.,* 2014]. Hence, CDSO3 has been discovered as one of the first drug entities capable of triple-inhibitory activities in emphysema *in vitro* as well as *in vivo*.

Recently, Sakagami et al. [2014] attempted pulmonary delivery of CDSO3 to repair lung damages in emphysematous lungs in the CSE-induced rat model of emphysema. The pathobiologically impaired “HIF-1α/VEGF deficiency” hypothesized in this research was shown in this model. Moreover, two week pulmonary administration of CDSO3 at 60 µg/kg significantly improved impaired exercise endurance by 50-70 % and restored increased airspace size by 42-73 %. When CDSO3 was pre-mixed with excess Fe^{2+} and a HIF-1α inhibitor, 2-methoxyestradiol, the reversal activities of

CDSO3 were opposed, supporting CDSO3's Fe^{2+} chelation-based HIF1α-mediated mechanism in this CSE-induced emphysema model. However, lung cell-specific repair and its mechanism have yet to be proven, while the reversal efficacy in differently-induced emphysema remain unknown. The latter could especially be critical, as the CSE-induced emphysema used in previous study [Sakagami 2014] has not yet been widely accepted as an experimental emphysema model. Furthermore, although CSE-induced emphysema causes necrosis, the VEGF receptor blocker model of emphysema induced with SU5416 has been shown to cause apoptosis and emphysema [Kasahara *et al*., 2000].

Table 1.3: The half-maximal inhibitory concentration (IC_{50}) and the Hill slope (HS) for CA, CD, and CDSO3 in the *in vitro* ant-elastase, anti-oxidative, and anti-inflammatory activity assessments [Saluja *et al*., 2013]

	Anti-elastase[1]		**Anti-oxidation**[2]		**Anti-inflammation**[3]
	IC_{50} [µM]	HS	IC_{50} [µM]	HS	IC_{50} [µM]
CA	NA	NA	16.82±1.16	2.9±0.5	>100
CD	2.82±0.20	1.1±0.1	6.15±0.33	3.3±0.6	~50
CDSO3	0.43±0.04	1.6±0.2	3.52±0.14	3.7±0.5	~10

[1]Anti-human neutrophil elastase (HNE) activity derived from the non-linear regression curve-fitting to the p-nitroanalide (pNA) generation *vs.* concentration profiles. Values are shown as mean±SD

[2]Anti-chemical oxidative activity derived from the non-linear regression curve-fitting to the $ABTS^{\bullet+}$ generation *vs.* concentration profiles. Values are shown as mean±SD

[3]Anti-inflammatory activity estimated from the TNFα-induced NFκB luciferase activity assay

CHAPTER 2

HYPOTHESIS AND SPECIFIC AIMS

The goal of this dissertation project was to further demonstrate the therapeutic potential CDSO3 as a novel macromolecular drug entity for pulmonary delivery in the treatment of emphysema and COPD. It was hypothesized that CDSO3 was capable of repairing lung damages and reversing emphysema. Specifically, this dissertation project was aimed to demonstrate 1) ferrous (Fe^{2+}) and ferric (Fe^{3+}) ion chelation activities of CDSO3 and their batch-to-batch differences, 2) the Fe^{2+}- and HIF-1α-dependent *in vitro* cytoprotective activity of CDSO3, and 3) the Fe - and HIF-1α-dependent lung repairing activities in an *in vivo* rat model of *established* pulmonary emphysema. Hence, the project is designed to test the following 3 hypotheses:

1. Despite differences in the elemental and physiochemical properties, two different synthetic batches of CDSO3 exert comparable, but potent Fe^{2+} chelating activity, and cytoprotective activity.
2. CDSO3 exerts potent Fe^{2+}- and HIF-1α-dependent *in vitro* cytoprotective activities against differently induced emphysematous cell death in alveolar macrophages, epithelial cells, and lung vascular endothelial cells.

3. Pulmonary delivery of CDSO3 reverses the functional and morphological impairments and normalize/stimulate HIF-1α and HIF-regulating proteins in an *in vivo* apoptotic rat model of *established* emphysema induced by VEGF receptor blockade

In Chapter 3, the ferrous and ferric ion chelating activities of CDSO3 were assessed using the *in vitro* chromogenic ferrozine and sulfosalicylic acid chelation-based competitive inhibition assays, respectively. Subsequently, the *in vitro* cytoprotective activities of CDSO3 and known iron chelators (DFO and EDTA) against differently induced emphysematous cell death in three different lung cell lines were assessed in Chapter 4. Cell death was measured using the trypan blue exclusion (TBE) and lactate dehydrogenase (LDH) assays, and the effects of HIF-1α inhibitors and excess Fe^{2+} or Fe^{3+} were tested to clarify the Fe^{2+} and HIF-1α-dependent mechanisms for CDSO3's cytoprotective actions. This led to Chapter 5, where the lung repairing activities of CDSO3 was assessed in the VEGF receptor blockade model of *established* emphysema in rats. Finally, Chapter 6 will summarize all the findings in this dissertation project and provide overall conclusions.

CHAPTER 3

ION CHELATING ACTIVITIES OF CDSO3 UPON SYNTHESES

3.1 INTRODUCTION

CDSO3 (Figure 3.1) has been chemo-enzymatically synthesized from caffeic acid (CA) monomers via a two-step method, oligomerization followed by sulfation, as described in Chapter 1. It was in 2006 that this CDSO3 synthesis was first published, and thereby CDSO3 was characterized as a dehydropolymer composed of 4-15 units of CA-based monomers with an average of 0.4 sulfates per monomer and a heterogeneous mixture of β-O-4 and β-5 linkages; its averaged weight-based molecular weight was reported to be 3,320 Da [Monien *et al*., 2006; Henry *et al.,* 2007]. Hence, CDSO3 was not a single chemical entity and rather a mixture of polymers with varying degrees of oligomerization and sulfation.

In this dissertation work, two batches of CDSO3, i.e., $CDSO3_{BH}$ and $CDSO3_{MT}$, prepared in the Desai laboratory, were used [Monien *et al.,* 2006; Thompson, 2015]. The samples were sent to Atlantic Microlab, Inc. (Norcross, GA) to be analyzed for their elemental composition. It is important to note that the nitrogen content for $CDSO3_{BH}$ and the oxygen content for $CDSO3_{MT}$ were not determined. Their elemental analysis

indicated that the ratio of sulfur to carbon (S/C) for $CDSO3_{BH}$ and $CDSO3_{MT}$ were 0.115 and 0.091, respectively. Furthermore, the sulfur content for $CDSO3_{BH}$ and $CDSO3_{MT}$ were 5.3 % and 3.7 %, respectively. As summarized in Table 3.1, their elemental compositions and distribution coefficients (log D), determined by Monien [2006] and Thompson [2015], were also different. Thus, as an oligomer hypothesized to stabilize HIF-1α and elevate VEGF though its ferrous ion (Fe^{2+}) chelating activity, it was crucial to first assess Fe^{2+} chelating activities and ensure their equipotent activities between these two batches. Therefore, in this chapter, Fe^{2+} chelating activities of CDSO3 in the two batches were determined using an *in vitro* chromogenic ferrozine chelation-based competitive inhibition assay. In addition, $CDSO3_{MT}$ was further examined for its ferric ion (Fe^{3+}) chelating activity by a similar competitive chelation inhibition assay using sulfosalicylic acid (SAA) in relation to its use in the *in vitro* anti-cell death activities described in Chapter 4. The Fe^{2+} chelating activities of two other known chelators, deferoxamine (DFO) and ethylenediaminetetraacetic acid (EDTA) were also assessed. It should be noted that batch-to-batch comparison was further extended with respect to *in vitro* anti-cell death activities, which is described in Chapter 4.

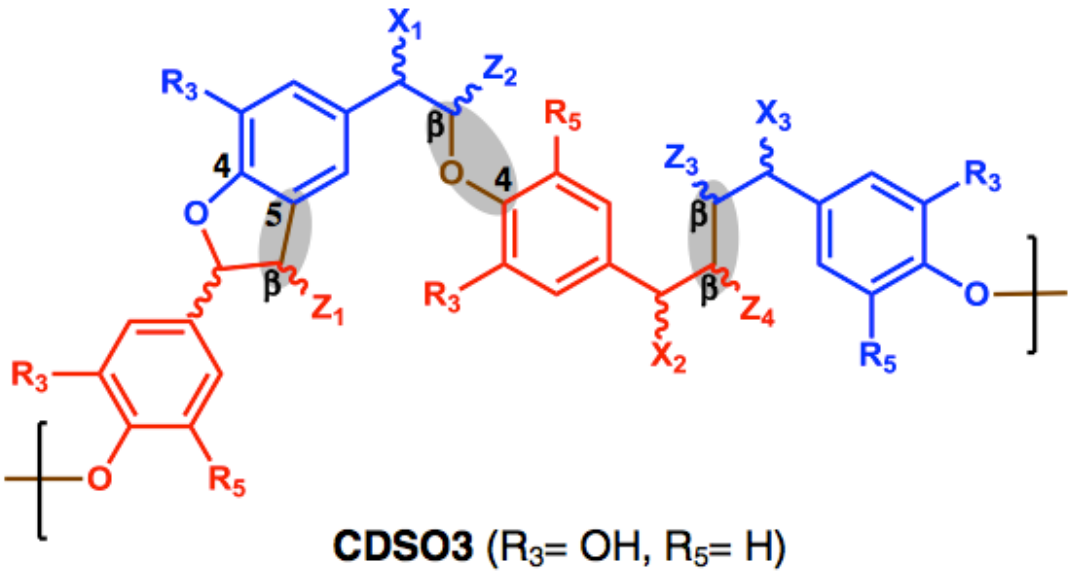

Figure 3.1: Chemical structure of CDSO3 (sulfated dehydropolymer of caffeic acid). Its primary linkages were reported to be β-O-4, β-5, and β-β (shaded). X_1, X_2, and X_3 are substituents at the α-position and may be –H, -OH, or $–OSO_3Na$. Z_1, Z_2, and Z_3 may be –H or –COONa [Henry et al., 2014].

Table 3.1: Elemental compositional analysis and measured distribution coefficient values (log D) for CDSO3 in two different batches [Monien *et al*., 2006; Thompson, 2015]

	Percent (%) elemental compositions[1]					**Log D**
	Carbon	Hydrogen	Oxygen	Nitrogen	Sulfur	
$CDSO3_{BH}$	46.1	4.0	36.7	ND	5.3	0.96±0.09
$CDSO3_{MT}$	40.5	3.6	ND	0.55	3.7	0.87±0.09

[1]Samples were sent to Atlantic Microlab, Inc. for their elemental composition analysis
ND: not determined

3.2 MATERIALS AND METHODS

3.2.1 Materials

CDSO3 was prepared in two batches ($CDSO3_{BH}$ and $CDSO3_{MT}$) in the Desai laboratory, as described in Chapter 1. $CDSO3_{BH}$ was supplied as a 5 mM solution in phosphate buffered saline (pH 7.4), while $CDSO3_{MT}$ was supplied as a lyophilized powder. Both batch were aliquoted and stored at -20 ^{o}C prior to use; careful precaution was taken to prevent the batches from being left at room temperature for > 2 h. Ferrous (Fe^{2+}) sulfate heptahydrate ($FeSO_4 \cdot 7H_2O$) was purchased from Sigma-Aldrich and stored at 4 ^{o}C, prior to use. Ferric (Fe^{3+}) chloride ($FeCl_3$; >98.0 % purity) was purchased from Spectrum Chemical Mfg. Corp (Gardena, CA) as an anhydrous sublimed powder and stored in a desiccator at room temperature prior to use. Ethylenediaminetetraacetic acid (EDTA; 99.0 % purity) was purchased from Sigma-Aldrich as a disodium salt, and stored at room temperature. Deferoxamine (DFO; ≥92.5 %purity) was a mesylate salt also obtained from Sigma-Aldrich and stored at -20 ^{o}C until use. Ferrozine (3-(2-pyridyl)-5,6-diphenyl-1,2,4-triazine-p,p'-sulfonic acid monosodium salt hydrate) was purchased from Sigma Aldrich, and sulfosalicylic acid (SAA; >99.6% purity) was purchased from Fisher Scientific; both were stored at 4 ^{o}C, prior to use.

3.2.2 Ferrous ion (Fe^{2+}) chelating activity assessment

The ferrous chelating activity of $CDSO3_{BH}$ and $CDSO3_{MT}$ were assessed using the *in vitro* chromogenic ferrozine chelation-based competitive inhibition assay, adapted and modified from Dinis *et al*. [1994]. A series of concentrations ranging from 0-1000 µM were tested in triplicates (n=3). In a 96-well plate, 15 µl of CDSO3 samples and 15 µl of 0.4 mM $FeSO_4$ were first added to 105 µl deionized, distilled water (DDW), and incubated in the dark at room temperature for 10 minutes. Subsequently, 15 µl of 2 mM ferrozine was added, so that competitive chelation was assessed in total 150 µl in each well. In order to accurately measure the absorbance generated only from ferrozine-Fe^{2+} chelation, in an additional reference well (n=1), 15 µl of ddH_2O was added in place of 2 mM ferrozine. The absorbance was measured at 562 nm using a multi-mode microplate reader (Synergy2, Biotek, Winooski, VT) and Gen5 Data Analysis Software (Biotek, Winooski, VT). The absorbance of the reference well was subtracted from that of the sample wells and then plotted as a function of concentration in a logarithmic scale. The half-maximal inhibitory concentration (IC_{50}) and Hill slope (HS) values were floated for determination from the plots by curve-fitting to the following equation (Equation 1) using a non-linear regression analysis software, Scientist (Micromath, St. Louis, MO):

$$Y = Ymin + \frac{(Y0 - Ymin)}{\left[1 + \left(\frac{C}{IC50}\right)^{HS}\right]}$$

Where Y = fraction of Fe^{2+} bound to ferrozine; Y_0 = fraction of Fe^{2+} bound to ferrozine in the absence of the test compound, fixed to 1; Y_{min} = lowest asymptotic fraction of Fe^{2+}

bound to ferrozine at the highest concentration, fixed to 0; and C = concentration [µM]. The "goodness-of-fit" of the curve-fitting was assessed using the Scientist-deriving statistical values for the coefficient of determination (COD) and model selection criterion (MSC); these were satisfactorily high at ≥0.98 and ≥3.0, respectively. The Fe^{2+} chelating activities of DFO and EDTA were similarly determined under the same experimental procedure and protocol.

3.2.3 Ferric ion (Fe^{3+}) chelating activity assessment

The ferric chelating activity of $CDSO3_{MT}$ was assessed using the *in vitro* chromogenic SSA chelation-based competitive inhibition assay, adapted and modified from Pozdnyakov *et al.* [2006]. A series of CDSO3 concentrations ranging from 0-50 µM were tested in triplicate (n=3). In a 96-well plate, 15 µl of CDSO3 samples and 15 µl of 2 mM $FeCl_3$ were first added to 105 µl deionized, distilled water (DDW), and incubated in the dark at room temperature for 10 minutes. Subsequently, 15 µl of 4 mM SAA was added, so that competitive chelation was assessed in total 150 µl in each well. In order to accurately measure the absorbance generated only from SAA-Fe^{3+} chelation, in an additional reference well (n=1), 15 µl of ddH_2O was added in place of 4 mM SAA. The absorbance was measured at 505 nm using Synergy2 (Biotek). The absorbance of the reference well was subtracted from that of the sample wells and then plotted as a function of concentration.

3.2.4 Data analysis

Each data point was expressed as mean ± standard deviation (SD), while the mean data were used for curve-fitting. The derived IC_{50} and HS values were statistically compared based on their 95 % confidence interval values (95% CI).

3.3 RESULTS

3.3.1 Fe^{2+} chelating activity of CDSO3 in two batches

Figure 3.2 shows the remaining Fe^{2+} fraction bound by ferrozine for (a) $CDSO3_{BH}$ and (b) $CDSO3_{MT}$ as a function of concentration. Table 3.2 shows the IC_{50} and HS values derived through curve-fitting along with the "goodness-of-fit" parameters. The IC_{50} values were 23.3±2.1 (95 % CI: 18.6, 28.0) and 17.0±1.4 (95% CI: 13.6, 20.5) μM, respectively, demonstrating that the Fe^{2+} chelating activity for the two batches of CDSO3 significantly different. However, the HS values were consistent,1.2±0.1 (95 % CI: 0.9, 1.4) and 1.4±0.2 (95 % CI: 1.0, 1.8), respectively.

(a)

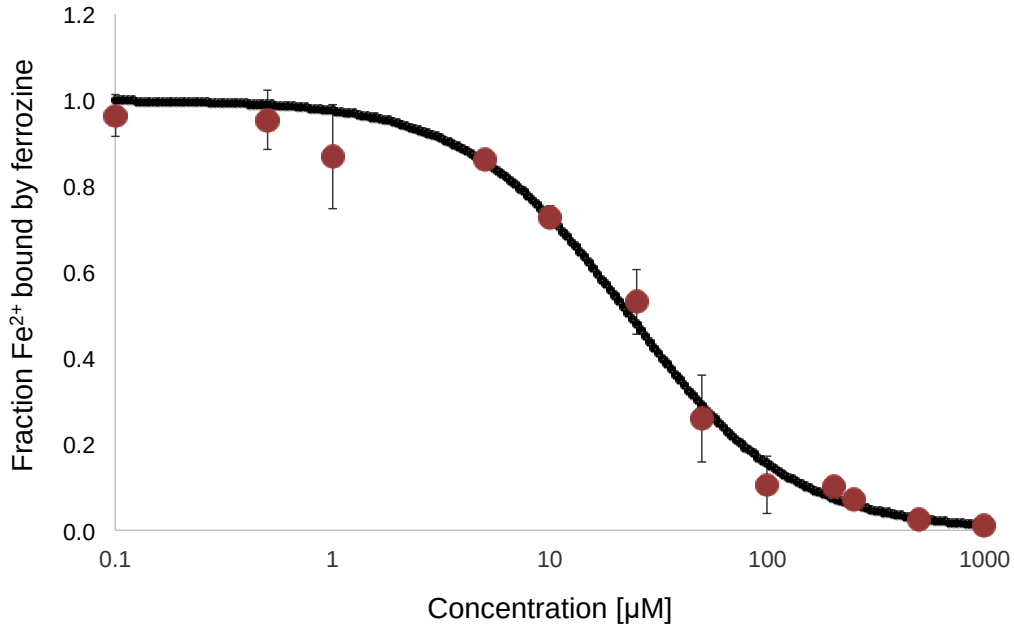

(b)

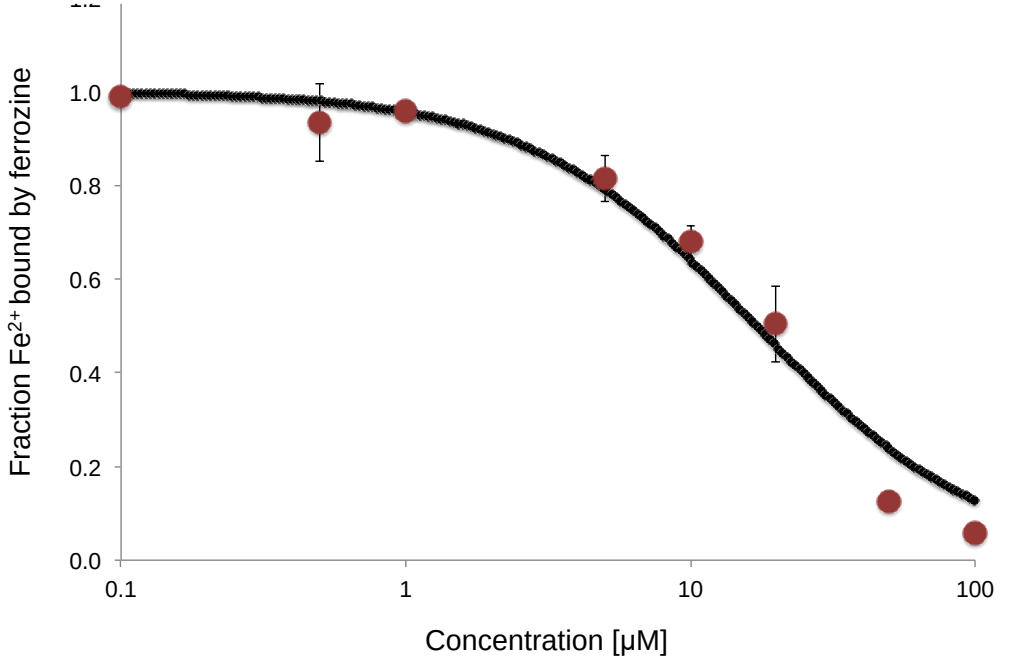

Figure 3.2: Remaining Fe^{2+} fraction bound by ferrozine for (a) $CDSO3_{BH}$ and (b) $CDSO3_{MT}$ as a function of concentration; Data are mean±SD from n=3. The solid lines are the results of curve-fitting.

Table 3.2: *In vitro* half-maximal inhibitory concentrations (IC_{50}) and Hill slope (HS) values for $CDSO3_{BH}$ and $CDSO3_{MT}$ in the ferrozine chelation inhibition assay, along with the COD and MSC values for curve-fitting

	$CDSO3_{BH}$	**$CDSO3_{MT}$**
IC_{50}[1]	23.3±2.1 (18.6, 28.0)	17.0±1.4 (13.6, 20.5)
HS[2]	1.2±0.1 (0.9, 1.4)	1.4±0.2 (1.0, 1.8)
COD[3]	0.99	0.99
MSC[4]	4.11	4.02

[1]Half-maximal inhibitory concentration (µM); derived mean ± SD (95% CI)
[2]Hill slope coefficient; derived value ± SD (95% CI)
[3]Coefficient of determination; ≥0.98 was considered satisfactory
[4]Model selection criterion; ≥3.0 was considered satisfactory

3.3.2 Fe^{2+} chelating activity of DFO and EDTA

Figure 3.3 shows the chelating activity profiles for known ion chelator molecules, (a) DFO and (b) EDTA. The IC_{50} values were derived to be 31.8±2.1 (95% CI: 27.1, 36.6) and 24.6±4.8 (95% CI: 13.6, 35.6) µM, respectively, which were slightly less potent than that of CDSO3's. The HS values for DFO and EDTA were 0.8±0.04 (95 % CI: 0.7, 0.9) and 1.0±0.2 (95 % CI: 0.6, 1.5), respectively. These data demonstrated that CDSO3 was as potent as DFO and EDTA in its Fe^{2+} chelating activity despite being a large 3.3 kDa non-peptidic macromolecule.

(a)

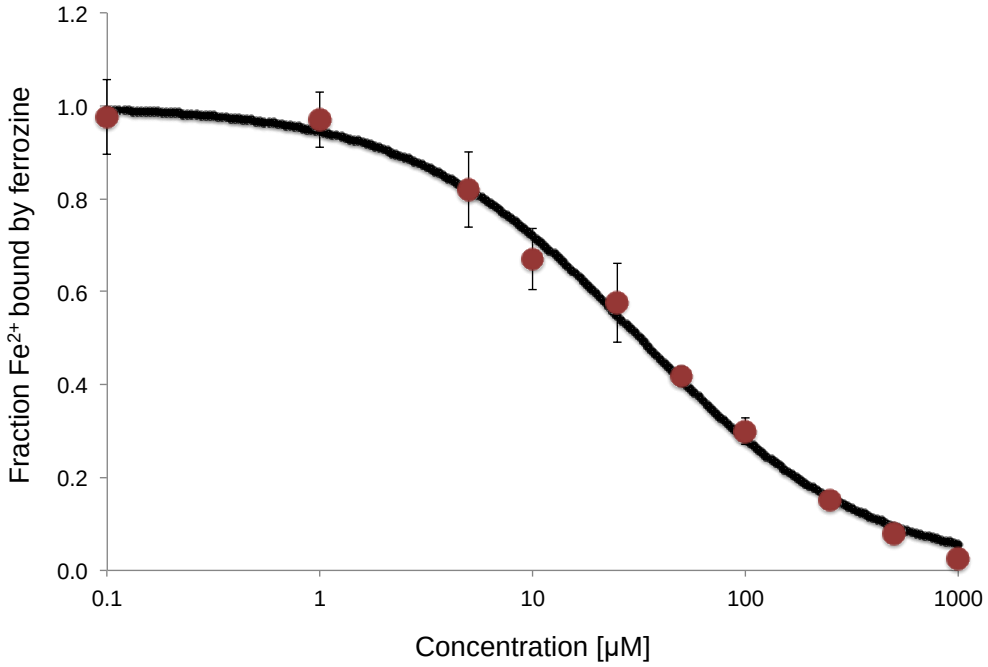

(b)

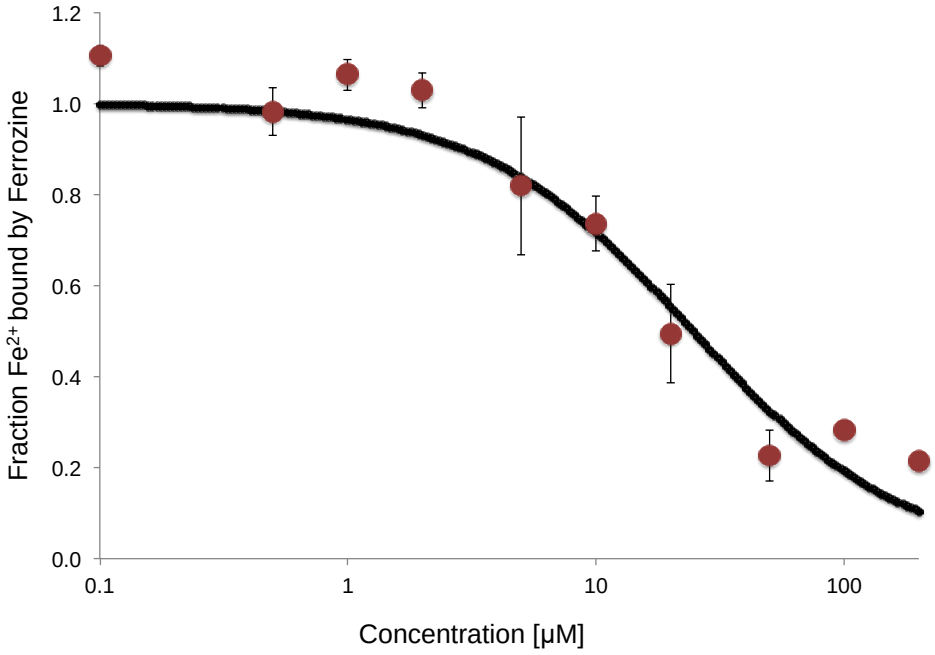

Figure 3.3: Remaining Fe^{2+} fraction bound by ferrozine for (a) DFO and (b) EDTA as a function of concentration; Data are mean ±SD from n=3. The solid lines are the result of curve-fitting.

Table 3.3: *In vitro* half-maximal inhibitory concentrations (IC_{50}) and Hill slope (HS) values for DFO and EDTA in the ferrozine chelation inhibition assay, along with the COD and MSC for curve-fitting

	DFO	EDTA
IC_{50}[1]	31.8±2.1 (27.1, 36.6)	24.6±4.8 (13.6, 35.6)
HS[2]	0.8±0.04 (0.7, 0.9)	1.0±0.2 (0.6, 1.5)
COD[3]	0.99	0.94
MSC[4]	4.92	2.48

[1]Half-maximal inhibitory concentration (μM); derived mean ± SD (95% CI)
[2]Hill slope coefficient; derived value ± SD (95% CI)
[3]Coefficient of determination; ≥0.98 was considered satisfactory
[4]Model selection criteria; ≥3.0 was considered satisfactory

3.3.3 Fe^{3+} chelating activity of CDSO3

In order to clarify ion selectivity of CDSO3's activity, such as cytoprotection studied in chapter 4, it was of interest to assess its Fe^{3+} chelation activity. Figure 3.4 shows the Fe^{3+} chelating activity for $CDSO3_{MT}$ up to 50 µM. CDSO3 appeared to be devoid of Fe^{3+} chelating activities. This in turn suggests that CDSO3's chelating activities are selective to divalent ions.

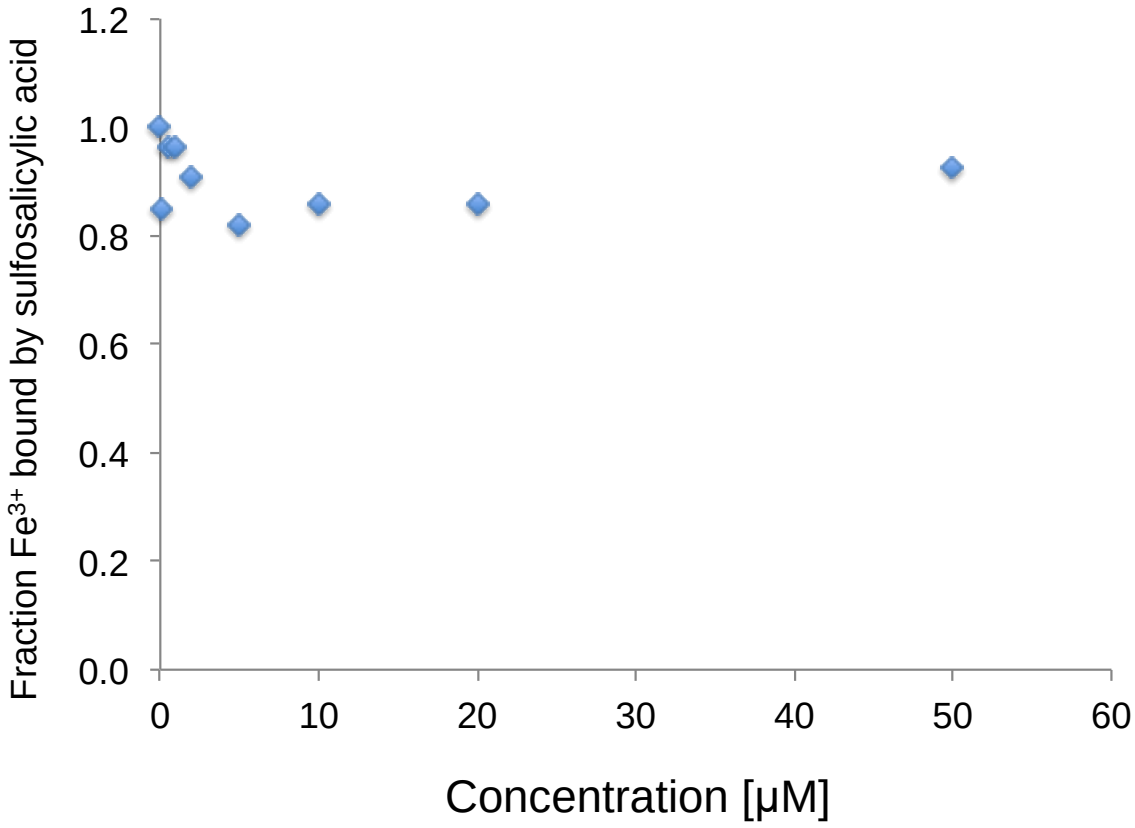

Figure 3.4: Remaining Fe^{3+} fraction bound by sulfosalicylic acid (SAA) as a function of $CDSO3_{MT}$ concentration

3.4 DISCUSSION

CDSO3 is a polymer consisting of 4-15 units of caffeic acid (CA) monomers with an average molecular weight of 3,320 Da. Its polydispersity and heterogeneous mixture of linkages, stereochemistry, and functional group substitutions result in a large number of possible sequences. Therefore, by nature of its complex structure, there is great difficulty in characterizing its structural and physiochemical properties, leading to the challenge of reproducibility and minimizing batch-to-batch differences. Measurements of the log D values and elemental analysis of two different batches of CDSO3 synthesized by two different chemists revealed that they had different physiochemical characteristic and elemental composition. The biggest difference between the batches was the sulfur content, with $CDSO3_{BH}$ having 5.3 % whereas $CDSO3_{MT}$ had 3.7 % sulfur. This difference was potentially due to a greater amount of time to undergo de-sulfation [Thompson, 2015]. It was hypothesized in Chapter 1 that CDSO3's pharmacologic inhibition of HIF-PHD by depleting the essential Fe^{2+} could be a means of stabilizing HIF-1α, and thereby overcoming the mechanistically critical 'HIF-1α/VEGF deficiency' in emphysema by increasing angiogenesis and preventing cell death. Therefore, the batch-to-batch differences in sulfur content could essentially affect CDSO3's ability to stabilize HIF-1α/VEGF and prevent cell death because sulfate groups significantly contribute to ferrous ion chelating capacity. In fact, their derived IC_{50} values were different: 23.3±2.1 (95 % CI: 18.6, 28.0) and 17.0±1.4 (95% CI: 13.6, 20.5) µM, respectively. These data suggest that 3.5 % difference in sulfur content between these batches do significantly affect the ferrous chelating activity. Meanwhile,

the ferrous ion (Fe^{2+}) chelation activity of CDSO3 was found to be comparable to and otherwise, slightly more potent than those of the known chelators, DFO and EDTA (IC_{50} values: 31.8±2.1 (95% CI: 27.1, 36.6) and 24.6±4.8 (95% CI: 13.6, 35.6) µM, respectively). Even so, the HS values for $CDSO3_{BH}$, $CDSO3_{MT}$, DFO, and EDTA are all approximately 1. CDSO3 appeared to be devoid of ferric ion (Fe^{3+}) chelation activity up to 50 µM. However, the development of a more sensitive assay is necessary to confirm these findings. This presumably suggests that CDSO3's chelating activities are selective for divalent ions.

3.5 CONCLUSIONS

The complex nature of CDSO3's chemical structure raises a concern about reproducibility and batch-to-batch variance, as potentially causing significant changes in its ferrous chelating activity. However, it was found that the variability in its elemental composition and physiochemical properties had only small effects on *in vitro* ferrous chelating activity. This assures that different batches of CDSO3 will produce relatively consistent results, and data from different batches can be treated collectively. Furthermore, the ferrous chelating activity of DFO and EDTA were also found to be similar to that of CDSO3, with DFO being the least potent. Although CDSO3 was shown to exhibit in vitro ferrous ion (Fe^{2+}) chelation activity with an IC_{50} of about 17-23 µM, it does not seem to have ferric ion (Fe^{3+}) chelation activity. These findings will enable further investigation into CDSO3's Fe^{2+} chelation-dependent mechanism of its cytoprotection in Chapter 4.

CHAPTER 4

FE^{2+}- AND HIF-1α-DEPENDENT ANTI-CELL DEATH ACTIVITY OF CDSO3

4.1 INTRODUCTION

A new pathobiologic concept of emphysema has been recently proposed, based on an imbalance of increased lung cell death and impaired cell proliferation, caused by "HIF-1α/VEGF deficiency". HIF-1α is a transcription factor which controls many downstream genes for various functions, including cell death and cell proliferation, yet its levels are primarily regulated by Fe^{2+}-dependent catalyzing enzymes (HIF-PHDs) for degradation. Therefore, reversal of the "HIF-1α/VEGF deficiency" via Fe^{2+} chelation has been proposed as a novel lung repairing strategy in emphysema. In Chapter 3, our non-peptidic, relatively lipophilic CDSO3 was shown to potently chelate Fe^{2+}, exerting 23 µM of IC_{50} value in the ferrozine assay. Hence, this chapter was designed to assess the Fe^{2+}- and HIF-1α-dependent cytoprotective activities of CDSO3 against various emphysematous insults via inflammation (CSE), oxidation (CSE and H_2O_2), elastolysis (HSE), and apoptosis (TSA and SU5416). In addition, the cytoprotective activities of two known iron chelators, DFO and EDTA, will also be assessed to clarify whether Fe^{2+} chelating activity was sufficient to exhibit cytoprotective activity.

4.2 MATERIALS AND METHODS

4.2.1 Materials

CDSO3 and CD were prepared as sulfated and sulfated CA dehydropolymers, respectively, in the Desai laboratory, as described in Chapter 1. They were supplied as either a solution ($CDSO3_{BH}$) or lyophilized powder ($CDSO3_{MT}$) and stored at -20 ^{o}C prior to use. The monomer CA was purchased from Sigma-Aldrich (St. Louis, MO). Research-grade cigarettes, 3R4F, were obtained from the Kentucky Tobacco Research and Development Center (University of Kentucky, Lexington, KY). Prior to each experiment, cigarette smoke extract (CSE) was freshly prepared by bubbling one research cigarette into 3 ml of the incubation media under ice using a smoking apparatus provided from Dr. Chu of the Hunger Holmes McGuire Richmond, VA Medical Center (Figure 4.1); this was considered to be 100 % CSE. Hydrogen peroxide (H_2O_2, ACS reagent, 30% (w/v)) solution was purchased from ACROS Organics (New Jersey, NJ). Its stock solution was prepared at 8.82 M (300mg/ml) in phosphate buffered saline (PBS; pH 7.4, Quality Biological) and stored at 4 ^{o}C prior to use. Human sputum elastase (HSE) certified as 875 U/mg protein (100 % protein and >95.0 % purity) was purchased from Elastin Products Company, Inc. (Owensville, MO) as a lyophilized powder. Its stock solution was prepared at 8,750 U/ml (10 mg/ml) in 50 % glycerol (Fisher Scientific) and 50 % 0.02 M sodium acetate (NaOAc; pH 5; Sigma Aldrich), stored in 50 µl aliquots at -20 ^{o}C, as recommended by the manufacturer for maximal stability. Trichostatin A (TSA; >98.0% purity) was purchased from Sigma-

Aldrich (St. Louis, MO) as a powder, and its stock solution was prepared at 6.61 mM (2 mg/ml) in ethanol (Fisher Scientific) and stored in 20 µl aliquots at -20 ^{o}C. SU5416 was a gift from Dr. Voelkel (VCU Pulmonary Medicine) and stored at -20^{o}C prior to use. The stock solution was prepared at 126 mM (30mg/ml) by dissolving SU5416 in dimethylformamide (DMF; Acros Organics) purged with nitrogen bubbled over 1 minute. Ferrous (Fe^{2+}) sulfate heptahydrate ($FeSO_4 \cdot 7H_2O$) and ferrous (Fe^{2+}) chloride ($FeCl_2$; >98.0 % purity) were purchased from Sigma-Aldrich and respectively stored at 4 and -20 ^{o}C, prior to use. Ferric (Fe^{3+}) chloride ($FeCl_3$; >98.0 % purity) was purchased from Spectrum Chemical Mfg. Corp (Gardena, CA) as an anhydrous sublimed powder and stored in a desiccator at room temperature prior to use. Ethylenediaminetetraacetic acid (EDTA; 99.0 % purity) was purchased from Sigma-Aldrich as a disodium salt, and stored at room temperature. Deferoxamine (DFO; ≥92.5 %purity) was a mesylate salt also obtained from Sigma-Aldrich and stored at -20 ^{o}C until use. Echinomycin (Ech) and CAY10585 (CAY) were purchased from Cayman Chemical (Ann Arbor, MI) as crystalline solids; and their stock solutions were respectively prepared at 23 mM (10 mg/ml) and 1.8 mM (2 mg/ml) in dimethyl sulfoxide (DMSO; Fisher Scientific) purged with nitrogen; they were stored in 50 µl aliquots at -20^{o}C.

Figure 4.1: Smoking apparatus used to prepare cigarette smoke extract (CSE)

4.2.2 Cell culture

Rat alveolar macrophage NR8383 cells and human adenocarcinomic alveolar epithelial A549 cells were obtained from the American Type Culture Collection (ATCC; Manassas, VA) and maintained as frozen cell banks at the Sakagami laboratory. NR8383 cells were seeded at concentrations of 0.1-0.4 x 10^6 cells/mL and A549 cells were seeded at concentrations of 0.002-0.01 x 10^6 cells/cm^2, and propagated through culture in 10 or 15 ml of the culture media in 25 or 75 cm^2 culture flasks (Corning Costar; Cambridge, MA), according to the protocol published by ATCC [Product Information Sheet: NR8383 (CRL-2192), ATCC; Product Information Sheet: A549 (CCL-185), ATCC]. The media were the F-12K Medium (Kaighn's Modification of Ham's F-12 Medium; ATCC) supplemented with 15% or 10% (v/v) fetal bovine serum (Invitrogen, Carlsbad, CA), respectively, and 1% (v/v) penicillin-streptomycin (Sigma-Aldrich). The passages 8-30 were used in experiments. In contrast, human lung microvascular endothelial (HMVEC-L) cells were purchased at passage 5 from Lonza (Walkersville, MD) and propagated in culture flasks according to the protocols published by Lonza [Product Information Sheet: Clonetics Endothelial Cell System, Lonza]. The cells were seeded at a density of 5,000 cells/cm^2 and cultured in 10 or 15 ml of the Endothelial Growth Medium (EGM-2MV; Lonza). The passages 5-10 were used in experiments. The NR8383, A549, and HMVEC-L cells were all maintained under the humidified 95% (v/v) air and 5% (v/v) CO_2 at 37 ^oC in the incubator (Model 5410, NAPCO, Milliville, NJ) connected to a CO_2 cylinder (National Welders, Richmond, VA). The culture media were changed two to three times weekly, during which cell growth was monitored under

the Nikon-TMS phase contrast microscope (Image Systems, Columbia, MD). Typically, the NR8383 and A549 cells reached confluence by 5-7 days and the HMVEC-L cells reached confluence by 5-9 days. Upon confluence, the cells were passaged into well plates for experiments and/or new flasks for further propagation; otherwise they were frozen for cell bank storage following scraping (NR8383) or trypsin-EDTA treatment (A549 and HMVEC-L) with 95 % complete growth medium and 5 % DMSO (NR8383 and A549) or 80 % EGM, 10 % DMSO, and 10 % FBS (HMVEC-L) in liquid nitrogen.

4.2.3 *In vitro* pro-inflammatory TNF-α release

The NR8383 cells were plated at 0.05 x 10^6 cells/well in 0.2 ml F-12K media supplemented with 1% FBS in 48-well plates. The cells were incubated with 0-25 µM CDSO3 in the absence or presence of 1 % CSE. After 18 h incubation, the supernatants were obtained via centrifugation at 11,752 x g (12,000 rpm; Eppendorf 5415 C; Westbury, NY) for 2 min. The supernatants were then analyzed to determine TNF-α released from the cells using the enzyme-linked immunosorbent assay (ELISA) kit (eBioscience), according to the manufacturer's protocol [Product Information Sheet: Mouse TNF alpha ELISA Ready-SET-Go!; eBioscience].

4.2.4 *In vitro* trypan blue exclusion assay

In vitro protective activities were determined using the trypan blue exclusion (TBE) and lactate dehydrogenase (LDH) assays upon incubation with or without test

molecules (i.e. CDSO3, CD, CA, DFO, and EDTA) and/or CAY, Ech, Fe^{2+} ($FeSO_4$ and $FeCl_2$) and Fe^{3+} ($FeCl_3$). On day 1, the cells were seeded in a 200-µl system at a density of 0.05-0.15 x 10^6 cells/well of 48-well plates in FBS-depleted culture media (1% FBS). Cell death was induced with 3-50 % CSE, 0.1 mM H_2O_2, 1 U/ml HSE, 1-2 µM TSA, or 1-50 µM SU5416. CDSO3, CD, CA, DFO, and EDTA were tested at 0-25 µM. In some experiments, addition of HIF-1α inhibitors (Ech, 10 µM; or CAY,10 µM) or excess Fe^{2+} or Fe^{3+} at 50 µM were further added to explore and clarify CDSO3's Fe^{2+}- and HIF-1α-dependent mechanism for cytoprotective (i.e. anti-cell death) activities. Following 18-24 h incubation at 37 ^{o}C, cell death was assessed using the TBE and LDH assays, as described in Appendix 1. Briefly, while the incubation media were taken for the LDH release assay, the cells were harvested using trypsin-EDTA (A549 and HMVEC-L) or scraping (NR8383) for the TBE assay. The cells were centrifuged at 11,752 x g (12,000 rpm; Eppendorf 5415 C; Westbury, NY) for 3-4 minutes, and the cell pellets were re-suspended with 100 µl fresh incubation media. Trypan blue solution, 4% (Amresco; Solon, OH) was added to the re-suspended cells and left at room temperature for 4-5 minutes. The cell suspension was centrifuged again at 11,752 x g (12,000 rpm) for 3-4 min, and the cell pellets were re-suspended with 200 µl of fresh media and plated into new 48-well plates, and allowed to settle at room temperature for at least 2 h. Using a microscope (Omax, Kent, WA) connected to ToupViewX (Omax, Kent, WA), at least 8-10 pictures were randomly captured to assure ≥300 cells to be counted. For some preliminary experiments, only 100-200 cells were counted. Figure 4.2 shows a representative microscopic field image of the A549 cells following trypan blue staining.

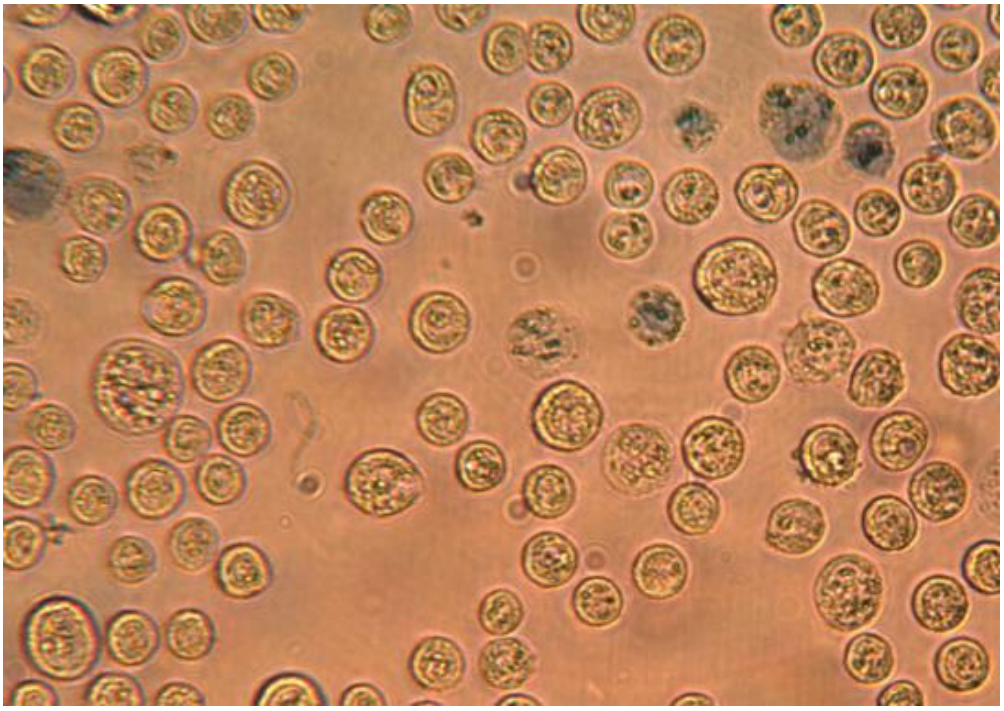

Figure 4.2: Representative microscopic field image of the A549 cells stained with trypan blue. Dead cells are stained blue, while live cells remain clear.

Following identification of over 300 cells, % dead cells was calculated from the following equation:

$$\%\ dead\ cells = \left(\frac{number\ of\ blue\ cells}{total\ number\ of\ cells}\right) \times 100$$

4.2.5 *In vitro* LDH release assay

The cells were seeded and treated, as discussed in 4.2.4. After 18-24 h incubation, the cell supernatants and cell lysates were taken for the LDH assay and

centrifuged at 11,752 x g (12,000 rpm; Eppendorf 5415 C; Westbury, NY) for 3-4 minutes. The supernatants and cell lysates were analyzed by the LDH release assay according to the manufacturer's protocol [Product Information Sheet TOX7: In vitro Toxicology Assay Kit, Lactic Dehydrogenase based Sigma-Aldrich]. The metabolic and chemical basis of the LDH assay is illustrated in Figure 4.3. In principle, damaged cells release LDH, an enzyme that reduces nicotinamide adenine dinucleotide (NAD) to NAD + hydrogen (NADH). The resulting NADH is utilized in the stoichiometric conversion of a tetrazolium dye, which can be measured spectrophotometrically at 490 nm using a multi-mode microplate reader (Synergy2, Biotek). The % LDH mass released is calculated as:

$$\%\ LDH\ mass = \left(\frac{LDH\ released\ from\ incubation\ media}{LDH\ released\ from\ incubation\ media + LDH\ from\ cell\ lysate}\right) \times 100$$

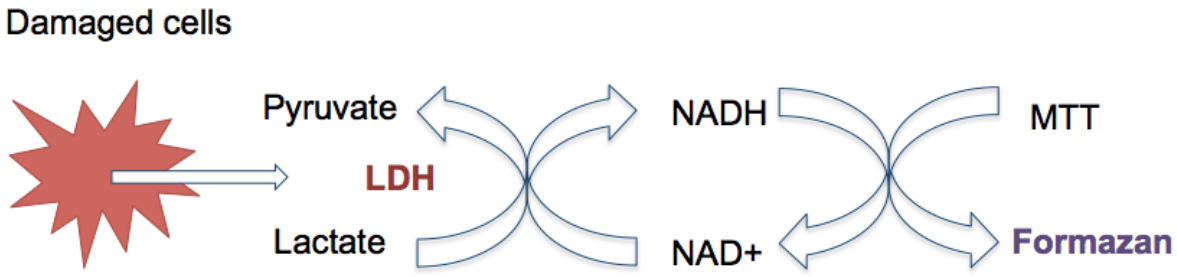

Figure 4.3: Metabolic and chemical basis of the LDH cytotoxicity assay.

4.2.6 Data Analysis

The data for each treatment groups were expressed as mean ± SD from more than triplicate experiments ($n \geq 3$). Analysis of variance (ANOVA) was used to test statistical differences for group values. In the event of significant difference in the ANOVA, the Tukey-Kramer multiple comparison test was carried out to identify group-by-group statistical differences or the Dunnett's test was carried out to identify statistical differences, compared to the negative control. In ANOVA, Tukey-Kramer multiple comparison test, and Dunnett's test, $p<0.05$ was considered to be statistically significant. JMP Pro 12 Software (SAS, Cary, NC) was used for these statistical analyses.

4.3 RESULTS

4.3.1 *In vitro* protective effects of CDSO3 against CSE-induced pro-inflammatory TNF-α release

Cigarette smoke contains thousands of chemical components, including ~ 10^{15} reactive species in the gas phase alone, particularly high levels of nitric oxide, while the tar phase has an equally abundant number of reactive oxygen and nitrogen species (ROS, RNS), including phenols and quinone [Yoshida *et al.,* 2007]. Failure of survival to cigarette smoke insults for alveolar macrophage is one of the early events in the pathobiologic cascade toward development of emphysema [Roth, 2008; Demedts *et al.,*

2006]. It is believed that exposure to irritants such as cigarette smoke first activates alveolar macrophages to recruit neutrophils into the airways and cause epithelial inflammation via release of chemotactic factors like interleukins and chemokines [Barnes, 2004]. Indeed, it was recently reported that the pro-inflammatory mediator, TNF-α, was primarily released from alveolar macrophages, and this is integral to cause inflammatory cell infiltration in cigarette smoke-induced emphysema [Churg *et al.,* 2004]. In this context, CDSO3 was tested for its protective activity against CSE-induced pro-inflammatory tumor necrosis factor α (TNF-α) release in rat alveolar NR8383 macrophages. Figure 4.4 shows the TNF-α release into the incubation media supernatants of the NR8383 macrophages after exposure to 1 % CSE in the absence or presence of CDSO3 at 1-25 µM. CSE caused a significant 19.8-fold increase in TNF-α release, compared to the vehicle control (40.3 $\rightarrow$ 797.3 pg/ml; $p<0.05$). CDSO3 was shown to inhibit this CSE-induced TNF-α release in a concentration-dependent manner at 1-25 µM, reaching significance at 5 µM. CDSO3 at 5, 10, and 25 µM caused significant 49.3, 79.4, and 94.3 % inhibition, respectively ($p<0.05$). Based on these results, it appears that CDSO3 is protective against CSE-induced pro-inflammatory TNF-α release by alveolar macrophages.

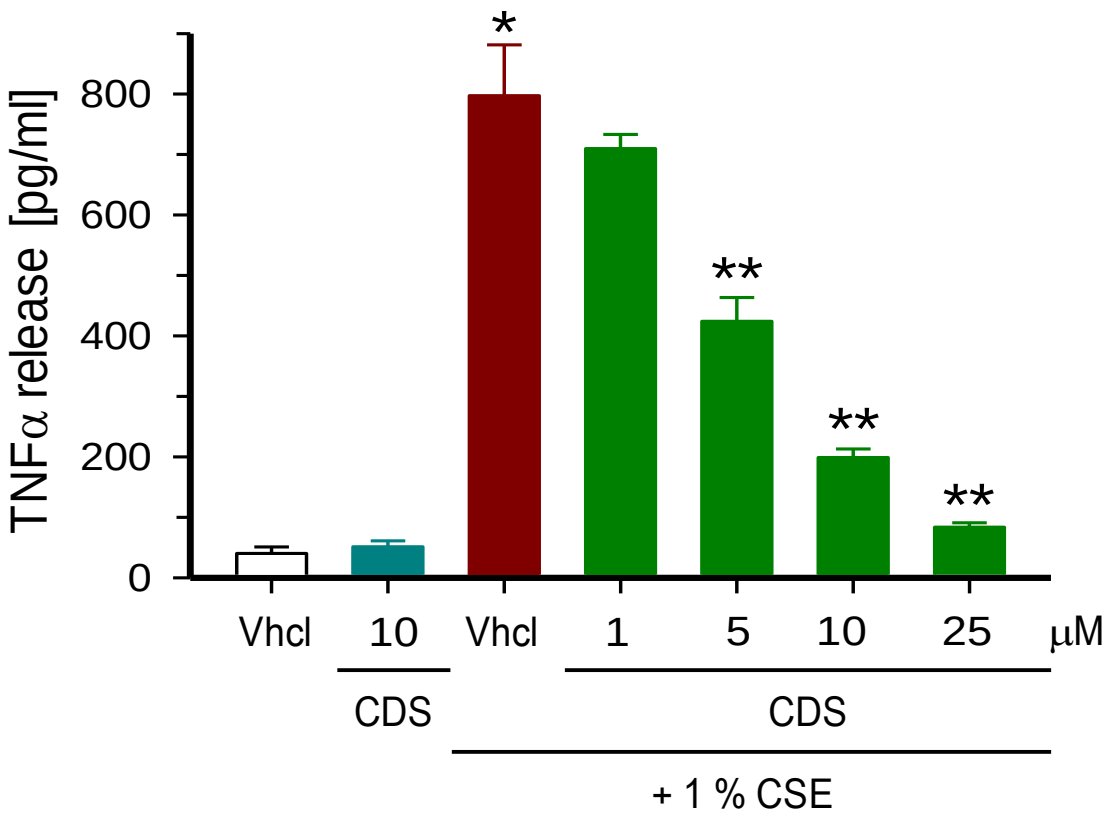

Figure 4.4: TNF-α release recovered from the incubation media supernatants of the rat alveolar NR8383 macrophages after exposure to vehicle (Vhcl) or 1 % CSE in the absence or presence of 1-25 μM CDSO3. Data represents mean±SD from n=4; *p<0.05, compared to the vehicle (negative) control; **p<0.05, compared to the CSE-stimulated (positive control), by ANOVA and Tukey's multiple comparison test.

4.3.2 *In vitro* protective activities of CDSO3 against cell death induced with cigarette smoke extract (CSE) in the alveolar macrophage NR8383 cells

Once the alveolar macrophages are activated upon exposure to cigarette smoke, they recruit neutrophils into the airways and cause oxidative stress and inflammation. This induced oxidative stress and excessive production of elastolytic enzymes then progressively cause the alveolar wall destruction and airspace enlargement in emphysema [Barnes, 2004]. Thus, studies for CDSO3's cytoprotective activities were also conducted in rat alveolar macrophage NR8383 cells upon cell death induced with CSE. Figure 4.5 shows the effects of CSE concentration on NR8383 cell death, as determined by the (a) TBE and (b) LDH assays. When the TBE assay was used, CSE at 3-50 % was shown to significantly cause cell death in a concentration-dependent manner, resulting in 4.3- and 8.7- fold greater % dead cells at 10 and 50 %, respectively, compared to the vehicle control ($p<0.05$; Figure 4.5.a). Since the TBE assay could not avoid subjectivity in measurements, these TBE assay-based results were compared with those determined by a more objective, colorimetric method of LDH release assay, as shown in Figure 4.5.b. Measured with increased absorbance at 490 nm, CSE caused NR8383 cell death, again in a concentration-dependent manner, and became significant upon 10 and 50 % CSE exposure ($p<0.05$), but not at 1 %. Based on these results, 10 % CSE was chosen to assess CDSO3's cytoprotective activities in subsequent studies.

Figure 4.6 shows the cytoprotective activities of CDSO3 at 1-25 μM against 10 % CSE-induced NR8383 cell death, alongside those of the unsulfated oligomer CD and

the monomer CA at 10 or 25 µM, as determined by the (a) TBE and (b) LDH release assays. Using the TBE assay in Figure 4.6.a, CDSO3 at 1-25 µM was shown to significantly inhibit CSE-induced NR8383 cell death in a concentration-related fashion. In fact, 12.7 and 13.5 % dead cells seen for CDSO3 at 10 and 25 µM, respectively, were almost comparable with 8.3 % dead cells in the vehicle control, implying that CDSO3's protective activities against this CSE-induced cell death were almost complete at these concentrations. In contrast, CD (the unsulfated oligomer) produced only 46.5 % protection at 25 µM, which was less potent than CDSO3 (83.9 % protection at 25 µM); this % protection for CD was comparable to that for CDSO3 at 5 µM (Figure 4.6.a). In Figure 4.6.b, the cytoprotective activities measured by the LDH release assay are shown for CDSO3 (1-25 µM), CD (10 µM) and the monomer CA (10 µM). Although statistical significance could not be established due to high variability values, a similar trend was seen that CDSO3 inhibited CSE-induced LDH release, i.e., cell death, in a concentration-related fashion. Moreover, neither CD nor CA was cytoprotective at 10 µM. It appeared, based on these results, that CDSO3 was potently protective against CSE-induced cell death and that the TBE assay enabled more sensitive and reproductive assessments of cell death and cytoprotective activities, compared to the LDH release assay.

(a)

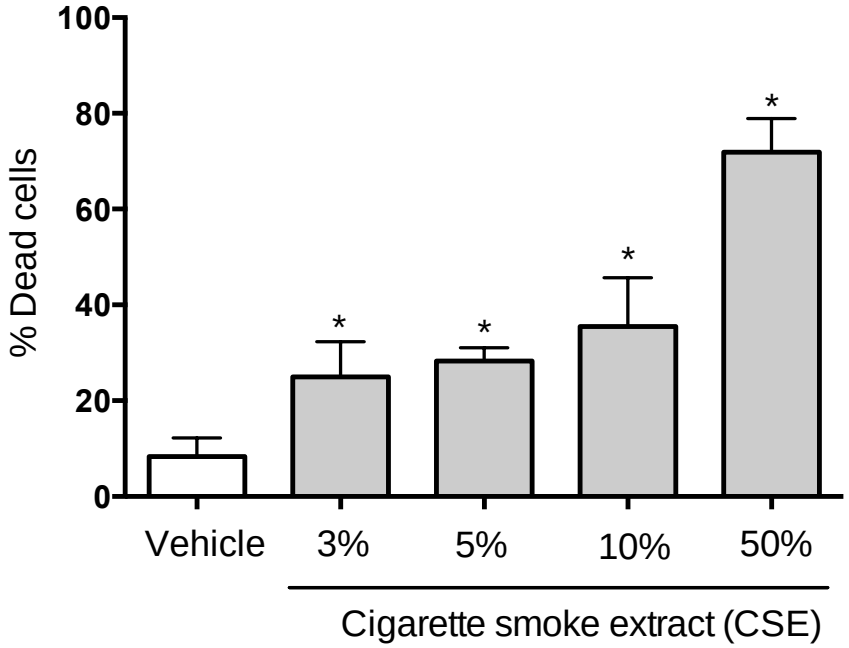

(b)

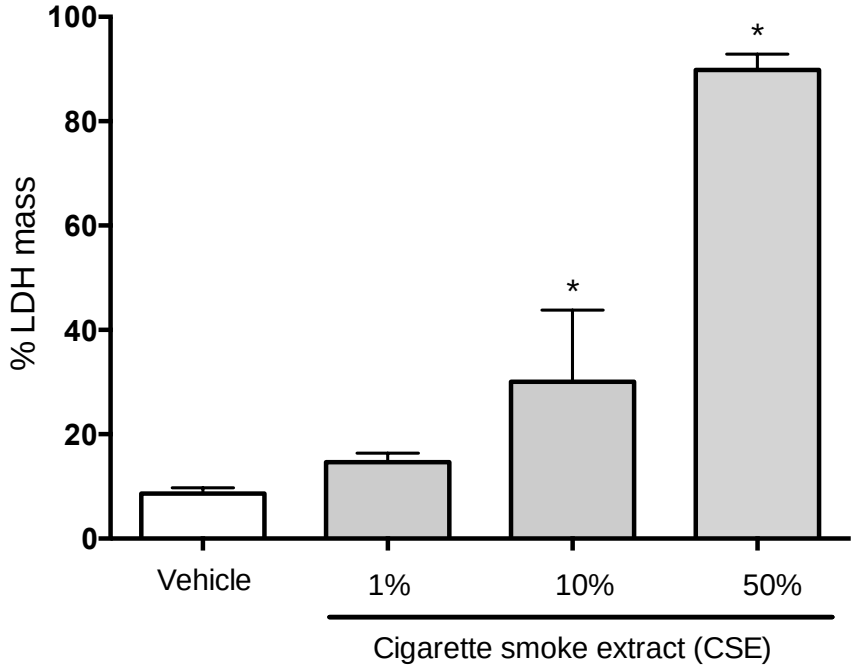

Figure 4.5: Concentration-dependent CSE-induced cell death in NR8383 cells, as determined by the (a) TBE and (b) LDH assay. Data represent mean±SD from n≥3; *p<0.05, compared to vehicle control by, ANOVA and Dunnett's test

(a)

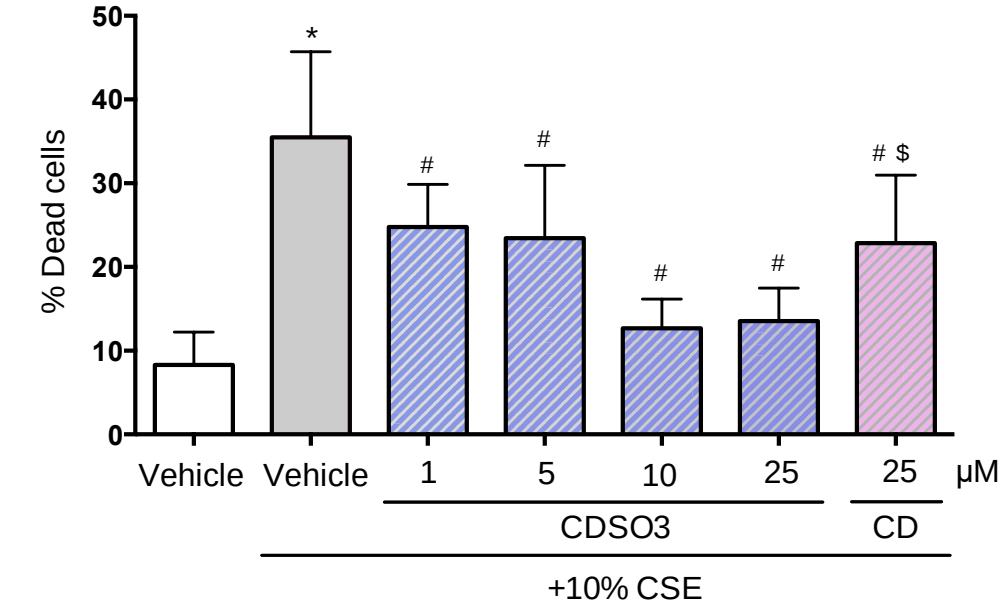

(b)

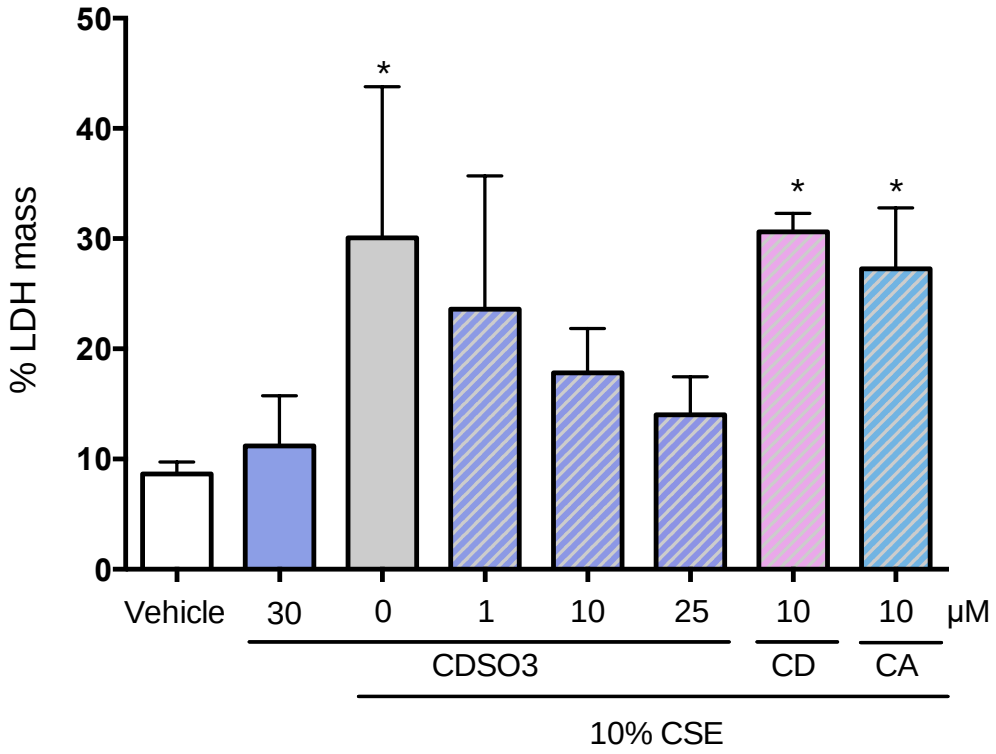

Figure 4.6*: In vitro* cytoprotective effects of CDSO3, CD, and CA in CSE-induced cell death in NR8383 cells, as determined by the (a) TBE and (b) LDH assays. Data represent mean±SD from n≥3; *p<0.05, compared to vehicle control; #p<0.05, compared to the CSE-induced control; $^{\$}$p<0.05, compared to the CSE-induced and 25 μM CDSO3-treated group , by ANOVA and Tukey's multiple comparison test.

4.3.3 *In vitro* protective activities of CDSO3 against CSE-induced cell death in the alveolar epithelial A549 cells and pulmonary vascular endothelial HMVEC-L cells

Numerous studies have identified increased endothelial cell apoptosis in human COPD/emphysema [Fallica *et al.,* 2014], and targeted induction of endothelial cell death has been shown to promote apoptosis of both endothelial cells and type II alveolar epithelial cells within the alveolar-capillary unit, resulting in emphysematous tissue remodeling [Giordano *et al.,* 2008]. Therefore, the protective activities of CDSO3 against 10 % CSE-induced cell death were further assessed in the (a) human alveolar epithelial A549 and (b) human pulmonary vascular endothelial HMVEC-L cells, determined by the TBE assay, as shown in Figure 4.7. In both cell types, CDSO3 at 10 µM alone did not cause cell death, while 10 % CSE increased % dead cells by 3.3- and 1.5-fold, respectively. However, CDSO3 at 10 µM caused significant 99.4 and 153.6 % protection against this induced cell death ($p<0.05$), respectively. These results demonstrate that CDSO3 is also potently protective against lung epithelial and endothelial cell death induced with CSE.

(a)

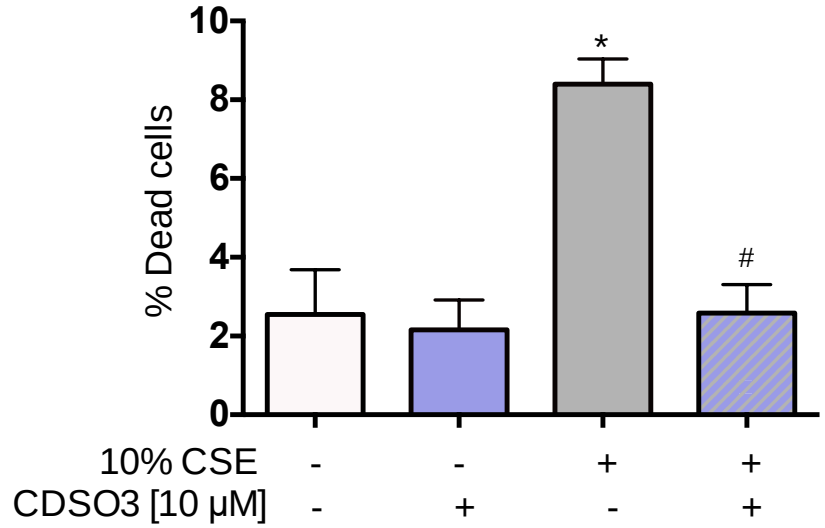

(b)

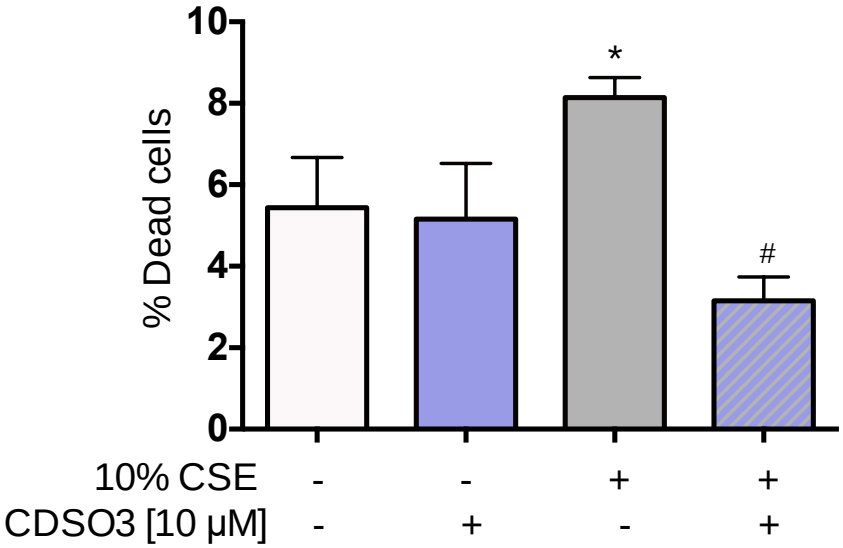

Figure 4.7: *In vitro* cytoprotective effects of CDSO3 against CSE-induced cell death in **(a)** A549 and **(b)** HMVEC-L cells, as determined by the TBE assay. + = present; - = absent. Data represent mean±SD from n≥3; *$p<0.05$, compared to the vehicle control; $^{\#}p<0.05$, compared to the CSE-induced control, by ANOVA and Tukey's multiple comparison test

4.3.4 *In vitro* protective activities of CDSO3 against oxidative and elastolytic cell death in the alveolar epithelial A549 cells

Because the alveolar wall septal destruction and loss in emphysema have been long known to be associated with induced oxidative stress and elastolytic activities in lungs, in addition to direct cigarette smoke insults [Yoshida, 2007], the cytoprotective activities of CDSO3 were then assessed in the A549 cells against (a) H_2O_2 and (b) HSE-induced cell death, respectively, determined by the TBE assay, as shown in Figure 4.8. H_2O_2 at 0.1 mM and HSE at 1 U/ml were found to induce A549 cell death significantly ($p<0.05$) by ~3.5 and ~4.5-fold, respectively. However, CDSO3 at 1 and 10 µM inhibited these induced cell death in a concentrated-related fashion. The results at 10 µM were remarkable, as producing complete 102.9 and 91.7 % protection, respectively.

(a)

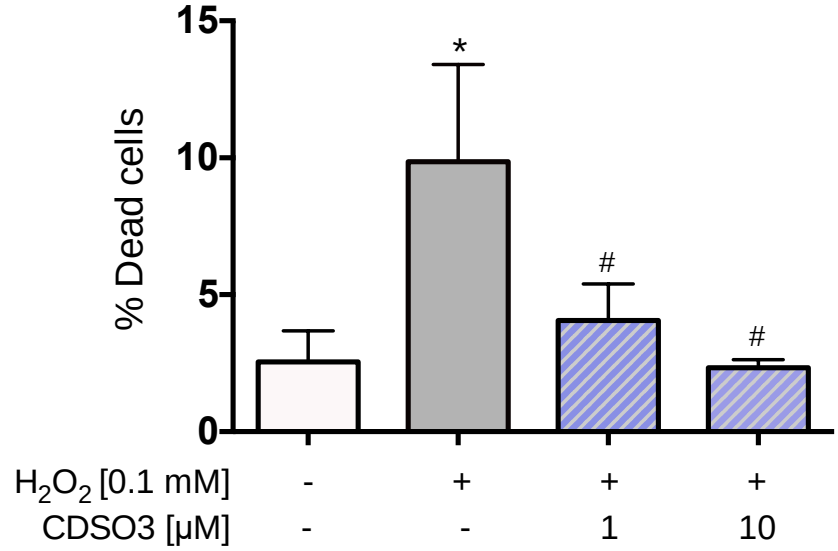

(b)

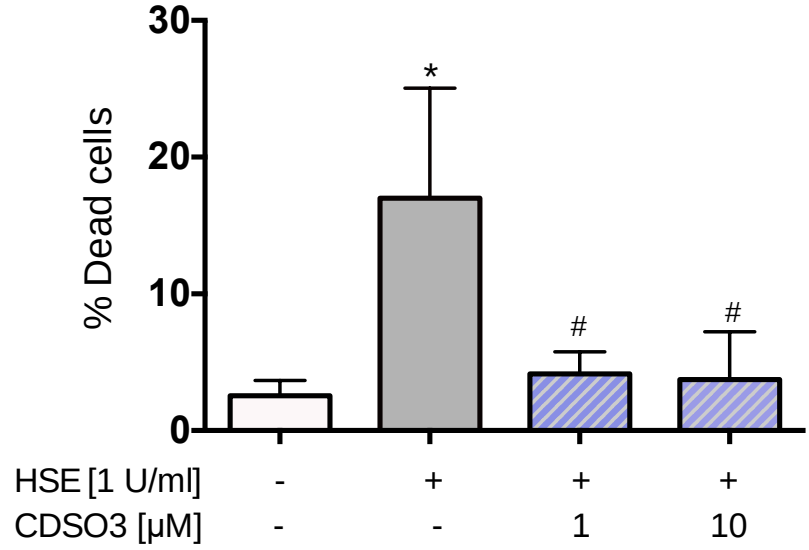

Figure 4.8: *In vitro* cytoprotective effects of CDSO3 at 1 or 10 μM against **(a)** 0.1 mM H_2O_2-induced and **(b)** 1 U/ml HSE-induced A549 cell death, as determined by the TBE assay. + = present; - = absent. Data represent mean±SD from n≥3; *p<0.05, compared to the vehicle control; #p<0.05, compared to the induced control, by ANOVA and Tukey's multiple comparison test

4.3.5 *In vitro* protective activities of CDSO3 against apoptotic lung cell death

In addition to oxidative stress and elastolysis, epigenetic modifications have been recently investigated in emphysematous lungs, thereby identifying reduced HDAC2 activity, and induced alveolar epithelial and endothelial cell death via necrosis, apoptosis, and autophagy, alongside cellular matrix instability and breakdown [Mizuno *et al*., 2011]. Therefore, the *in vitro* protective effects of CDSO3 against cell death induced with an HDAC inhibitor, TSA, in the (a) A549 and (b) HMVEC-L cells, were also tested, as determined by the TBE assay (Figure 4.9). TSA at 2 μM significantly increased % dead cells in the A549 and HMVEC-L cells by about 3.5- and 4.6- fold, respectively. However, CDSO3 at 10 μM again significantly inhibited such TSA-induced cell death by 68.6 and 63.6 % ($p<0.05$), respectively, suggesting that CDSO3 was also capable of potent cytoprotection against apoptotic cell death induced with the epigenetic HDAC inhibitor, TSA.

(a)

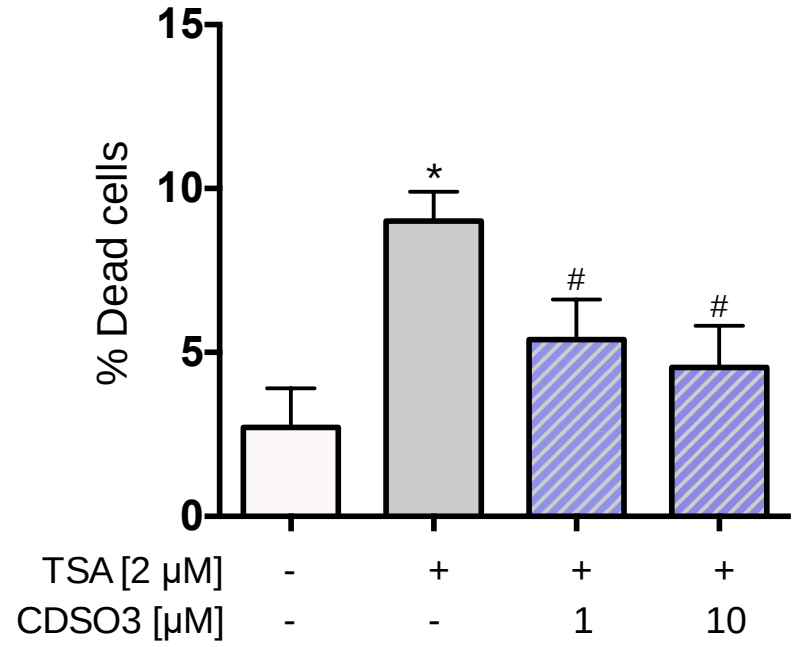

(b)

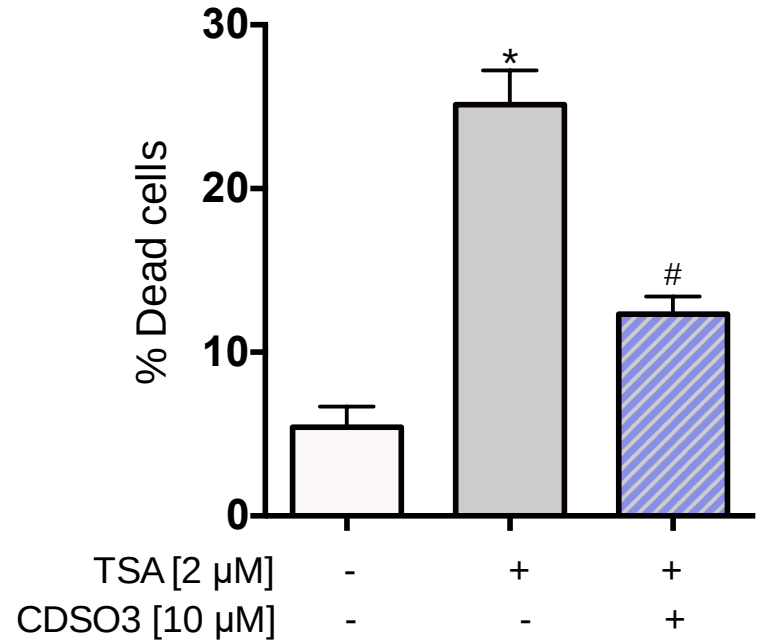

Figure 4.9: *In vitro* cytoprotective effects of CDSO3 at 1 or 10 µM against 2 µM TSA-induced cell death in **(a)** A549 and **(b)** HMVEC-L cells, as determined by the TBE assay. + = present; - = absent. Data represent mean±SD from n≥3; *p<0.05, compared

to the vehicle control; #p<0.05, compared to the TSA-induced control, by ANOVA and Tukey's multiple comparison test

Epigenetic modifications of HDAC inhibition are suggested to lead to apoptotic cell death in emphysematous lungs, at least in part, via impaired VEGF and its receptor signaling [Mizuno *et al.,* 2011; Kasahara *et al.,* 2000]. In fact, as shown in Figure 4.10, a VEGF receptor antagonist, SU5416, caused A549 cell death in a concentration-dependent manner, reaching significance in its cell death induction at ≥ 10 μM ($p<0.05$). Hence, the in vitro protective activities of CDSO3 at 10 μM were examined in the HMVEC-L cells against cell death induced with SU5146 at 10 or 25 μM, determined by the TBE assay, as shown in Figure 4.11. SU5416 increased % dead cells by ~3.5 and ~5.0-fold at 10 and 25 μM, respectively. Against these induced cell death, CDSO3 at 10 μM was able to produce significant inhibition by 86.1 and 50.7 %, respectively ($p<0.05$). It became clear therefore that CDSO3 potently inhibited lung cell death induced by VEGF receptor blockade.

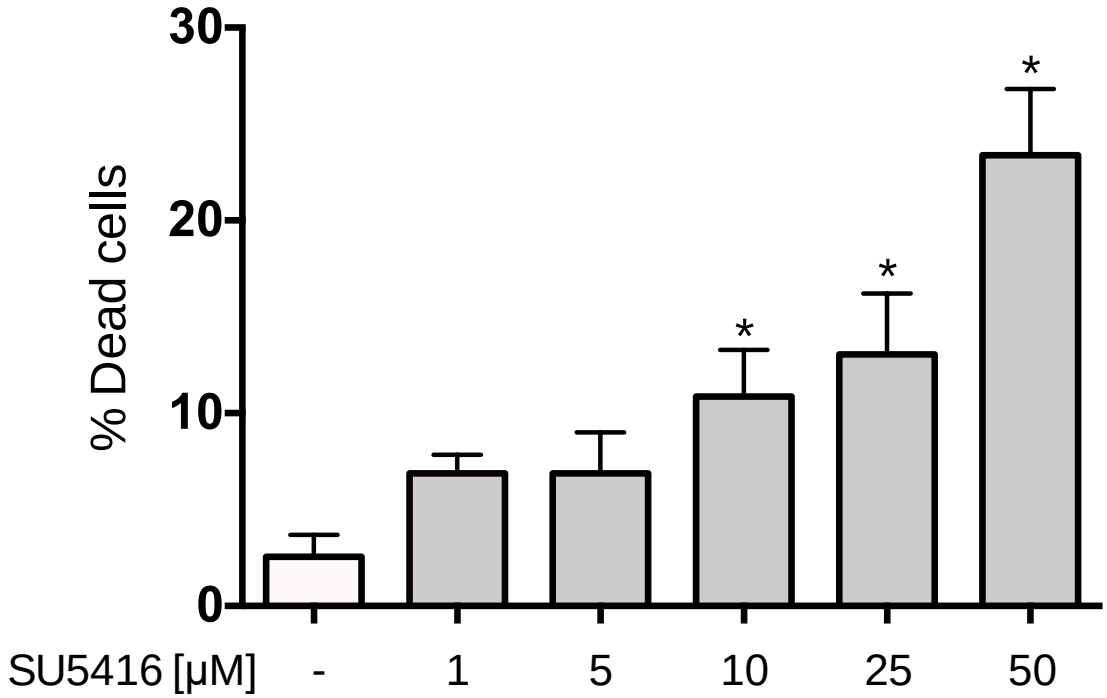

Figure 4.10: Effects of SU5416 concentration on A5419 cell death induction, as determined by the TBE assay. Data represent mean±SD from n≥3; *p<0.05, compared to the vehicle control, by ANOVA and Dunnett's test.

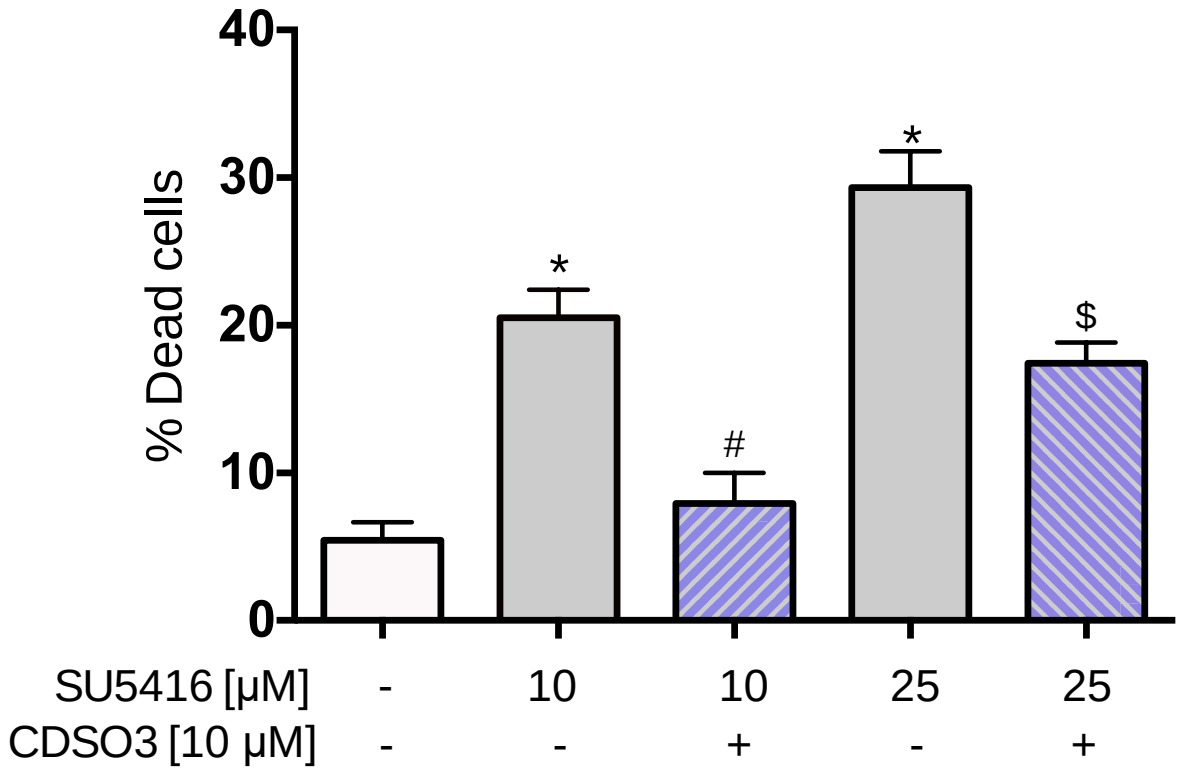

Figure 4.11: *In vitro* protective activities of 10 μM CDSO3 against 10 or 25 μM SU5416-induced HMVEC-L cell death, as determined by the TBE assay. + = present; - = absent. Data represent mean±SD from n≥3; *p<0.05, compared to the vehicle control; $^{\#}$p<0.05, compared to the SU5416 (10 μM)-induced control; $^{\$}$p<0.05, compared to the SU5416 (25 μM)-induced control, by ANOVA and Tukey's multiple comparison test

4.3.6 Fe^{2+}- and HIF-1α-dependent mechanisms for CDSO3's anti-cell death activities

While CDSO3 at 10 μM consistently exhibited potent protective activities against lung epithelial and endothelial cell death induced with different emphysematous insults, its mechanism was still unknown. Based on a hypothesis that CDSO3's Fe^{2+} chelating activity inhibits Fe^{2+}-dependent HIF-degrading enzymes, HIF-PHDs, thereby stabilizing HIF-α and elevating HIF-regulating VEGF, for these anti-cell death activities, effects of HIF-1α inhibitors (Echinomycin and CAY) and excess Fe^{2+} or Fe^{3+} on CDSO3's protective activities were studied in the A549 and HMVEC-L cells upon cell death induced with CSE, TSA, or SU5416, as shown in Figures 4.12-4.16. In the A549 cells, as shown in Figures 4.12 and 4.13, 99.4 and 68.6 % protective activities for CDSO3 at 10 μM against the CSE- and TSA-induced cell death, respectively, were near completely opposed by addition of HIF-1α inhibitors, 10 μM Ech and CAY, as well as excess Fe^{2+} (50 μM $FeSO_4$). In the HMVEC-L cells, as shown in Figures 4.14-4.16, 50.7-86.1 % protective activities for 10 μM CDSO3 against the TSA- and SU5416-induced cell death were again near completely negated by addition of Ech, CAY, and excess Fe^{2+} (50 μM $FeSO_4$ or $FeCl_2$). However, as shown in Figure 4.16, addition of excess Fe^{3+} (50 μM $FeCl_3$) failed to oppose CDSO3's anti-cell death activities. Collectively, these results were consistent with CDSO3's Fe^{2+}- and HIF-1α-dependent mechanism, as hypothesized in this dissertation research.

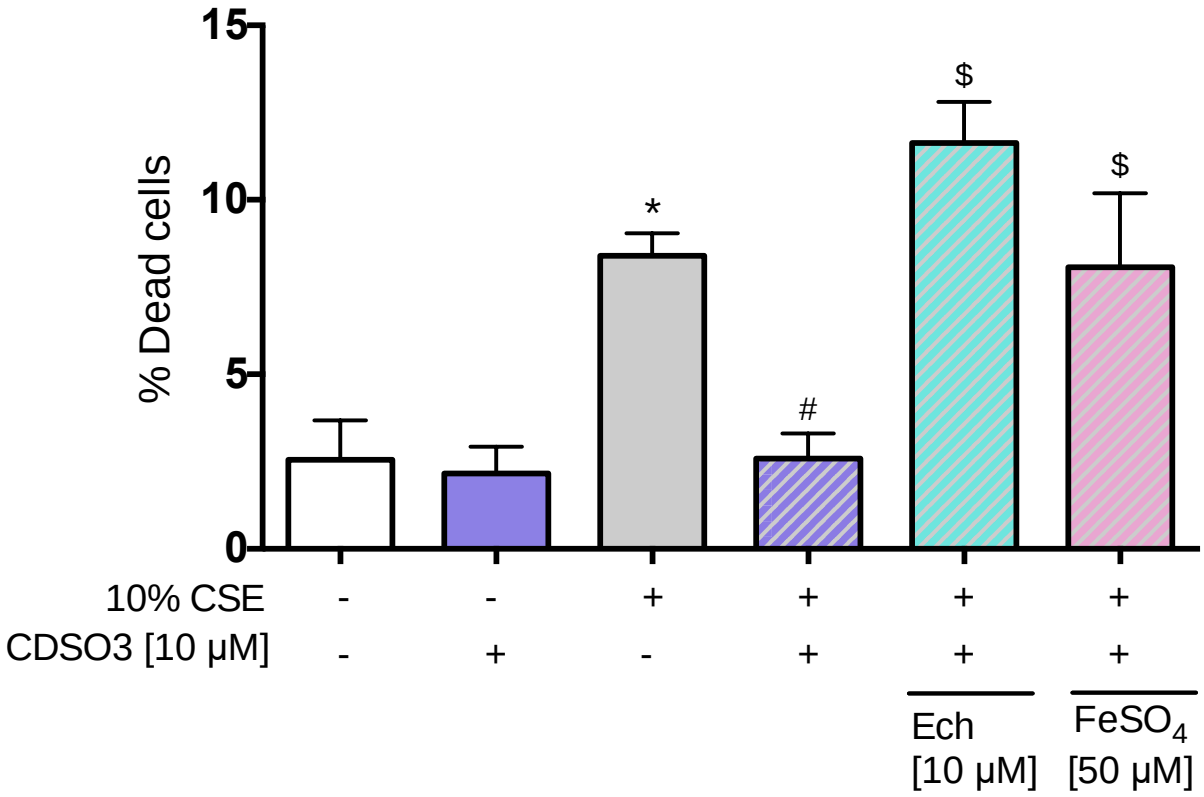

Figure 4.12: Effects of 10 μM echinomycin (Ech; a HIF-1α inhibitor) and 50 μM $FeSO_4$ (i.e., excess Fe^{2+}) on CDSO3's protective activities at 10 μM against 10 % CSE-induced cell death in A549 cells, as determined by the TBE assay. + = present; - = absent. Data represent mean±SD from n≥3; *p<0.05, compared to the vehicle control; $^{\#}$p<0.05, compared to the CSE-induced control; $^{\$}$p<0.05, compared to the TSA-induced and CDSO3-treated group, by ANOVA and Tukey's multiple comparison test

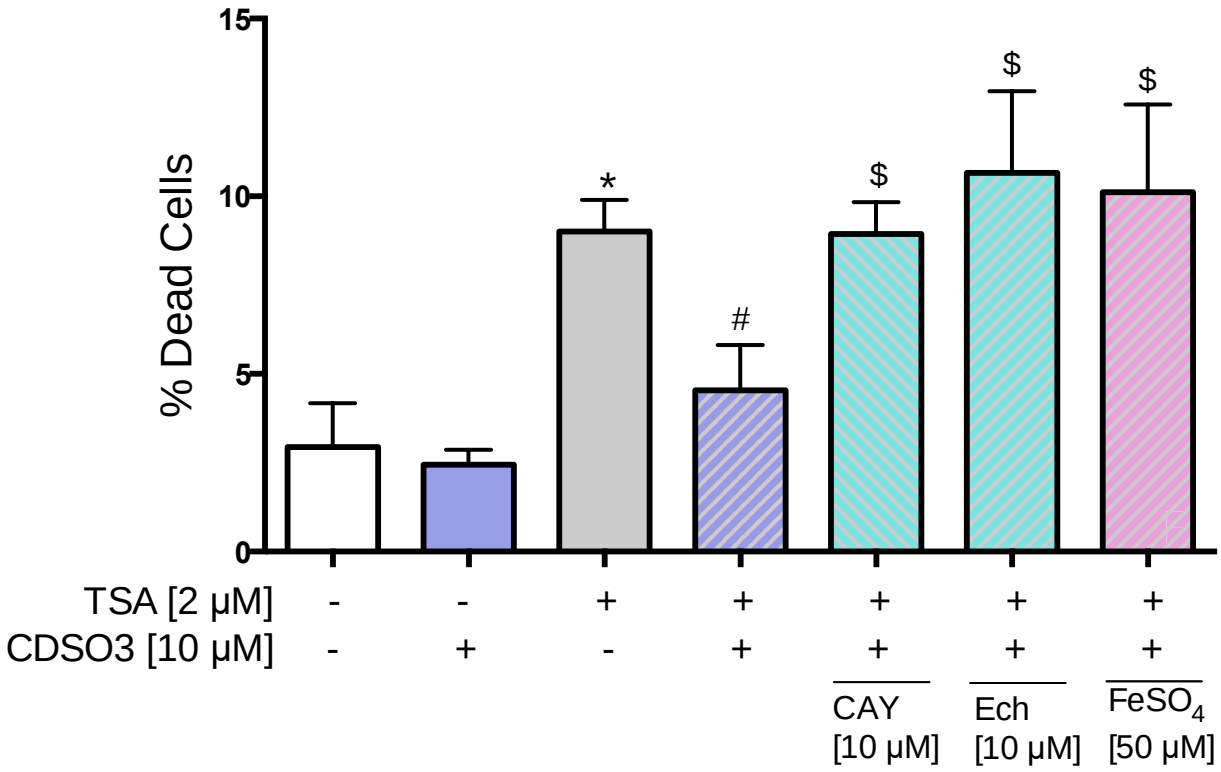

Figure 4.13: Effects of 10 μM CAY10585 (CAY; a HIF-1α inhibitor), 10 μM echinomycin (Ech; a HIF-1α inhibitor) and 50 μM $FeSO_4$ (i.e., excess Fe^{2+}) on CDSO3's protective activities at 10 μM against 2 μM TSA-induced cell death in A549 cells, as determined by the TBE assay. + = present; - = absent. Data represent mean±SD from n≥3; *p<0.05, compared to the vehicle control; $^{\#}$p<0.05, compared to the TSA-induced control; $^{\$}$p<0.05, compared to the TSA-induced and CDSO3-treated group, by ANOVA and Tukey's multiple comparison test

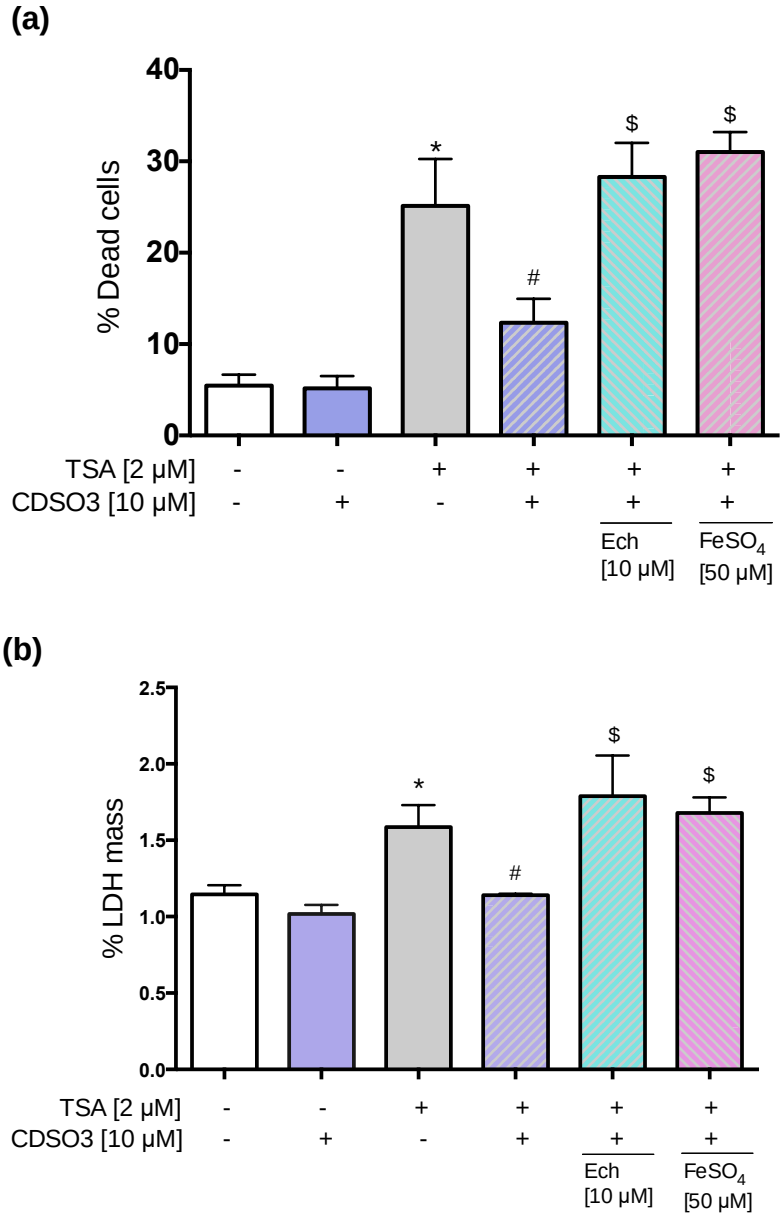

Figure 4.14: Effects of 10 µM echinomycin (Ech; a HIF-1α inhibitor) and 50 µM $FeSO_4$ (i.e., excess Fe^{2+}) on CDSO3's protective activities at 10 µM against 2 µM TSA-induced cell death in HMVEC-L cells, as determined by the (a) TBE and (b) LDH release assay. + = present; - = absent. Data represent mean±SD from n≥3; *p<0.05, compared to vehicle control; $^{\#}$p<0.05, compared to the TSA-induced control; $^{\$}$p<0.05, compared to the TSA-induced and CDSO3-treated group, by ANOVA and Tukey's multiple comparison test

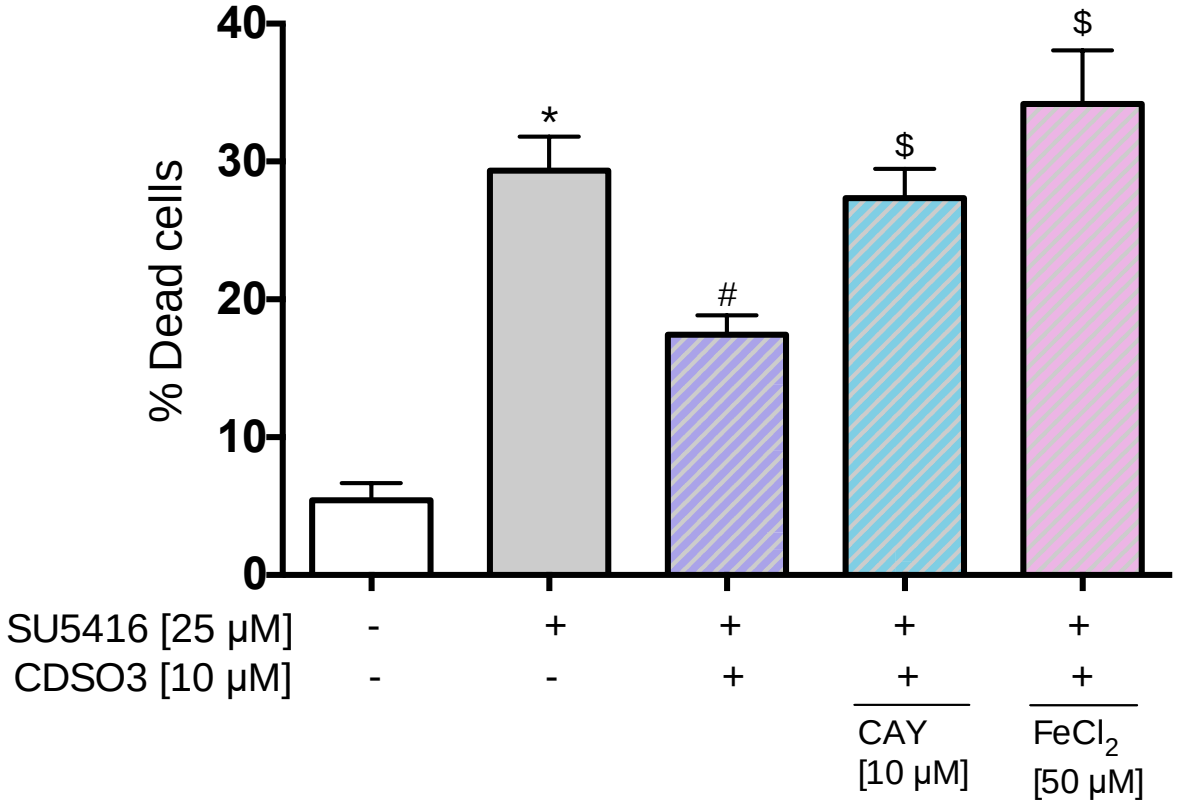

Figure 4.15: Effects of 10 μM CAY10585 (CAY; a HIF-1α inhibitor) and 50 μM $FeCl_2$ (i.e., excess Fe^{2+}) on CDSO3's protective activities at 10 μM against 25 μM SU5416-induced HMVEC-L cell death, as determined by the TBE assay. + = present; - = absent. Data represent mean±SD from n≥3; *p<0.05, compared to the vehicle control; $^{\#}$p<0.05, compared to the SU5416-induced control; $^{\$}$p<0.05, compared to the SU5416-induced and CDSO3-treated group, by ANOVA and Tukey's multiple comparison test

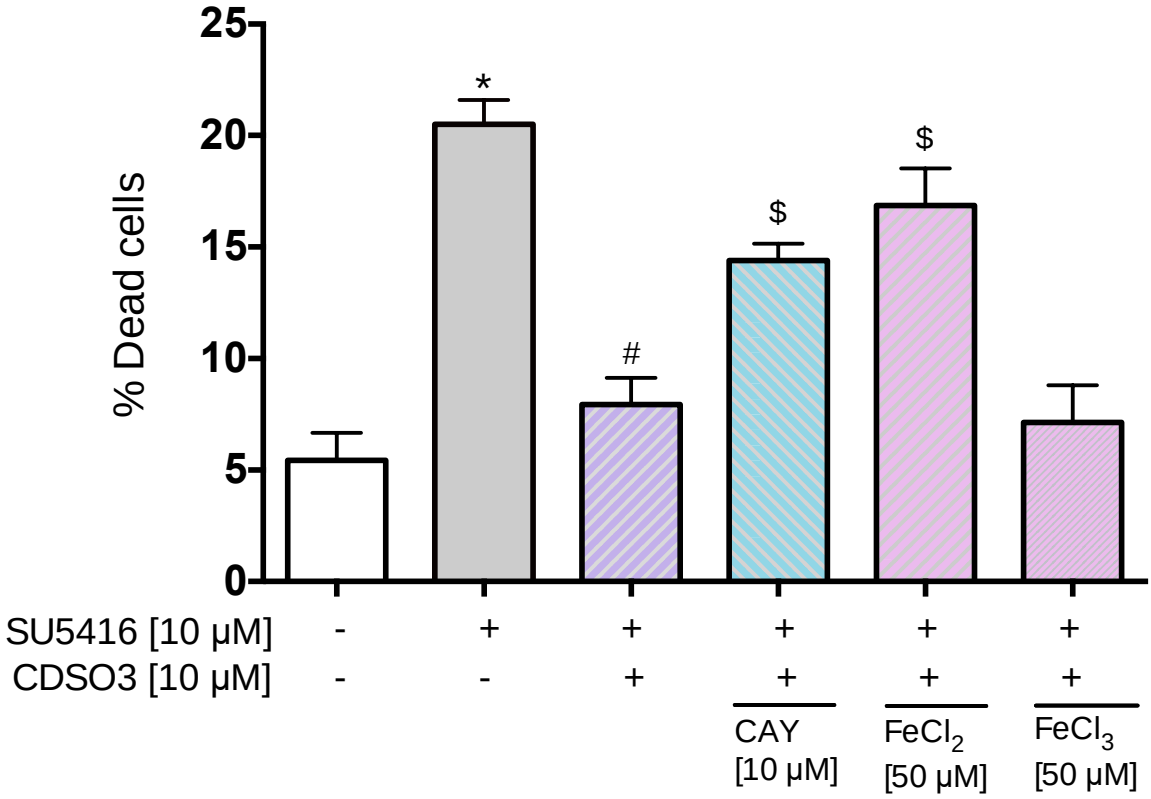

Figure 4.16: Effects of 10 μM CAY10585 (CAY; a HIF-1α inhibitor) and 50 μM $FeCl_2$ and $FeCl_3$ (i.e., excess Fe^{2+}) on CDSO3's protective activities at 10 μM against 10 μM SU5416-induced HMVEC-L cell death, as determined by the TBE assay. + = present; - = absent. Data represent mean±SD from n≥3; *p<0.05, compared to the vehicle control; $^{\#}$p<0.05, compared to the SU5416-induced control; $^{\$}$p<0.05, compared to the SU5416-induced and CDSO3-treated group, by ANOVA and Tukey's multiple comparison test

4.3.7 *In vitro* protective activities of other Fe^{2+} chelator molecules against SU5416-induced A549 cell death

To examine whether Fe^{2+} chelating activities alone universally produce protective activities against emphysematous cell death, two other known Fe^{2+} chelators molecules, DFO and EDTA, were tested for their cytoprotective activities against SU5416-induced A549 cell death determined by the TBE assay. As shown in Figure 4.17, unlike CDSO3 exerting 72.6 % cytoprotection, 4.0-fold increase of % dead cells induced with 10 µM SU5416 were unable to be inhibited by either DFO or EDTA at 10 µM. This in turn implied that CDSO3 is unique and different from DFO or EDTA as a Fe^{2+} chelator molecule capable of cytoprotection, presumably because CDSO3 is relatively lipophilic (log D ~ 1), while DFO and EDTA are hydrophilic and highly charged (log D ~ -2.2 and ~-0.8, respectively).

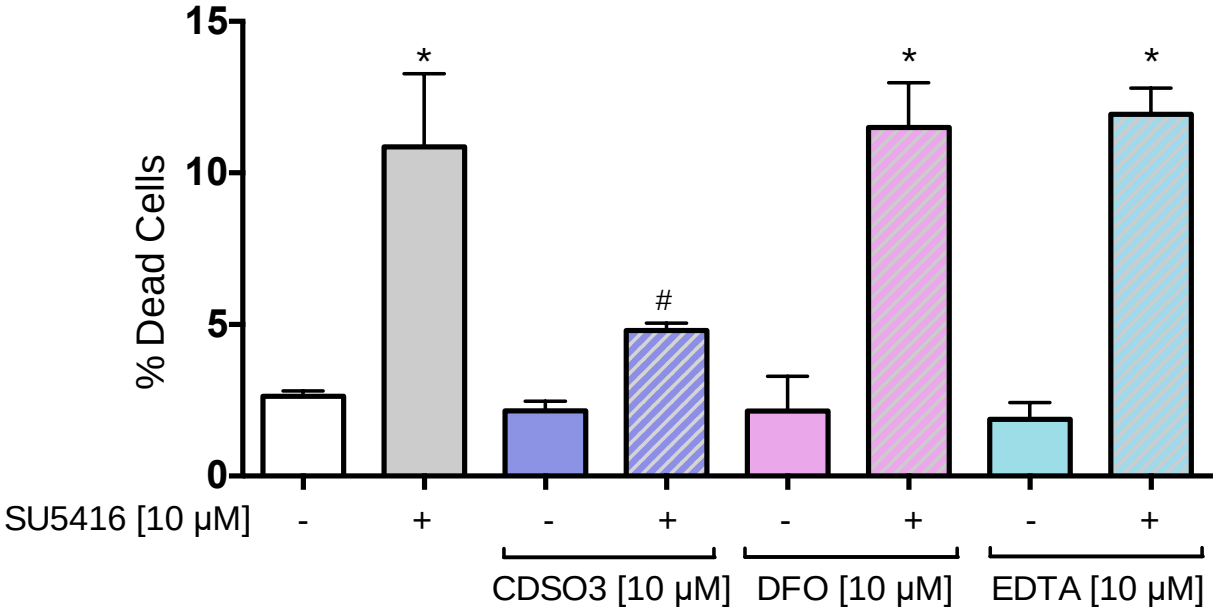

Figure 4.17: *In vitro* protective activities of CDSO3, DFO, and EDTA at 10 µM against SU5416-induced cell death, as determined by the TB assay. + = present; - = absent. Data represent mean±SD from n≥3; *p<0.05, compared to the vehicle control; #p<0.05, compared to the SU5416-induced control, by ANOVA and Tukey's multiple comparison test

4.3.8 Comparisons of the *in vitro* protective activities of two different batches of CDSO3

As discussed in Chapter 3, two different batches of CDSO3 were synthesized, i.e., $CDSO3_{BH}$ and $CDSO3_{MT}$ [Monien *et al.,* 2006; Thompson *et al.,* 2015], and provided for our experiments. As shown in Table 3.1, their elemental compositions and distribution coefficients (log D), determined by Monien [2006] and Thompson [2015], were different. The *in vitro* ferrous (Fe^{2+}) chelating activities of both batches were then determined in Chapter 3, revealing comparable IC_{50} values of 23.3±2.1 and 17.0±1.4 µM. It was therefore of interest to compare the *in vitro* cytoprotective activities of these two batches. Figure 4.18 shows the comparative *in vitro* cytoprotective effects of (a) $CDSO3_{BH}$ and (b) $CDSO3_{MT}$ at 10 µM against 10-µM SU5416-induced A549 cell death, as determined by the TBE assay. $CDSO3_{BH}$ and $CDSO3_{MT1}$ at 10 µM produced comparable 72.6±3.1 and 80.7±3.4 % protection against SU5416-induced A549 cell death, which were not significantly different.

(a)

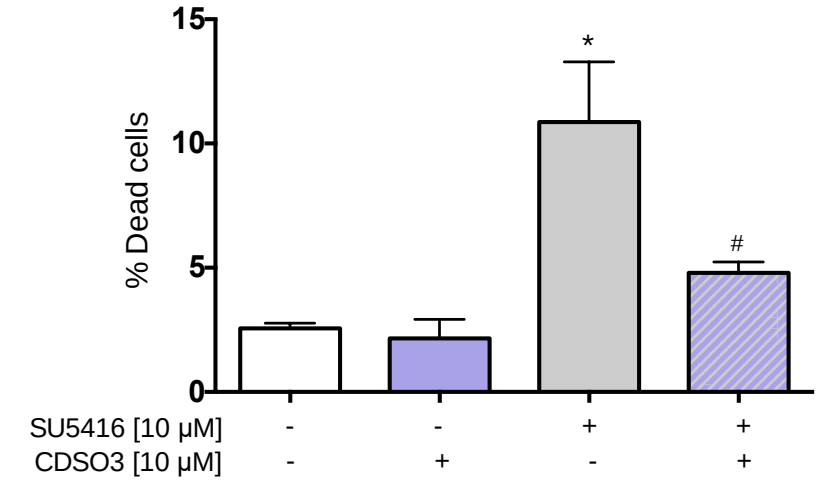

(b)

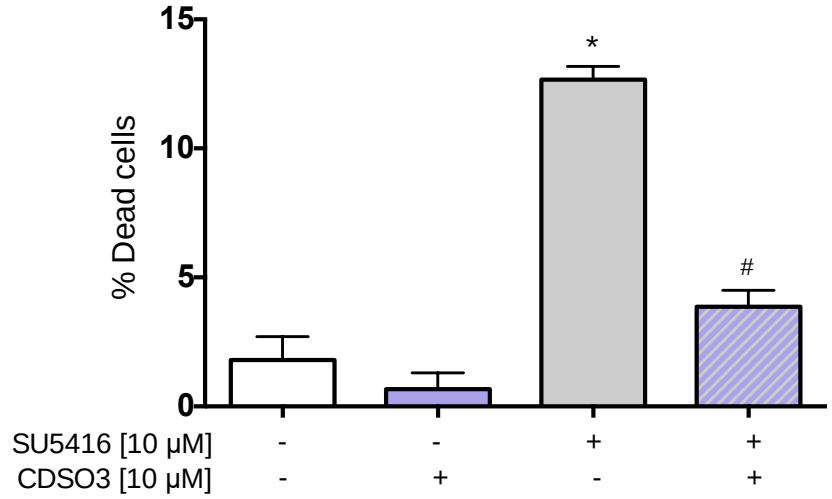

Figure 4.18: Protective effects of $CDSO3_{BH}$ and $CDSO3_{MT}$ at 10 µM against 10 µM SU5416-induced A549 cell death, as determined by the TBE assay. + = present; - = absent. Data represent mean±SD from n≥3; *p<0.05, compared to the vehicle control; $^{\#}$p<0.05, compared to the SU5416-induced control, by ANOVA and Tukey's multiple comparison test

4.4 DISCUSSION

In this chapter, the ELISA assay was used to assess CSE-induced pro-inflammatory TNF-α release in alveolar macrophages. In contrast, the TBE and LDH assays were employed to assess the Fe^{2+} chelation-dependent HIF-1α up-regulatory *in vitro* cytoprotective activity of CDSO3 against inflammatory, oxidative, elastolytic, and apoptotic cell deaths, in alveolar macrophages, epithelial, and endothelial cells. Furthermore, its cytoprotective activity of two other well-known chelators, DFO and EDTA were also assessed. CDSO3 was shown to protect against CSE-induced TNF-α release, while also being the only chelator shown to exhibit potent protective activities against these various stimuli, suggesting its unique ability to enter these cells that have been suggested in the pathobiological mechanism of emphysema in order to exert its cytoprotection. These findings of CDSO3's protective activities are promising to further study its ability to reverse lung damages in established emphysema *in vivo*.

4.4.1 CDSO3 as a cytoprotective drug against inflammatory, oxidative, and elastolytic cell death

The widely accepted cornerstones of emphysema pathogenesis are persistent inflammation, oxidative stress, and protease/anti-protease imbalance [Suki *et al.,* 2003; Barnes *et al.,* 2003]. First, the inhalation of noxious particles from cigarette smoke causes the massive influx of inflammatory cells, such as alveolar macrophages and neutrophils, into the luminal airways and lung tissues, which release pro-inflammatory mediators into the lung [Roth, 2008; de Boer WI *et al.,* 2005]. The pro-inflammatory

factors released by activated immune cells stimulate the resident cells to produce and secrete additional pro-inflammatory factors, thereby attracting more immune cells, sustaining the cycle of this inflammatory process [Roth, 2008]. Secondly, the inflammatory cells (macrophages and neutrophils) release proteolytic enzymes, which causes an imbalance between proteases and anti-proteases in the lungs, resulting in an increased in proteolytic activity [Demedts *et al.,* 2006; Roth, 2008]. And third, cigarette smoke or inflammatory leukocytes and epithelial cells also generate oxidants, resulting in oxidative stress. This oxidative stress can further contribute to the protease/anti-protease imbalance and the inflammatory reaction by activating the transcription of pro-inflammatory genes via activation of the transcription factor NF-κB [Demedts *et al.,* 2006]. Furthermore, oxidative stress can lead to cell death and can cause damage to the lung extracellular matrix [Demedts *et al.,* 2006].

The unsulfated and sulfated dehdryopolymers (DHPs), CD and CDSO3, alongside the caffeic acid (CA) monomer, have recently been shown to exhibit triple inhibitory activity against elastase, oxidation and inflammation *in vitro*, with CDSO3 being most potent, as summarized in Table 1.4 [Saluja *et al,* 2013]. CDSO3 was also shown to inhibit 1% CSE-induced TNF-α release in a concentration-dependent manner from 1-25 μM, with 5, 10, and 25 μM causing significant 49.3, 79.4, and 94.3 % inhibition, respectively ($p<0.05$; Figure 4.4). It was therefore hypothesize that CDSO3 could also protect against emphysematous cell death induced by these three known mechanisms. Thus, the cytoprotective activity of CDSO3, along with CD and CA, were tested against inflammatory (CSE)-, oxidative (CSE and H_2O_2)-, and elastolytic (HSE)-induced alveolar macrophage, epithelial, and endothelial cell death using the TBE and

LDH assays. It was found that CD at 25 µM could only produce 46.5 % protection, which was less potent than CDSO3 (83.9 % protection at µM), assessed by the TBE assay; however, neither CD nor CA was cytoprotective at 10 µM against 10 % CSE, when assessed by the LDH assay. CDSO3 at 10 µM exhibited potent 84.0-153.9 % cytoprotection against 10% CSE-, 0.1 mM H_2O_2-, and 1 U/ml HSE-induced alveolar macrophage, epithelial, and endothelial cells (Table 4.1). These data were encouraging to showing that CDSO3 produced triple protection against the multi-faceted mechanisms believed to be the cornerstones of the pathogenesis of emphysema.

4.4.2 CDSO3 as a cytoprotective drug against apoptotic cell death

It has been widely reported that increased apoptosis of alveolar septal cells is observed in the lungs of patients with COPD/emphysema [Demedts *et al.,* 2006; Imai *et al.,* 2005; Kasahara *et al.,* 2000; Yokohori *et al.,* 2004]. Furthermore, epigenetic modifications of HDAC inhibition are suggested to lead to apoptotic cell death in emphysematous lungs, at least in part, via impaired VEGF and its receptor signaling [Mizuno *et al.,* 2011; Kasahara *et al.,* 2000]. Therefore, the protective activity of CDSO3 was assessed against alveolar epithelial and endothelial cell death induced with TSA (an HDAC inhibitor) and SU5416 (a VEGF receptor blockade) using the TBE. CDSO3 at 10 µM potently inhibited these induced cell deaths by 63.6-86.1 % in both alveolar epithelial and endothelial cells (Table 4.1), clearly suggesting that CDSO3 was protective against cell death induced with an epigenetic HDAC inhibitor as well as a VEGF receptor blocker.

Table 4.1: The % inhibition of CDSO3 at 10 µM against emphysematous cell death induced with different stimuli in alveolar macrophages (NR8383), epithelial (A549), and endothelial (HMVEC-L) cells, as determined by the trypan blue exclusion (TBE) assay.

	NR8383		A549		HMVEC-L	
	Cell death induction[1]	% inhibition[2]	Cell death induction[1]	% inhibition[2]	Cell death induction[1]	% inhibition[2]
10 % CSE	4.3-fold	84.0±12.8	3.3-fold	99.4±12.5	1.7-fold	153.9±18.2
0.1 mM H_2O_2	-	-	3.9-fold	102.9±3.9	-	-
1 U/ml HSE	-	-	6.7-fold	91.7±24.1	-	-
2 µM TSA	-	-	3.5-fold	68.6±19.5	5.0-fold	63.6±13.0
10 µM SU5416	-	-	4.3-fold	72.6±5.3	3.5-fold	86.1±14.2

[1]Increase in % dead cells, as compared to the vehicle (negative) control.
[2]Values shown as mean±SD from n≥3

4.4.3 CDSO3's cytoprotection is Fe^{2+}- and HIF-1α-dependent

While CDSO3 at 10 μM consistently exhibited potent protective activities against lung epithelial and endothelial cell death induced with different emphysematous insults, its mechanism was still unproven. Based on a hypothesis that CDSO3's Fe^{2+} chelating activity inhibits Fe^{2+}-dependent HIF-degrading enzymes, HIF-prolyl hydroxylases (PHD), thereby stabilizing HIF-a and elevating HIF-regulating VEGF, for these anti-cell death activities, effects of HIf-1α inhibitors (echinomycin and CAY10585) and excess Fe^{2+} or Fe^{3+} on CDSO3's protective activities were studied in the A549 and HMVEC-L cells upon cell death induced with CSE, TSA, or SU5416. The cytoprotective activities of CDSO3 at 10 μM were near completely opposed by addition of HIF-1α inhibitors, 10 μM echinomycin (Ech) and CAY10585 (CAY), as well as excess Fe^{2+} (50 μM $FeSO_4$). However, addition of excess Fe^{3+} (50 μM $FeCl_3$) failed to oppose CDSO3's anti-cell death activities. This can be explained by the lack of ferric (Fe^{3+}) chelating activity with CDSO3 at 10 μM, as discussed in Chapter 3. Collectively, these results were consistent with CDSO3's Fe^{2+}- and HIF-1α-dependent mechanism.

4.4.4 DFO and EDTA are Fe^{2+} chelators but not cytoprotective

To examine whether Fe^{2+} chelating activities alone universally produce protective activities against emphysematous cell death, two other known Fe^{2+} chelators molecules, deferoxamine (DFO) and ethylenediaminetetraacetic acid (EDTA), were tested for their cytoprotective activities against SU5416-induced A549 cell death determined by the

TBE assay. As shown in Figure 4.17, unlike CDSO3 exerting 72.6 % cytoprotection, the 4-fold increased % dead cells induced with 10 µM SU5416 were unable to be inhibited by either DFO or EDTA at 10 µM. This implied that CDSO3 is unique and different from DFO or EDTA as a Fe^{2+} chelator molecule capable of cytoprotection. It was reported Thompson [2015] that the log D value of CDSO3 is ~1, making it 10 times more concentrated in the organic phase than the aqueous phase. Although CDSO3 is a large molecule containing charges, its aromatic backbone imparts over hydrophobic character, allowing it to penetrate the membrane and enter the cell where it exerts its effects. Conversely, DFO (log D = -2.2) and EDTA (log D = -0.8) are known to be highly hydrophilic molecules, therefore, although they both have Fe^{2+} chelation IC_{50} values of 31.8±2.1 (95% CI: 27.1, 36.6) and 24.6±4.8 (95% CI: 13.6, 35.6) µM (Chapter 3), these molecules are not able to penetrate the membrane to exert their effects inside the cell.

4.5 CONCLUSIONS

CDSO3 was clearly shown to exhibit potent cytoprotective activity against release of the pro-inflammatory cytokine, TNF-α, in alveolar macrophages. CDSO3 was also protective against inflammatory (CSE), oxidative (CSE and H_2O_2), elastolytic (HSE), and apoptotic (TSA and SU5416) cell death, in alveolar macrophages, epithelial, and endothelial cells. Furthermore, the molecular mechanism of this anti-cell death activity is suggested to involve Fe^{2+} chelation up-regulation HIF-1α. However, the Fe^{2+} chelators, DFO and EDTA, did not exhibit the same cytoprotection, implying that

CDSO3 is unique as a Fe^{2+} chelator molecule capable of cytoprotection due to its lipophilic nature.

CHAPTER 5

REVERSAL OF EMPHYSEMA INDUCED BY VEGF RECEPTOR BLOCKADE IN RATS FOLLOWING LUNG DELIVERY OF CDSO3

5.1 INTRODUCTION

As a triple-action inhibitor of oxidative stress, inflammation, and neutrophil elastase, CDSO3 remarkably attenuates the development of emphysema, when dosed to the lung in a preventative and interventional manner [Saluja *et al*., 2013,2014]. However, it is more important to reverse emphysema so as to develop a cure, such that epigenetic modifications in the emphysematous lung have received considerable attention to identify the responsible factor for progressive destruction and loss of the alveolar septa. Hypothesizing that CDSO3 is a lipophilic Fe^{2+} chelator enabling protection against epigenetically-induced apoptotic lung cell death, CDSO3's cytoprotective activities for repairing emphysematous lungs via recovery of "HIF-1α/VEGF deficiency" were assessed against various emphysematous cell death in Chapter 4. In Chapter 4, CDSO3's mechanism for cytoprotection was also clarified. However, it was still uncertain whether CDSO3 is also effective *in vivo* in the animal model of emphysema, in the especially epigenetically-relevant model. Hence, this chapter was designed to test CDSO3's Fe^{2+}- and HIF-1α-dependent reversal of lung

damages in an *in vivo* rat model of apoptotic emphysema induced by VEGF receptor blockade [Kasahara et al., 2000]. It was also aimed to clarify whether lung functional activity could be correlated with alveolar morphological airspace enlargement and destruction, to define established emphysema. The *in vivo* functional activity was assessed by the treadmill exercise endurance (EE) test, whereas the *in vivo* morphological alveolar airspace enlargement and destruction were quantified by measuring the mean linear intercept (MLI) and destructive index (DI), respectively. The lung tissue expressions of HDAC2, HIF-1a, VEGF, BAX, and cleaved caspase-3 were measured by Western blot in an attempt to clarify the mechanism of CDSO3's reversal of *established* emphysema.

5.2 MATERIALS AND METHODS

5.2.1 Materials

CDSO3 was prepared as described in previous chapters at the Desai laboratory, and stored at -20 ^{o}C prior to use. Only one batch referred to as $CDSO3_{BH}$ in Chapter 3 was used, supplied as 5 mM lyophilized powder. SU5416 was a gift from Dr. Voelkel (VCU Pulmonary Medicine) and stored at -20 ^{o}C prior to use. $FeSO_4 \cdot 7H_2O$ was purchased from Sigma-Aldrich and stored at 4 ^{o}C, prior to use. Agarose solution at 0.5 % was prepared by slowly adding agarose (Invitrogen, Carlsbad, CA) into 80 ^{o}C DDW to complete its dissolution in a beaker on a magnetic hotplate stirrer; temperature was

then maintained at 50 ^{o}C prior to use. Isoflurane was purchased from Webster Veterinary Supply, Inc. (Sterling, MA) and stored at room temperature.

5.2.2 Animals

This research adhered to the NIH Principles of Laboratory Animal Care (NIH publication #85-23, revised in 1985) under the protocol approved by the Institutional Animal Care and Use Committee (IACUC) at Virginia Commonwealth University (VCU; Protocol AD20086). Male Sprague-Dawley rats (specific-pathogen free, 8-9 weeks of age), weighing 250-275 g, were received from Hilltop Lab Animals, Inc. (Scottdale, PA) and acclimated for more than 3 days prior to use. Temperature (20-23^{o}C), relatively humidity (40-70%) and light-dark cycling (12-12 h; the light cycle was between 6 a.m. and 6 p.m.) were tightly controlled and maintained.

5.2.3 Study protocol

Figure 5.1 outlines the overall experimental protocol to 1) develop and establish emphysema in rats, induced with SU5416; 2) treat emphysematous animals with CDSO3 or saline; and 3) to assess functional treadmill exercise endurance, followed by animal sacrifice and lung harvest. A total of 42 animals were used and divided into the following 5 groups:

	Induction	Treatment	N
Group 1	Saline	Saline	14
Group 2	Saline	CDSO3	2
Group 3	SU5416	Saline	10
Group 4	SU5416	CDSO3	12
Group 5	SU5416	CDSO3 + $FeSO_4$	4

Following acclimatization, rats were trained for two weeks to run on the rodent treadmill (Accuscan Instruments, Inc.; Figure 5.2), according to our in-house training protocol described in Appendix 2. On Day 1, rats were tested to ensure completion of their learning (pre-experimental EE), according to our testing protocol described in Appendix 2. Groups 3, 4, and 5 of animals received a single subcutaneous (SC) injection of SU5416 at 20 mg/kg to induce non-inflammatory, apoptotic, experimental emphysema [Kasahara et al., 2000]. SU5416 was suspended in saline or 0.9 % NaCl containing 0.5 % carboxymethylcellulose sodium, 0.9 benzylalcohol, and 0.4% Tween 80, and subcutaneously injected as 5 mg/ml suspension without a use of anesthesia; Groups 1 and 2 of animals received saline. Rats were left untreated in the animal facility for 3 weeks, while treadmill training continued to maintain their learning, as described in Appendix 2. On Day 21, their pre-dose exercise endurance was determined to ensure the development of emphysema from reduced EE times. Groups 2 and 4 received an orotracheal (OT) instillations of CDSO3 at 60 µg/kg three times a week for 2 weeks; Group 5 received OT CDSO3 at 60 µg/kg premixed with 10 mM $FeSO_4$; Groups 1 and 3 received OT saline. On Day 35, all animals were tested for their post-dose EE. The animals were then anesthetized with an intraperitoneal injection of urethane at 1 g/kg. The trachea was exposed and cannulated through an incision made on the trachea. After the chest cavity was opened, the animals were sacrificed by exsanguination by

cutting the abdominal aorta. The lung was carefully removed from the body, and the left lung was then inflated with ~ 8 ml of a 0.5 % agarose solution warmed at 45 ^{o}C through the tracheal cannula at a hydrostatic pressure of 20 cm; the bronchi to the right lung lobes were closed with a suture. The fully-inflated left lungs were placed on ice for ≥5 min to solidify the luminal agarose, followed by fixation in 10 % buffered formalin at 4^{o}C over 24 h. The fixed lung tissues were sent to the VCU Anatomical Pathology Laboratory to be embedded in paraffin blocks, followed by hematoxylin-eosin (HE) staining of their 4 μm-thick alveolar section slides. The lung sections were used to quantify airspace enlargement (mean linear intercept, MLI) and alveolar destruction (destructive index, DI). The right lung was used for Western blot analysis, as described in 5.2.8.

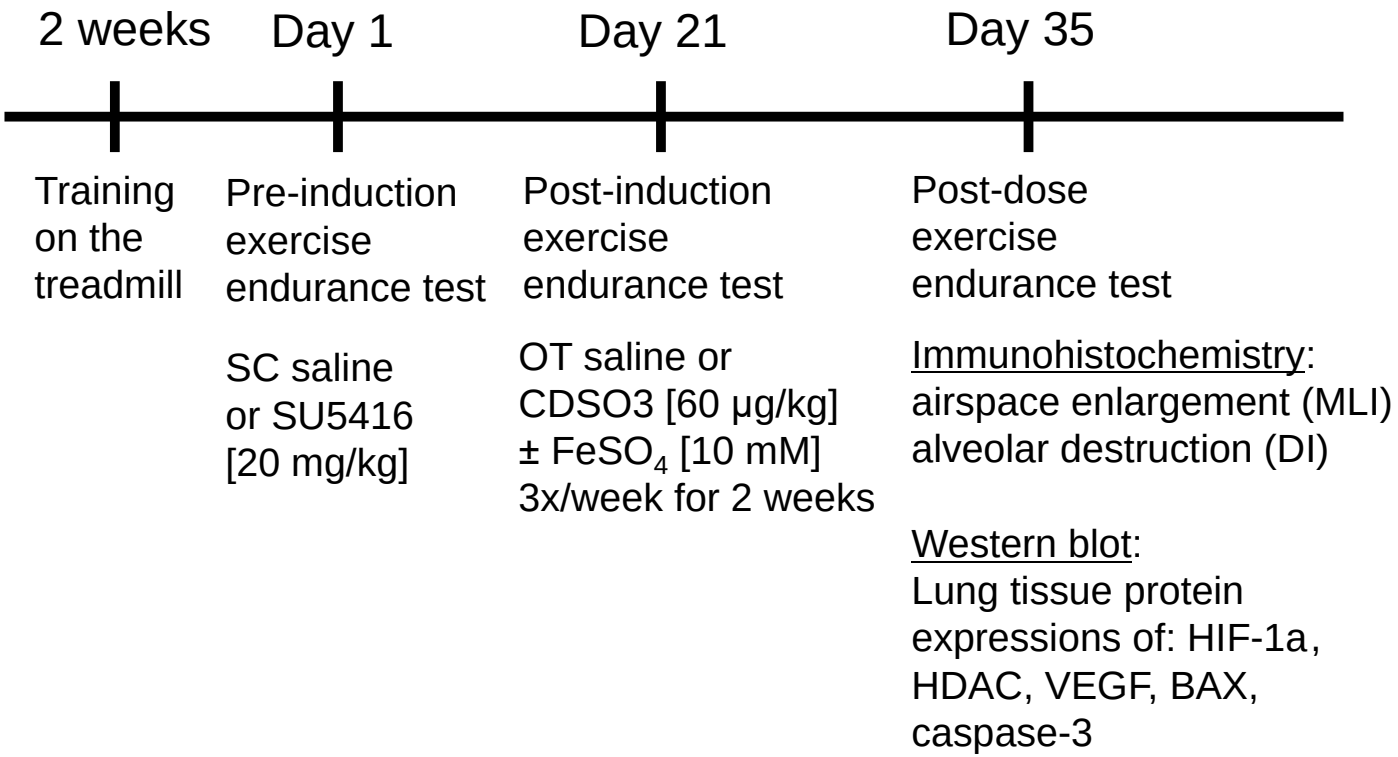

Figure 5.1: Experimental protocol to assess the *in vivo* lung repairing effects of CDSO3 administered into the lung in the VEGF receptor blockade-induced rat model of pulmonary emphysema

Figure 5.2: Treadmill used to test rat exercise endurance.

5.2.4 Orotracheal pulmonary instillation

CDSO3 or saline was administered to the lungs by orotracheal instillation under short anesthesia with isoflurane. Each rat was anesthetized in a chamber box with 4 % (v/v) isoflurance vapors generated from a vaporizer (Ohmeda Tech 4 Surgivet, Smiths Medical North America, Waukesha, WN) in 95% oxygen and 5% air as a carrier gas (National Welders, Richmond, VA) at 3.5 l/min. Sufficient anesthesia was typically attained in 5 min, ensured by the absence of corneal and pedal reflexes. Subsequently, the animal was placed in a supine position on a surgical board inclined at 60^{o} under a heat lamp. The tracheal entry lumen was visually confirmed through the oral cavity using a small animal fiber-optic laryngoscope (Welch Allyn, Skaneateles Falls, NY). Then, 0.1 ml of CDSO3 at 60 µg/kg or saline was directly instilled into the lung using a PennCentury Microsprayer (Wyndmoor, PA); the tip of the Microsprayer was positioned just before the tracheal bifurcation. The animals were held in an upright position for 1 min to avoid cough reflexes before returning to the cages. The entire instillation operation was typically completed within 6 min of the isoflurane anesthesia, after which the animals regained consciousness in 4 min.

5.2.5 Airspace enlargement

Alveolar airspace enlargement was quantified by measuring the MLI, as described by Thurlbeck [1967] and slightly modified in-house. The H&E-stained lung sections were viewed under the microscope at 25X magnification, and 5 airspace

images were randomly selected, photographed using the Axiovision software (Allied High Tech Products, Rancho Dominguez, CA) and printed out on 8x11-sized paper. On each image, 5 equally spaced lines (space: 513 μm; line length: 3540) were drawn (Figure 5.3), and their intercepts with the alveolar walls in the line length were counted to determine the MLI values (3540 μm/the number of intercepts). The MLI value for each animal was thus calculated as an average of the 25 MLI values (5 horizontal lines per image x 5 images). Each slide was coded, yet measured in a random order.

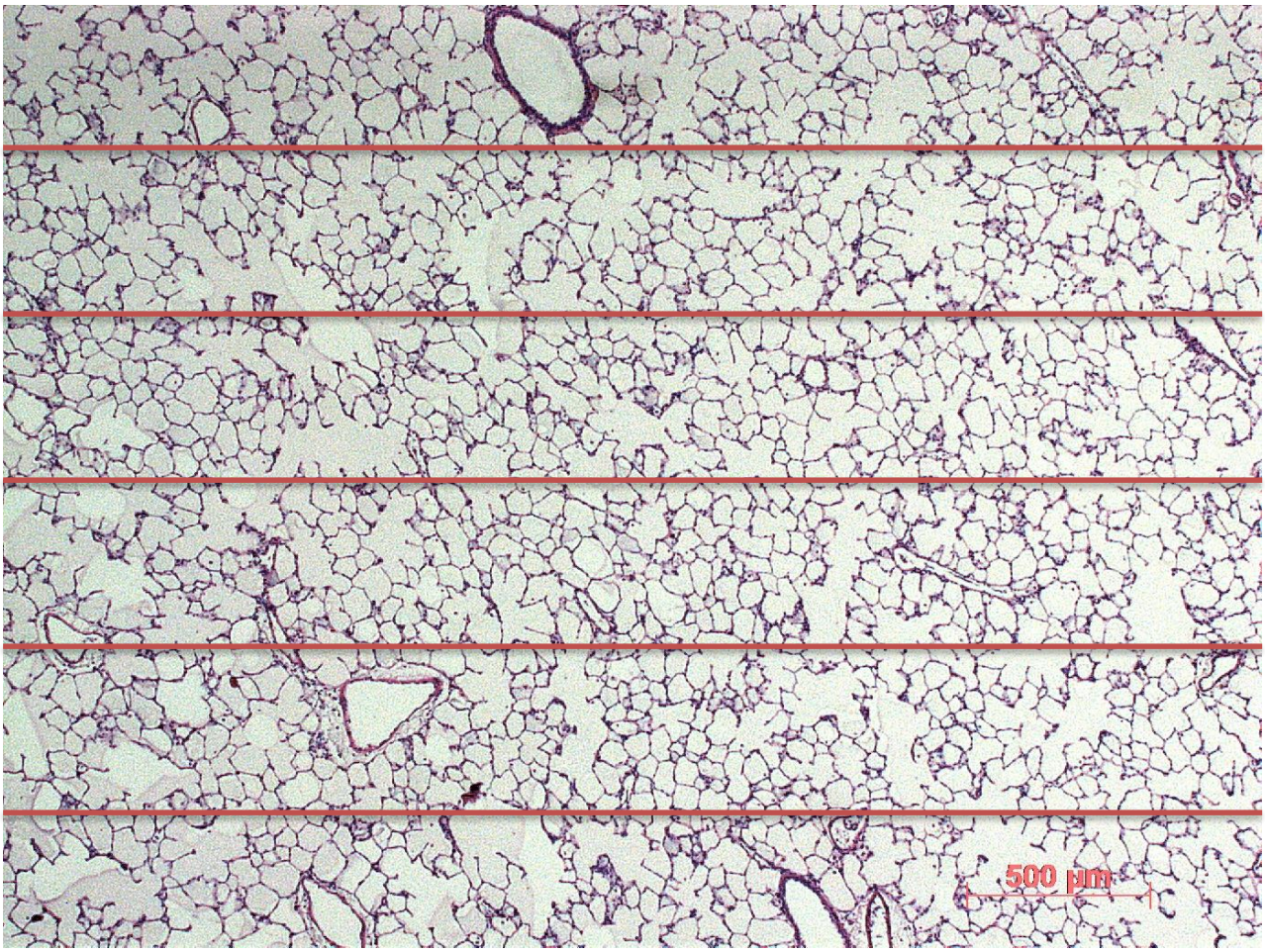

Figure 5.3: Representative histological hematoxylin-eosin (H&E)-stained micrograph of the left lung lobes taken on day 35 at 25x magnification used to determine the MLI. Five equally spaced lines (space: 513 µm; line length: 3540) are drawn over each image and their intercepts with the alveolar walls (stained purple) in the line length were counted to determine the MLI values (3540 µm/the number of intercepts).

5.2.6 Alveolar destruction

Alveolar destruction was quantified by measuring the destructive index (DI), as described by Eidelman [1991] and modified in-house. The H&E-stained lung sections were viewed under the microscope at 100X magnification and 50-60 airspace images were randomly taken (Figure 5.4). User Microsoft PowerPoint, each of the images was placed on a slide with a grid of 66 equally spaced dot points placed over each image. The alveolar spaces and duct spaces surrounding each point was carefully inspected and classified as either normal (N) or destroyed (D). Only dot points falling on whole alveoli and/or alveolar duct spaces were counted. Points falling on other structures, such as duct walls and alveolar walls, were not included. Both alveolar spaces and alveolar duct spaces were considered normal if they were surrounded by intact walls disrupted in only one place. A structure was considered to be destroyed if a) the wall of an avelolus was disrupted in two or more places, b) there were more than two disruptions of adjacent aloveli that opened into a single duct space, 3) when a duct space contained two or more islands of lung parenchyma within its lumen, or 4) when a structure was lined with cuboidal epithelium but was clearly not an airway, with or without breaks in the walls. Over 2,000 dot points were assessed, from which the % DI values were calculated using D/(D+N) x 100.

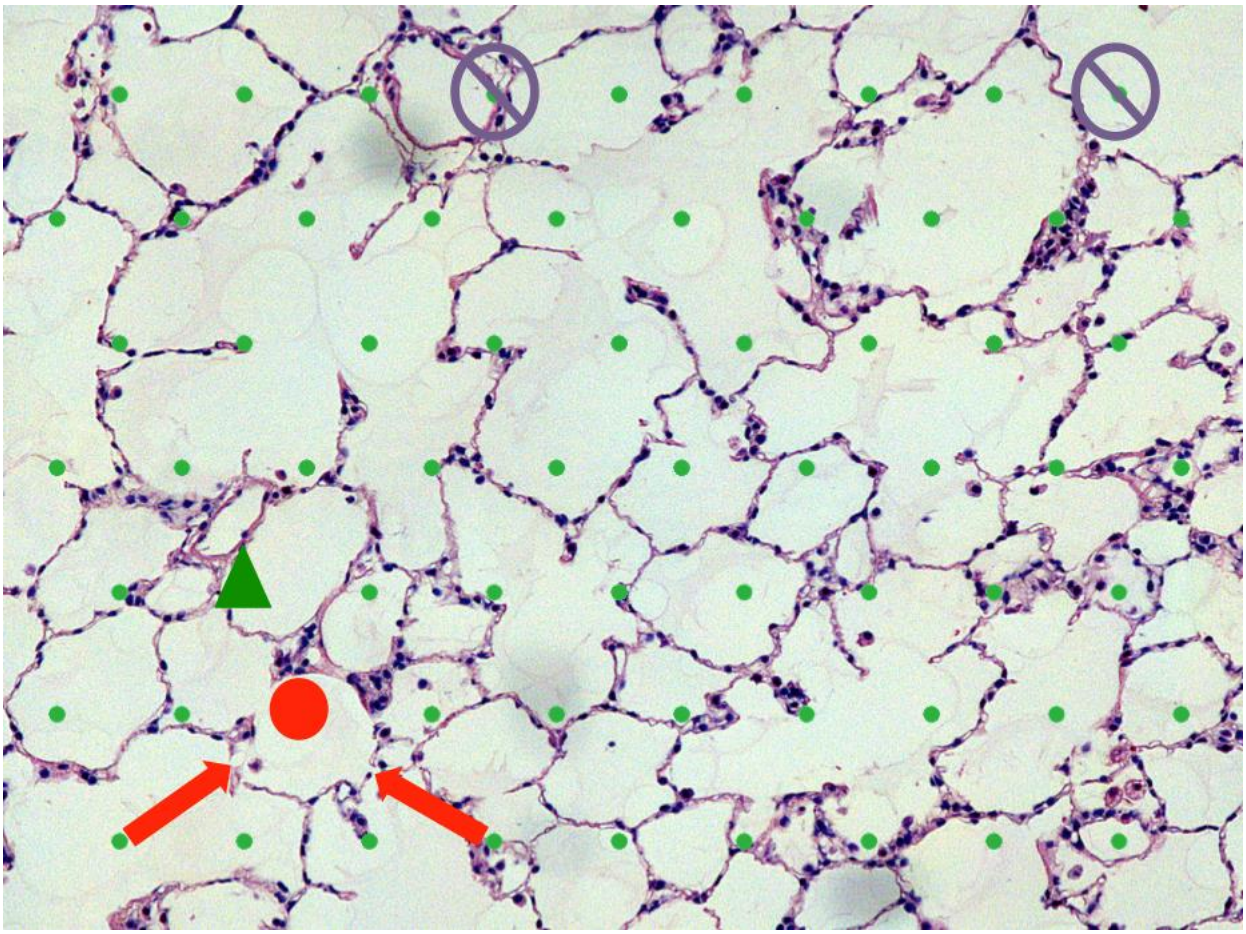

Figure 5.4: Representative histological hematoxylin-eosin (H&E)-stained micrograph (100x magnification) of the left lung lobe taken at day 35 used to determine the DI. The red arrows are pointed towards destruction in the alveolar walls, so that the ● = Destroyed, and ▲ = Normal.

5.2.7 Western blot

Lung tissue (300 mg) was minced and lysed in 1 ml of a lysis buffer containing 150 mM NaCl (Fisher Scientific), 50 mM Tris (pH 8.0, Bio-Rad Laboratories), 1% NP-40 (Fisher Scientific), and protease inhibitor (1 tablet in 10 ml of lysis buffer, Roche Diagnostics) using a homogenizer (Pro 200; Pro Scientific, Inc.) for 2 minutes. The tissue was allowed to rest for 15 minutes on ice, vortexed, and centrifuged (Aventi JE Centrifuge; Beckman Coulter) at 16,000 g at 4^{o}C. The supernatant was stored at -70^{o}C prior to use. The protein concentration was quantified by bicinchoninic acid assay (Pierce). The lung tissue samples were then prepared at a concentration of 2.5 µg/µl. In total, 40-70 µg of protein from the whole-lung lysates were loaded onto 10% Mini-Protean Precast Gels (Bio-Rad Laboratories) and subjected to Tris/Glycine/sodium dodecylsulfate (SDS)-polyacrylamide gel electrophoresis (Bio-Rad Laboratories) at 100 V for about 90 minutes. The protein was transferred from the gel to a 0.2 µm nitrocellulose membrane (Bio-Rad Laboratories) for ~90 minutes at 100 V. The membranes were washed in PBS containing 0.1% Tween-20 (pH 7.5) for 5 minutes, then blocked in 5% (w/v) non-fat dried milk (Kroger) in TBS or PBS for 60 minutes on a slow rocker at room temperature. The membrane was then incubated with primary antibodies against HDAC2 (rabbit monoclonal, Santa Cruz, sc-7899), HIF-1α (rabbit polyclonal, Santa Cruz, sc-10790), cleaved caspase-3 (rabbit monoclonal, Cell Signaling, 9664-s), VEGF (mouse monoclonal, Santa Cruz, sc-7269), or BAX (rabbit monoclonal, Cell Signaling, 2772s) for 60 minutes at room temperature on a slow rocker. The membranes continued to be incubated in the primary antibody at 4 ^{o}C on a slow rocker overnight. Subsequently, the membranes were then washed for 10 minutes

three times in PBS or TBS. The membrane was then allowed to incubate in anti-mouse or anti-rabbit secondary antibodies raised in goat conjugated with HRP (Bio-Rad Laboratories) on the slow rocker at room temperature for 80 minutes, then washed for 15 minutes three times in PBS or TBS. The membranes were allowed to incubate in SuperSignal West Pico Chemiluminescent Substrate (1:1 stable peroxide solution and liminal enhancer solution) for 1 minute, then developed onto BioExcell Autoradiographic Films.

5.2.8 Data analysis

The data for each treatment groups were expressed as mean ± SD. Analysis of variance (ANOVA) was used to test statistical differences for individual values. In the event of significant difference in the ANOVA, the Tukey-Kramer multiple comparison test was carried out to identify group-to-group statistical differences. In both ANOVA and Tukey-Kramer multiple comparison test, $p<0.05$ was considered to be statistically significant.

5.3 RESULTS

All animals tolerated SU5416 or saline SC injection and/or saline, CDSO3 and/or FeSO4 spray-instillations to the lung over the two week period, based on monitoring of appearance, posture, mobility, appetite, and body weight gain, with the exception of three animals (TR209, 210, and 211) that showed reduced body weight gain during the CDSO3 dosing period. Note however that these rats still exhibited improved exercise endurance, as shown in Figures 5.5 and 5.6.

5.3.1 Treadmill exercise endurance impairment and its improvement by CDSO3

Figures 5.5 show the treadmill EE time and its change in each animal receiving different treatment groups. Healthy, untreated control animals ran 43.3±6.8 min on the treadmill until exhaustion, and two-week lung administration of CDSO3 at 60 μg/kg alone did not alter the running times, i.e., 41.6±0.9 min. This demonstrated that CDSO3 by itself does not cause functional EE impairment. In contrast, SC injection of SU5416 at 20 mg/kg significantly ($p<0.05$) reduced the EE times by 80.8 % (8.3±2.8 min), shown as post-induction, pre-treatment EE values in Figure 5.5, which confirmed the development of emphysema. When these emphysematous rats were treated with saline for two weeks, the post-treatment EE values remained unimproved at 8.5±3.6 min, or impaired by average 80.4 %. However, when CDSO3 was administered to the lungs at 60 μg/kg for 2 weeks, the EE values were significantly ($p<0.05$) improved in all the rats by average 66.5 % to 31.9±7.4 min (Figure 5.5). These data strongly suggested that the CDSO3 treatment enabled reversal of the functional EE values presumably as a result of repair of lung damages. More intriguingly, when CDSO3 was pre-mixed with excess Fe^{2+} (i.e.,10 mM FeSO4) and then administered to the lungs of these emphysematous rats, the EE values remained abnormally reduced at 9.5±4.1 min, which was equivalent to those seen in the saline-treated emphysematous rats. This excess Fe^{2+}-induced failure of emphysema reversal was consistent with the mechanism of action for CDSO3, as hypothesized in this dissertation research, i.e., Fe^{2+} chelation-dependent HIF-1α stabilization and elevation. These findings are summarized in Figure 5.6.

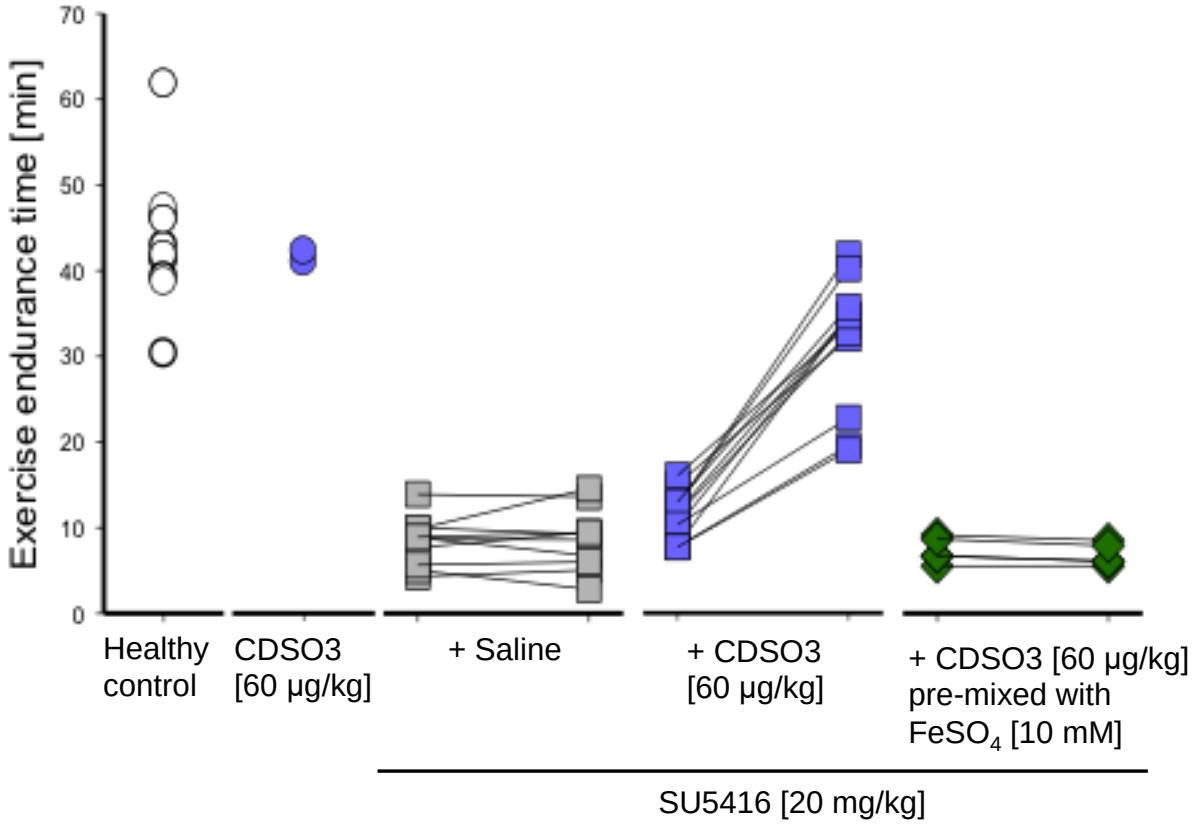

Figure 5.5: *In vivo* reversal of functional treadmill exercise endurance impairment by CDSO3 at 60 µg/kg against emphysema induced with VEGF receptor blockade

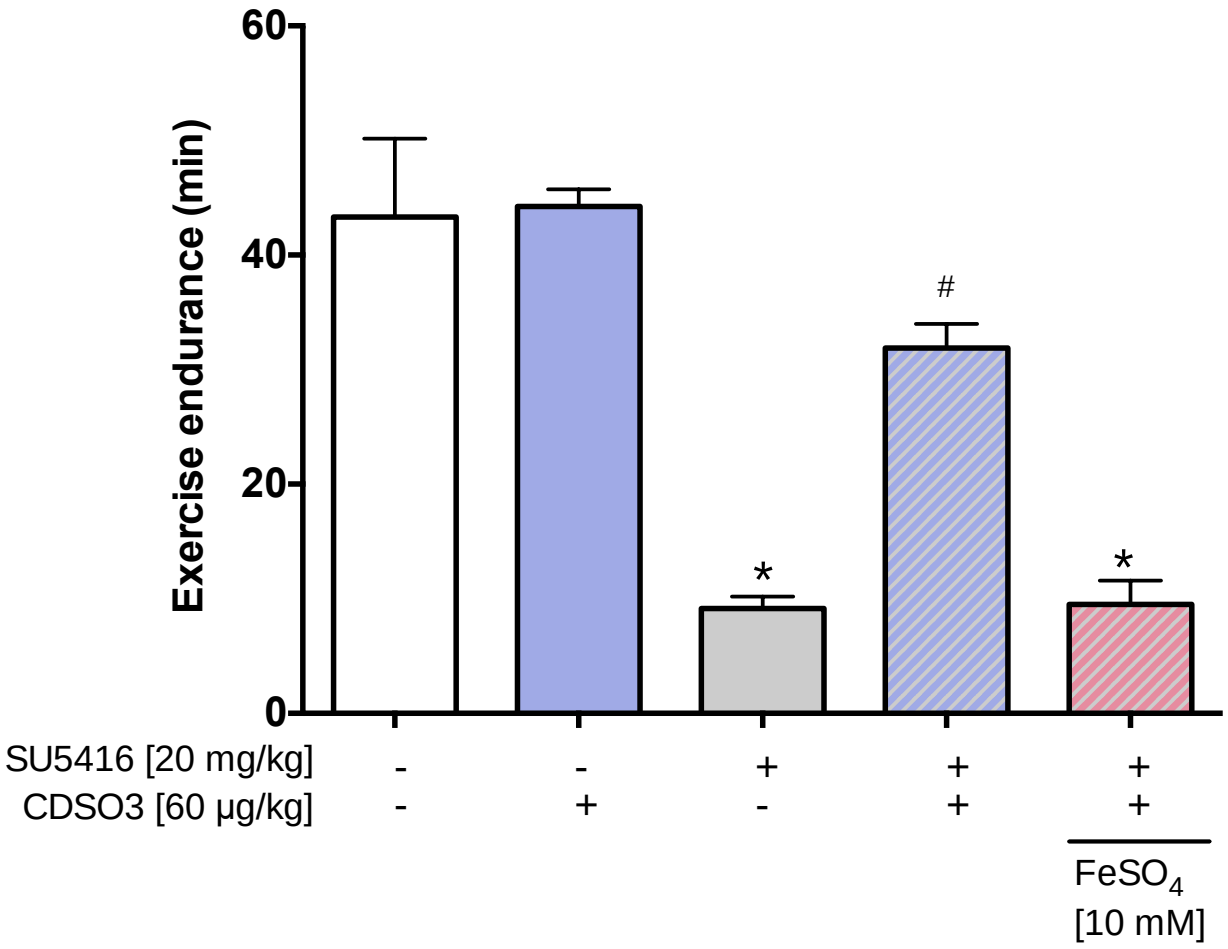

Figure 5.6: Exercise endurance (EE) values in 5 different treatment groups in a rat emphysema model induced by VEGF receptor blockade. Data represent mean±standard deviation (SD) from n=3-11; *p<0.05, compared to the healthy (negative) control; #p<0.05, compared to the SU5416-induced (positive) control, by ANOVA and Tukey's multiple comparison test

5.3.2 Airspace enlargement and its improvement by CDSO3

Figure 5.7 shows the representative histological H&E-stained micrographs of the left lung lobes taken on day 35 following different treatments. The mean linear intercept (MLI) values for the alveolar airspace size (e.g., enlargement) were determined from these micrographs at 25x magnification, as shown in Figure 5.8. While CDSO3 treatment alone at 60 μg/kg resulted in the MLI value of 49.5±4.7 μm, which was not significantly different from the MLI value of 56.1±6.0 μm for the healthy control rats. However, the absence of the alveolar walls was visually apparent in the SU5416-induced animals (Figure 5.6b) when compared to the healthy control animals (Figure 5.6a). As a result, this SU5416-induced airspace enlargement was quantified by a significant 46.5 % increase in the MLI value ($p<0.05$; 56.1±6.0 to 82.2±2.3 μm), as shown in Figure 5.7. In contrast, the 2-week treatment with CDSO3 at 60 μg/kg enabled significant recovery in the MLI value by 74.1 % ($p<0.05$; 82.2±2.3 to 62.9±5.2 μm). However, when CDSO3 at 60 μg/kg was pre-mixed with excess Fe^{2+}, and then administered to the lungs of these emphysematous rats, the alveolar airspace remained enlarged, comparable to those seen in the SU5416-indced emphysematous rats.

a) Healthy control (Saline + Saline)

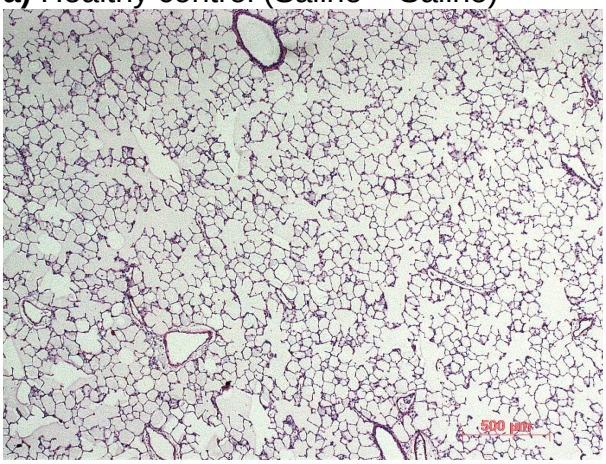

b) SU5416 + Saline

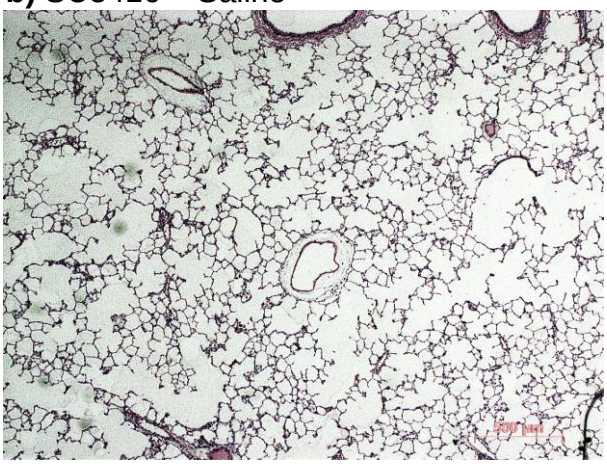

c) SU5416 + CDSO3 [60 µg/kg]

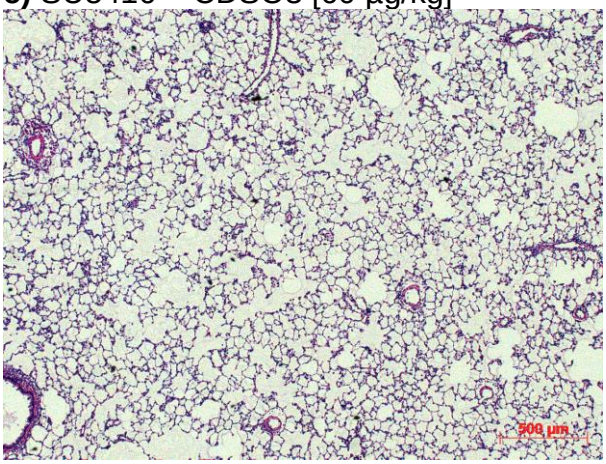

d) SU5416 + CDSO3 [60 µg/kg] pre-mixed with $FeSO_4$ [10 mM]

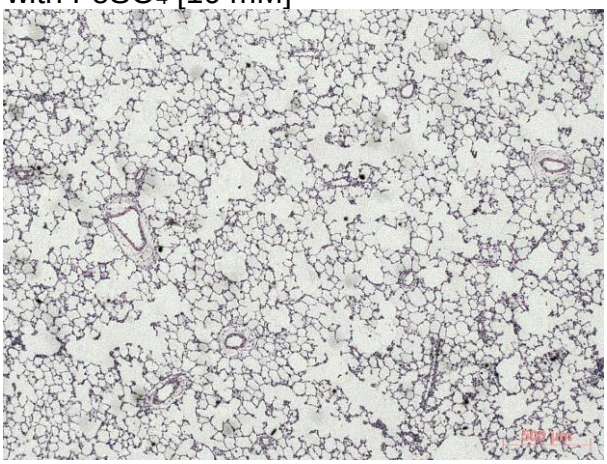

Figure 5.7: Representative histological hematoxylin-eosin (H&E)-stained micrographs of the left lung lobes taken on day 35 following SC injection of SU5416 or saline on day 1 and two-week pulmonary delivery with saline or CDSO3 60 µg/kg ± 10 mM $FeSO_4$. The micrographs are shown under 25X magnification; and the scale bars represent 500 µm.

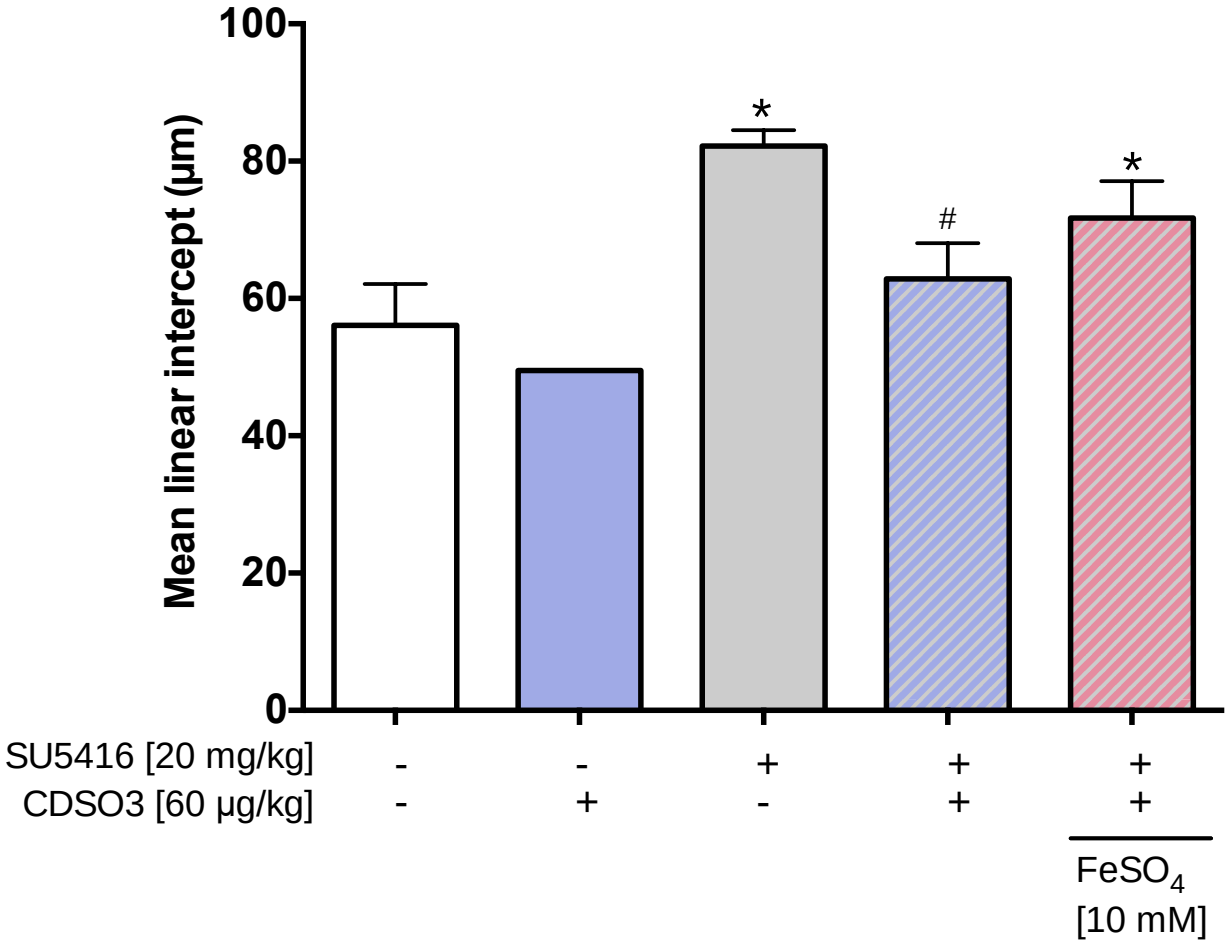

Figure 5.8: Mean linear intercept (MLI) values determined from the left lung lobes taken on day 35 following different treatment groups in the SU5416-induced rat model of emphysema. + = present; - = absent. Data represents mean±SD from n=2-11; *p<0.05, compared to the healthy control; #p<0.05, compared to the SU5416-induced control, by ANOVA and Tukey's multiple comparison test

5.3.3 Induced alveolar wall destruction and its improvement by CDSO3

The destructive index (DI) values were determined from the histological H&E-stained micrographs of the left lung lobes at 25x magnification, and are shown in Figure 5.9. Healthy control animals had a DI value of 5.6±2.4 %. SU5416-induced emphysematous animals had a significant 5-fold increase in the DI value ($p<0.05$; 5.6±2.4 % to 28.2±7.3 %), demonstrating the severe alveolar wall destruction due to SU5416. Treatment with CDSO3 at 60 µg/kg enabled significant recovery in the DI value by 87 % ($p<0.05$; 28.2±7.3 % to 8.5±1.5 %). However, when CDSO3 at 60 µg/kg was pre-mixed with excess Fe^{2+} and then administered to the lungs of these emphysematous rats, the alveolar structures remained destroyed, comparable to those seen in the SU5416-indced emphysematous rats (23.1±2.9%).

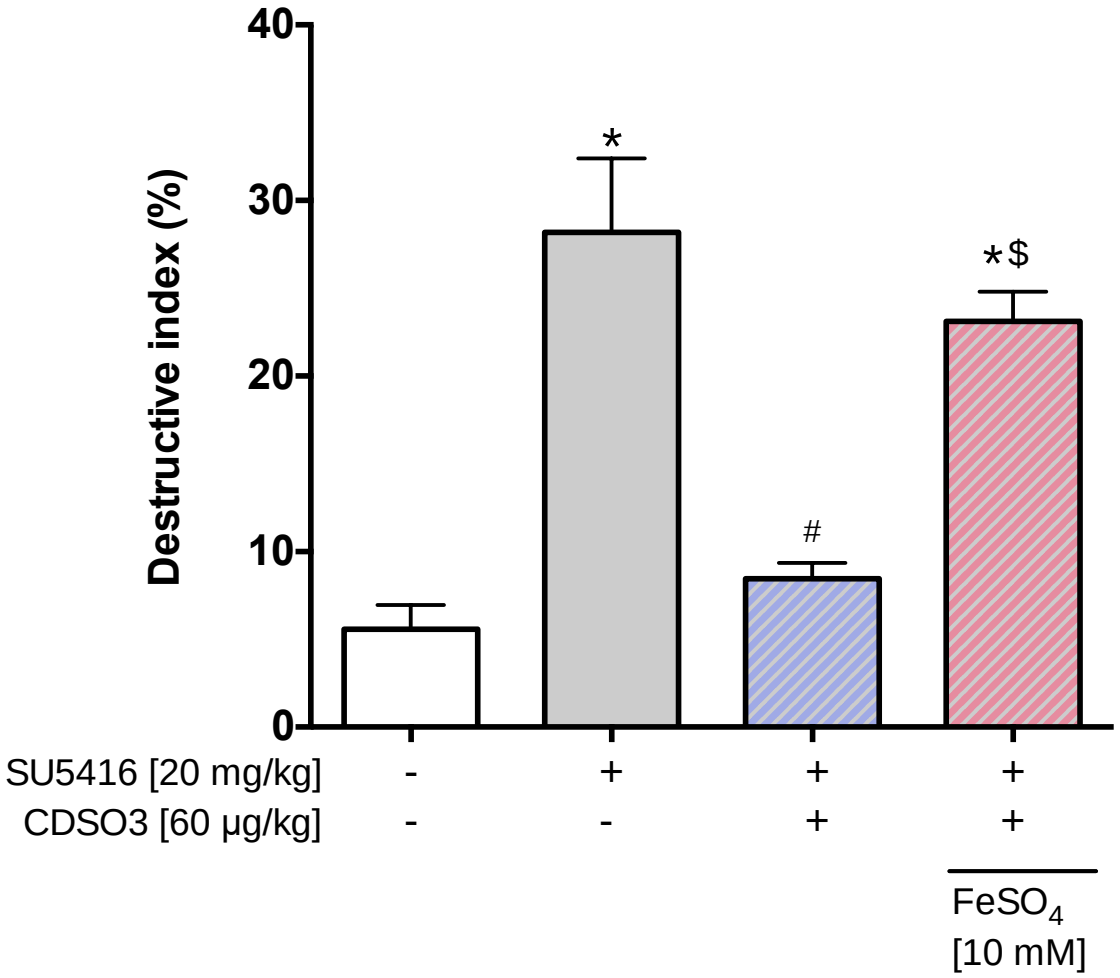

Figure 5.9: *In vivo* reversal of morphological alveolar destruction by CDSO3, as assessed by the destructive index. + = present; - = absent. Data represent mean±standard deviation (SD) from n=3; *p<0.05, compared to vehicle control; $^{\#}$p<0.05, compared to the SU5416-induced control; $^{\$}$p<0.05, compared to the SU5416-induced and CDSO3-treated group, by ANOVA and Tukey's multiple comparison test

5.3.4 EE, MLI, and DI correlations

The EE, MLI, and DI values for each animal in the four treatment groups were then plotted in Figures 5.10-5.12 to examine their three-way correlations. Correlations were clearly seen in that impaired functional EE was associated with emphysematous abnormalities of airspace morphology (MLI and DI), as shown in Figures 5.9 and 5.10, respectively. Lower EE correlated with larger MLI and DI values, suggesting that emphysematous rats with impaired exercise endurance exhibited increased alveolar airspace enlargement and destruction. In contrast, as shown in Figure 5.11, alveolar destruction/loss (DI) and size enlargement (MLI) in this disease animal model resulted in moderate correlations.

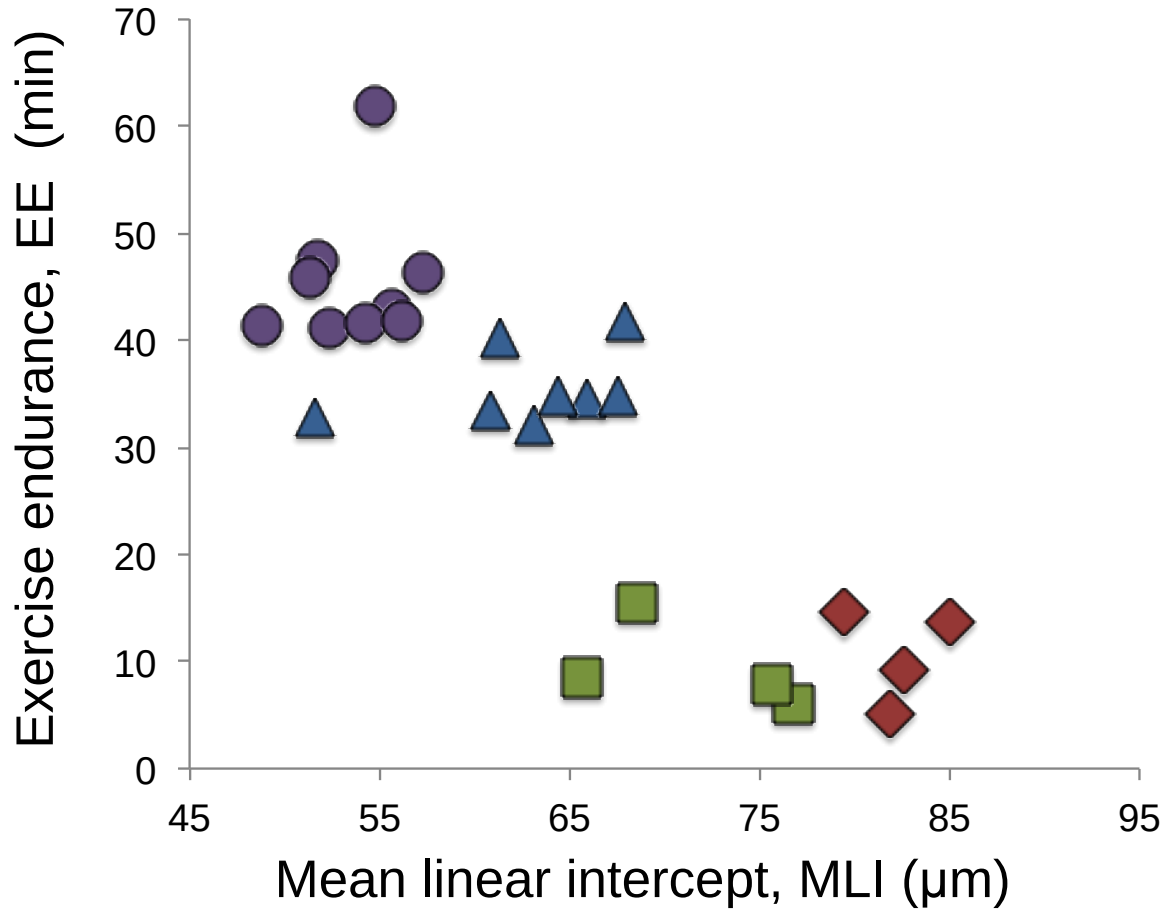

Figure 5.10: Correlation between functional EE and airspace enlargement (MLI). ● = Healthy control rats, ◆ = SU5416-induced, saline-treated rats, ▲ = SU5416-induced, CDSO3-treated rats, and ■ = SU5416-induced, CDSO3/FeSO4-treated rats

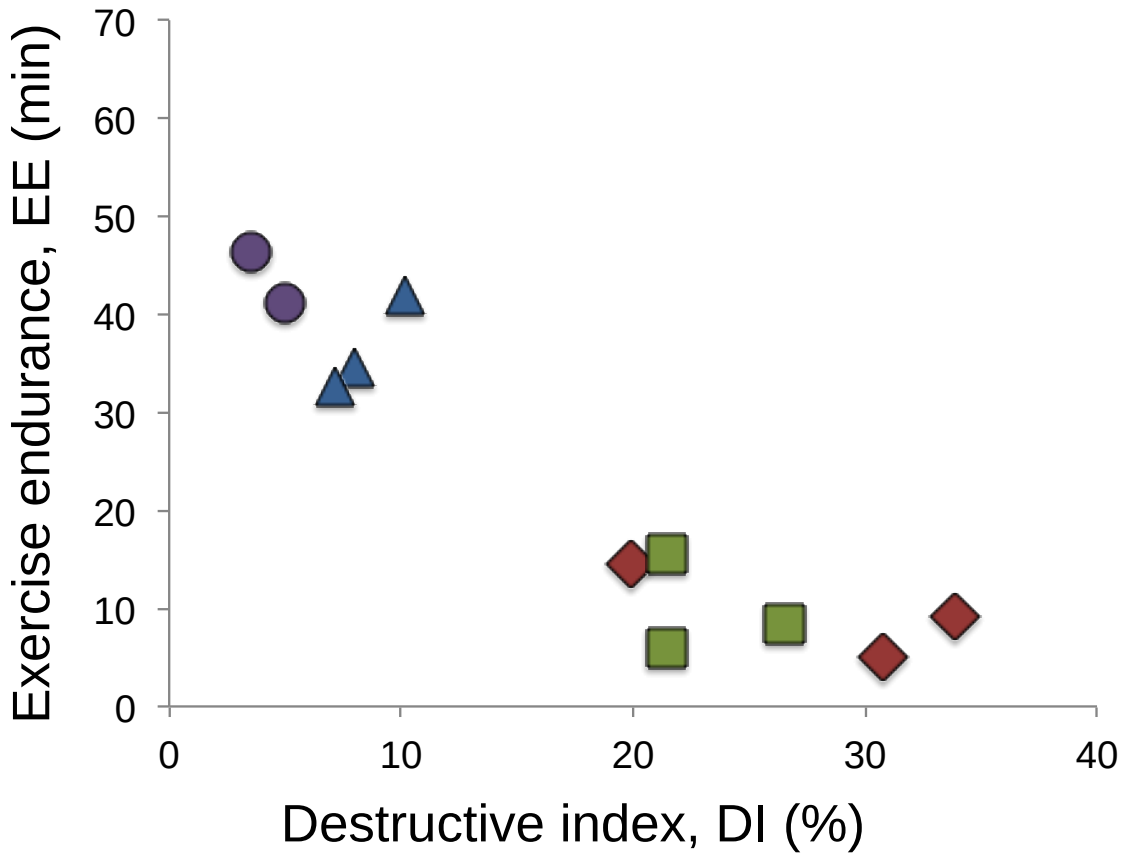

Figure 5.11: Correlation between functional exercise endurance (EE) and alveolar destruction (DI). ● = Healthy control rats, ◆ = SU5416-induced, saline-treated rats, ▲ = SU5416-induced, CDSO3-treated rats, and ■ = SU5416-induced, CDSO3/FeSO4-treated rats

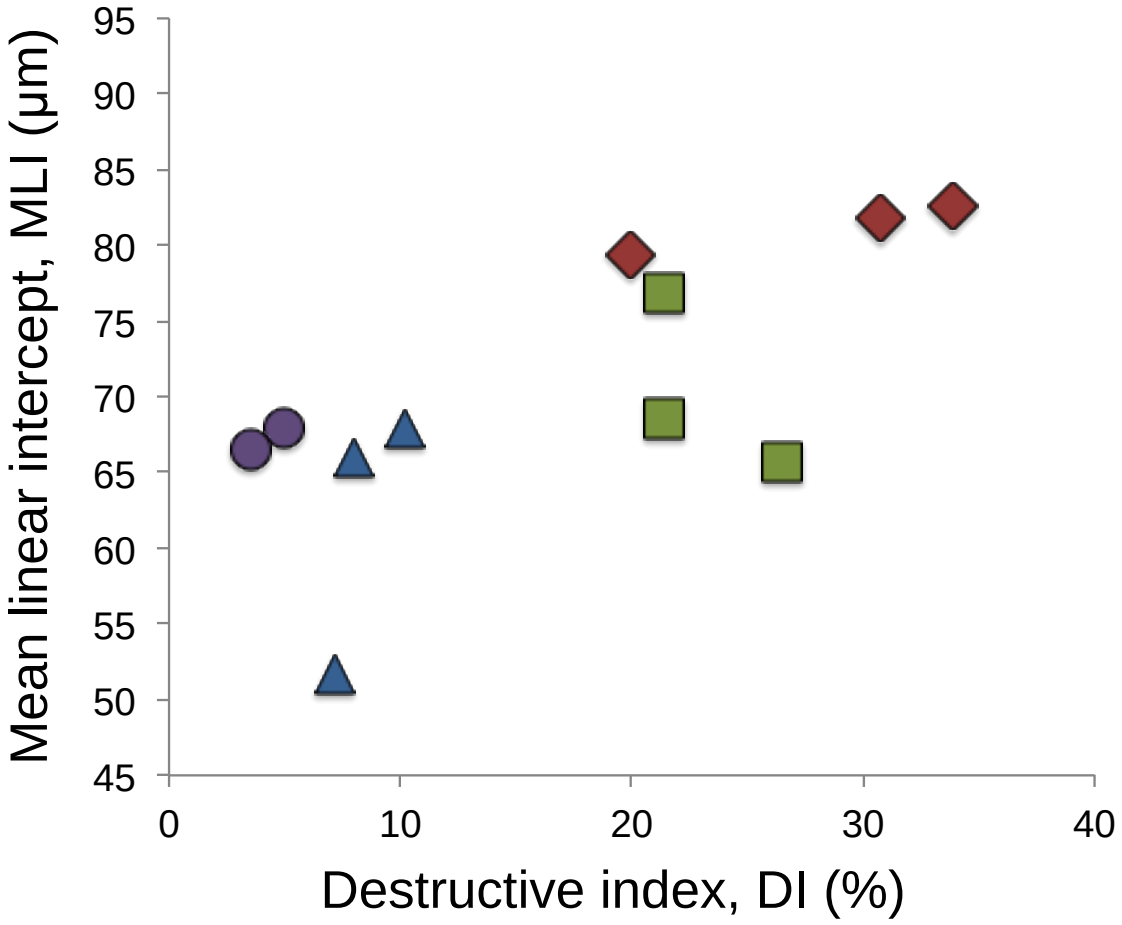

Figure 5.12: Correlation between alveolar airspace enlargement (MLI) and destruction (DI). ● = Healthy control rats, ◆ = SU5416-induced, saline-treated rats, ▲ = SU5416-induced, CDSO3-treated rats, and ■ = SU5416-induced, CDSO3/FeSO4-treated rats

5.3.5 Lung tissue expression of protein markers

The lung tissue expressions of several proteins were measured using Western blot analysis to clarify the mechanism of CDSO3's reversal of functional and morphological impairment, i.e. Fe^{2+} chelation-dependent hypoxia-inducible factor-1α (HIF-1α) stabilization/stimulation. Figure 5.13 show that VEGF receptor blockade with SU5416 did not significantly change the lung tissue expressions of histone deacetylase 2 (HDAC2) upstream. In addition, the lung tissue expressions of HIF-1α in cytoplasmic extracts were also unchanged, compared to those of the healthy control animals (Figure 5.14). Similarly, treatment with CDSO3 at 60 µg/kg also did not significantly change the expressions of HDAC2 or HIF-1α, when compared to both the healthy control animals and emphysematous animals. However, CDSO3 at 60 µg/kg administered into the lungs significantly increased the expression of VEGF by two-fold, compared to the healthy animals ($p<0.05$). Instillation of SU5416 significantly reduced the expression of VEGF by 52 % ($p<0.05$), but treatment with CDSO3 at 60 µg/kg in these emphysematous animals significantly normalized the expression of VEGF (Figure 5.15). Yet, the lung tissue expression of the pro-apoptotic marker, BAX, was unchanged across all treatment groups (Figures 5.16, 5.17). However, SU5416 at 20 mg/kg significantly increased the expression of cleaved caspase-3 by almost 1.5-fold, compared to the healthy control ($p<0.05$), and treatment with CDSO3 at 60 µg/kg in these emphysematous normalized the expression of cleaved caspase-3 almost to the level expressed in healthy control animals. Furthermore, when CDSO3 at 60 µg/kg was premixed with excess Fe^{2+} and then dosed to the lungs, the expression of cleaved

caspase-3 increased significantly by 3.3-fold compared to the expressions of healthy control animals ($p<0.05$).

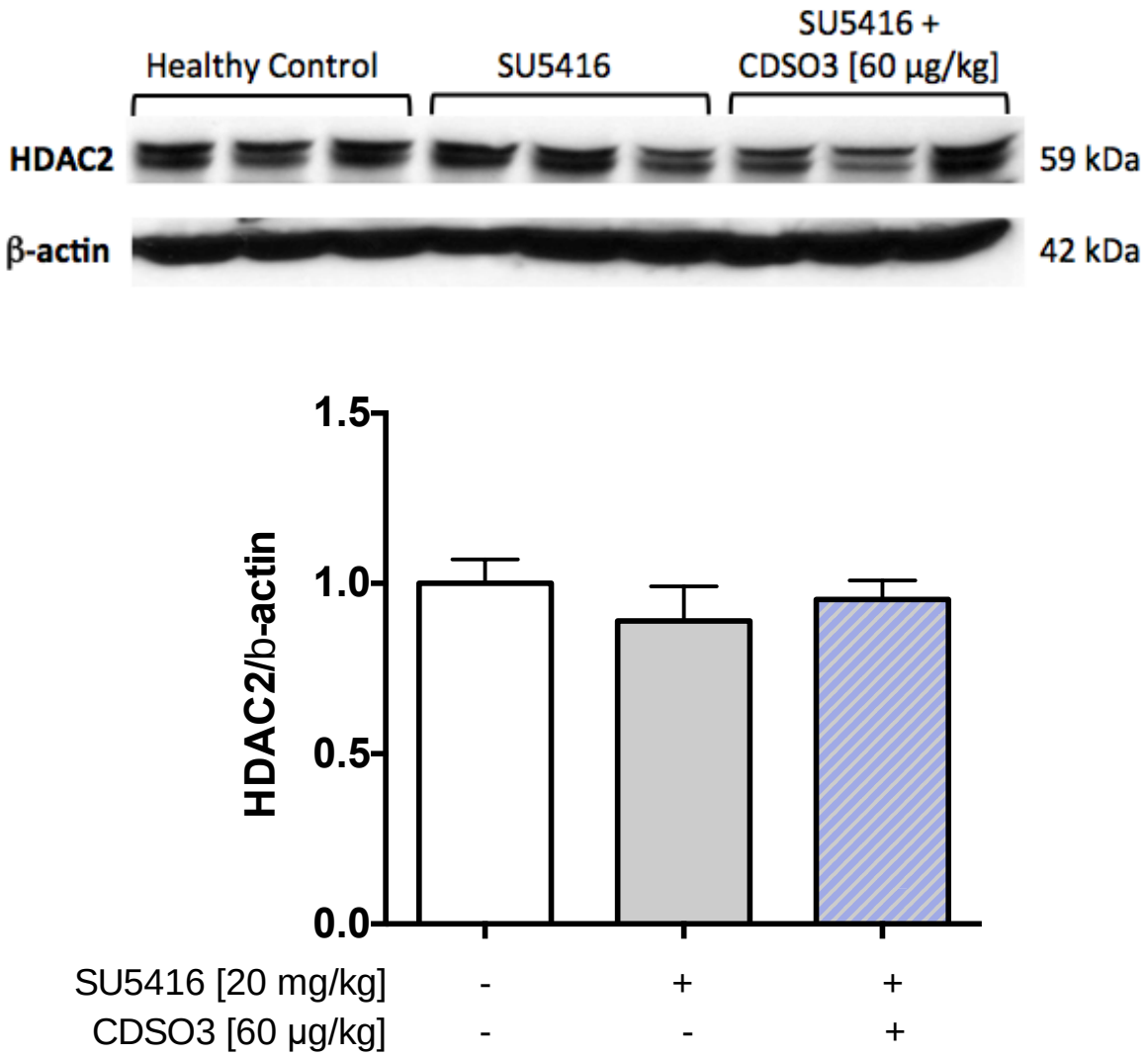

Figure 5.13. Rat lung tissue cytoplasmic expression of HDAC, as shown by bands at 59 kDa. Data represent mean±SD from n=3. + = present, - = absent

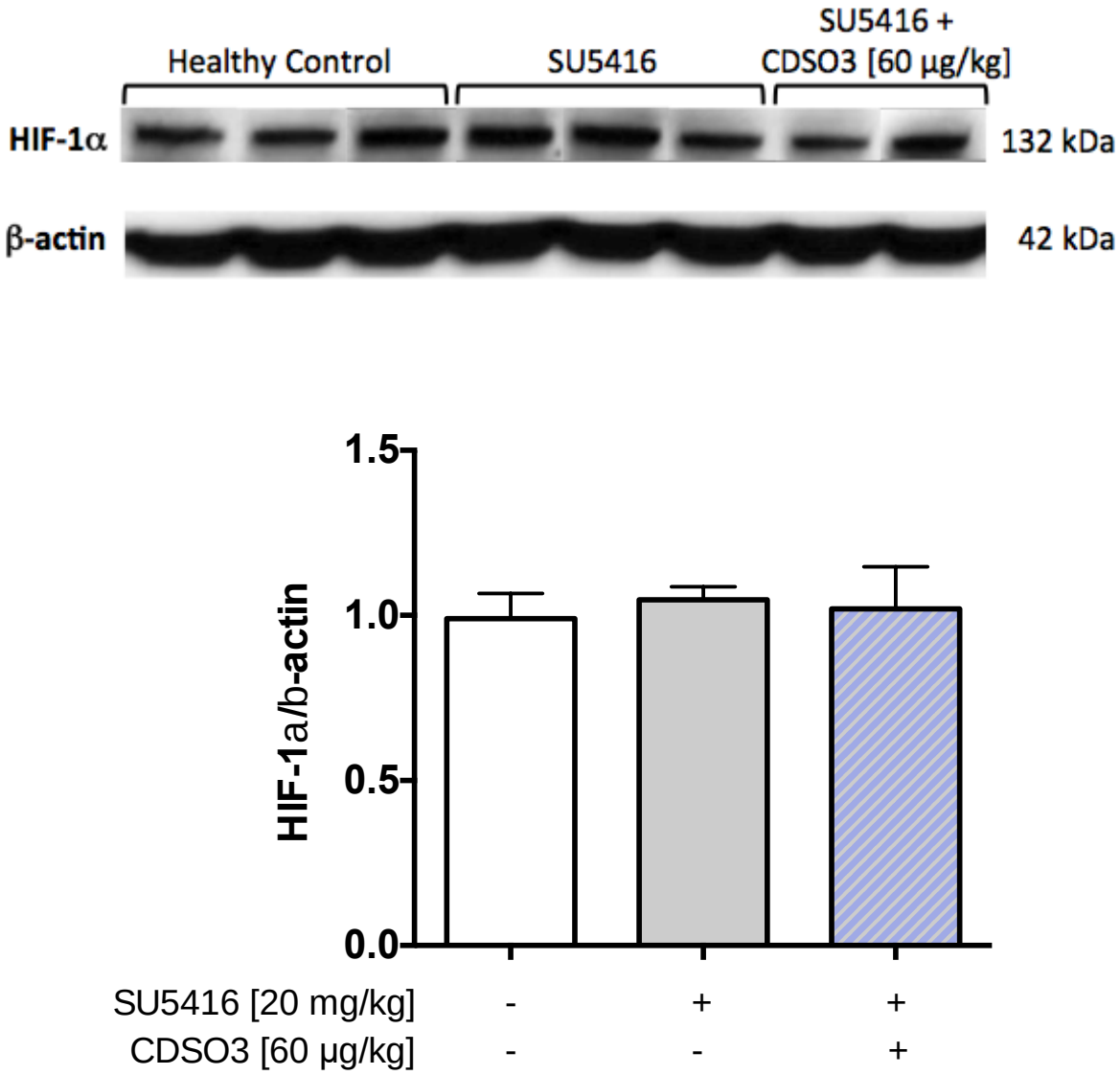

Figure 5.14. Rat lung tissue cytoplasmic expression of HIF-1α, as shown by bands at 132 kDa. Data represent mean±SD from n=3-4.

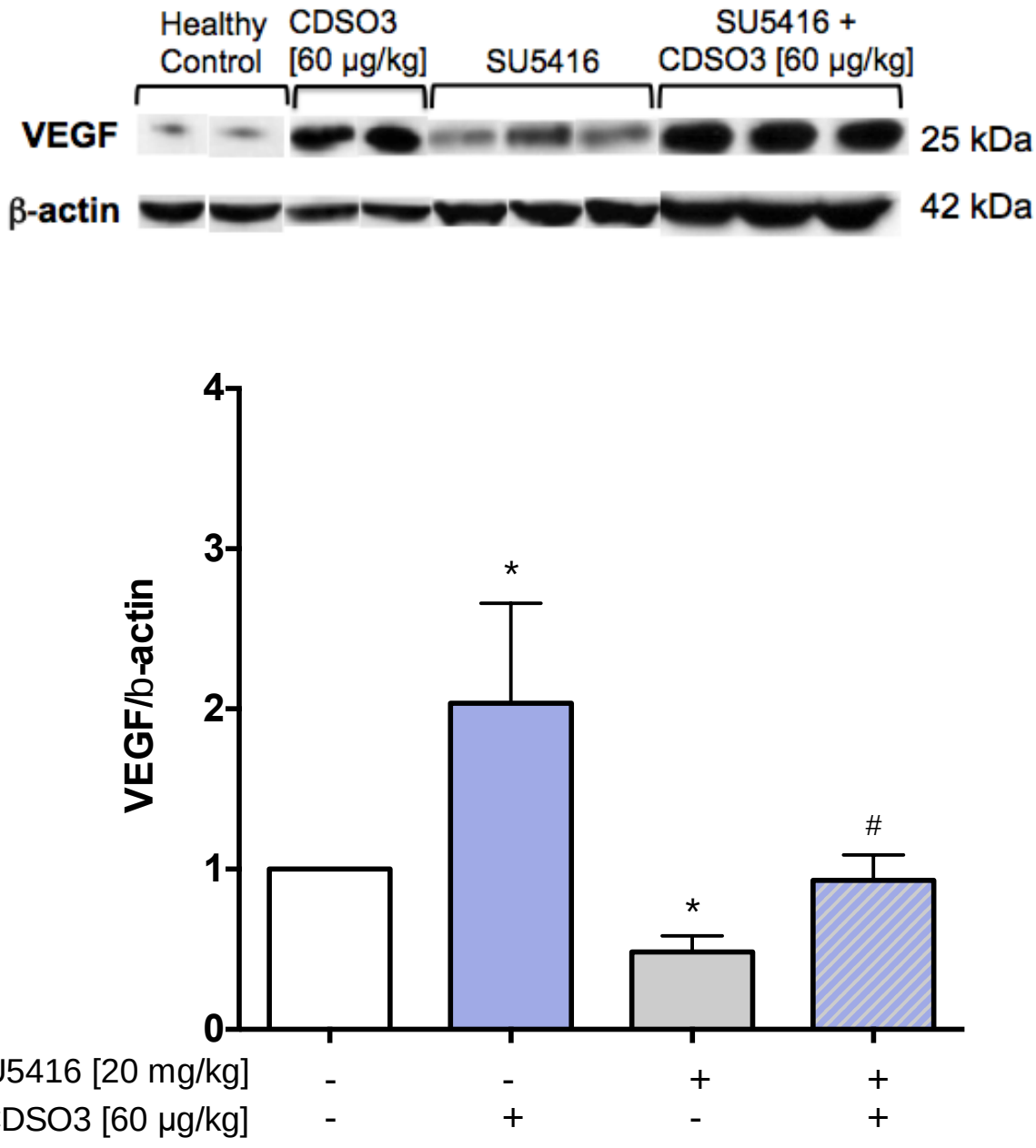

Figure 5.15. Rat lung tissue cytoplasmic expression of VEGF, as shown by bands at 25 kDa. Data represent mean±SD from n=3-4. *p<0.05, compared to the healthy control; #p<0.05, compared to the SU5416-induced animals, by ANOVA and Tukey's multiple comparison test

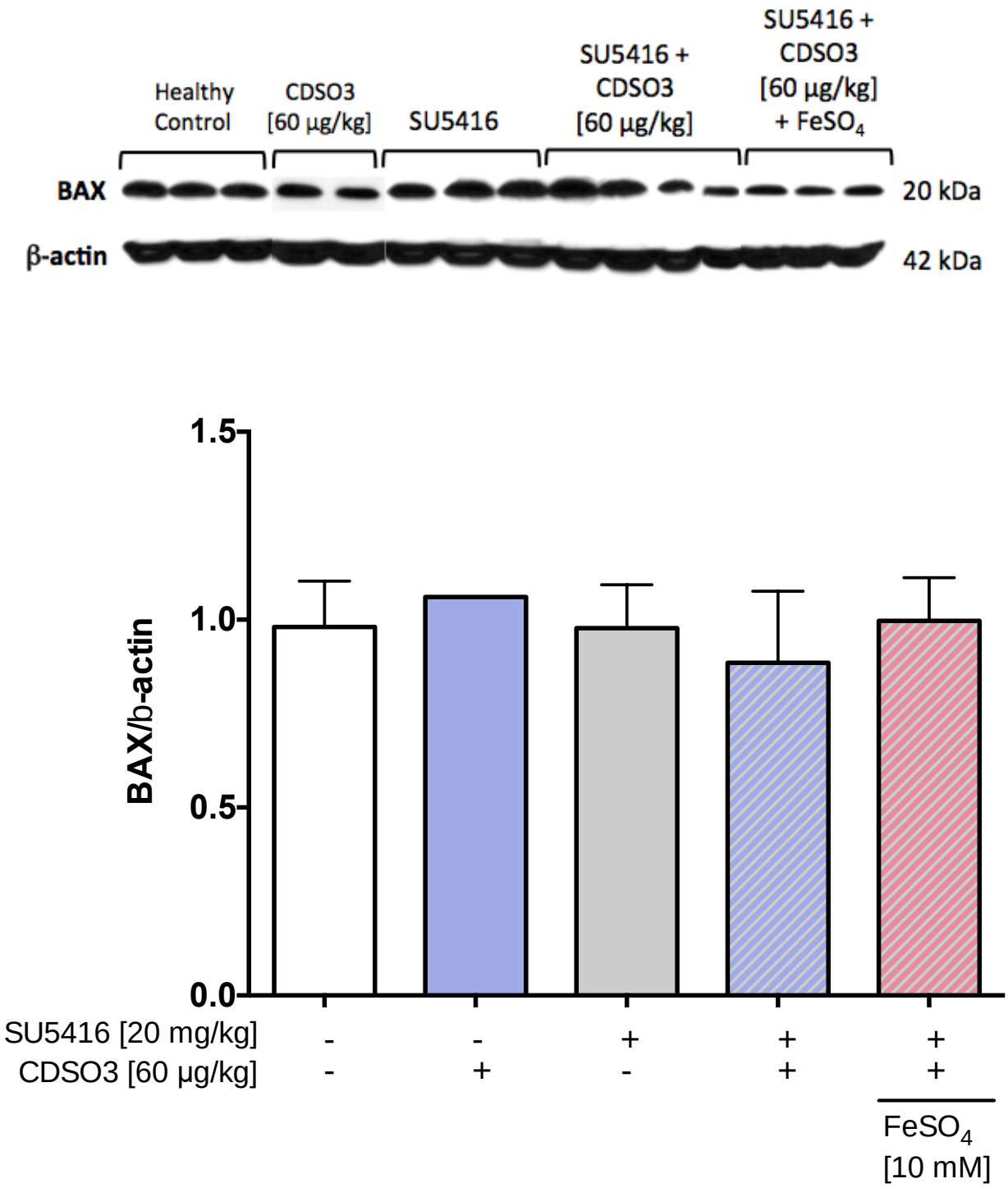

Figure 5.16. Rat lung tissue cytoplasmic expression of BAX, as shown by bands at 20 kDa. Data represent mean±SD from n=2-4.

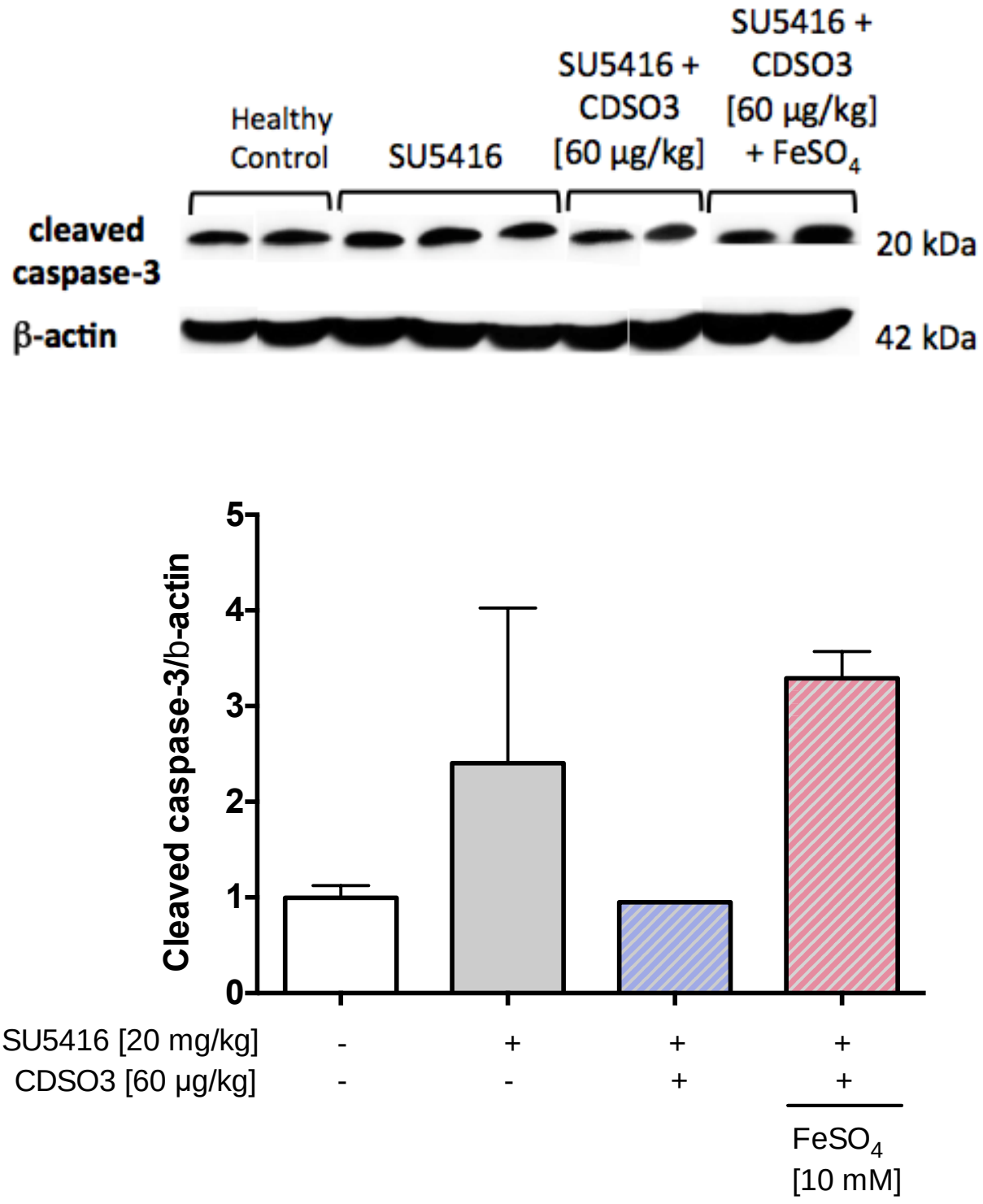

Figure 5.17. Rat lung tissue cytoplasmic expression of cleaved caspase-3. Data represent mean±SD from n=2-5.

5.4 DISCUSSION

The *in vivo* animal studies of pulmonary emphysema in this chapter have successfully demonstrated that pulmonary administration of the 3.3 kDa non-peptidic sulfated dehydropolymer of caffeic acid, CDSO3, significantly reversed functional and morphological impairments. The major findings for pulmonary administration of CDSO3 at 60 µg/kg are as follows: 1) SU5416-induced functional impairment (decreased EE), morphological airspace enlargement (increased MLI), and alveolar destruction (increased DI) were reversed by 66.5, 74.1, and 87.0 %; 2) the EE, MLI, and DI remained impaired when CDSO3 pre-mixed with excess Fe^{2+}; 3) reduced alveolar wall destruction is correlated with improvement in functional exercise endurance and airspace size; 4) decreased VEGF and increased caspase-3 are normalized.

5.4.1 CDSO3 reverses functional and morphological impairment

One SC injection of SU5416 at 20 mg/kg significantly ($p<0.05$) reduced the EE times by 80.8 % (43.3±6.8 → 8.3±2.8 min), and increased the MLI and DI by 46.5 % (56.1±6.0 → 82.2±2.3 µm) and 5-fold (5.6±2.4 → 28.2±7.3 %), respectively. Pulmonary administration of CDSO3 at 60 µg/kg for 2 weeks improved the EE, MLI, and DI by 66.5 % (8.3±2.8 min → 31.9±7.4 min), 74.1 % (82.2±2.3 → 62.9±5.2 µm), and 87.0 % (28.2±7.3 → 8.5±1.5 %). However, when CDSO3 was pre-mixed with excess Fe^{2+} (10 mM $FeSO_4$) and then administered to the lungs of these emphysematous rats, the alveolar structures remained destroyed, comparable to those seen in the SU5416-

induced rats, suggesting a Fe^{2+} chelation-dependent mechanism. These findings are consistent with CDSO3's reversal effects in the HSE/CSE and CSE models of pulmonary emphysema [Saluja *et al.,* 2014; Sakagami 2016].

5.4.2 Reduced alveolar wall destruction is correlated with improvement in functional exercise endurance and airspace size

Correlations were clearly seen in that impaired functional EE was associated with emphysematous abnormalities of airspace morphology (MLI and DI), suggesting that functional treadmill exercise endurance is a non-invasive test to predict emphysematous changes in the lung. Furthermore, alveolar destruction/loss (DI) resulted in a moderate correlation, yet still suggesting that their association in this disease model. These correlations confirm the definition of emphysema, as characterized by the destruction of the alveolar walls leading to airspace enlargement and reduced surface area for gas exchange, resulting in difficulty breathing.

5.4.3 CDSO3 increases the expression of VEGF and cleaved caspase-3, but not HDAC, HIF-1α, or BAX

SC SU5416 at 20 mg/kg reduced the expression of VEGF by two-fold and increased the expression of cleaved caspase-3 by about 1.5-fold, whereas pulmonary treatment with CDSO3 at 60 µg/kg significantly normalized both of these protein. However, neither induction with SU5416 at 20 mg/kg nor treatment with CDSO3 were

shown to alter the expressions of HDAC2, HIF-1α, or the pro-apoptotic marker, BAX. It is notable to mention that the expression of HIF-1α was measured from cytoplasmic extracts of lung tissue, which is rapidly degraded by HIF-PHD. It is the stabilized HIF-1α that translocates into the nucleus, where it is expected to dimerizes with HIF-1β to bind the hypoxia response element (HRE) of target genes to up-regulate VEGF, as discussed in Chapter 1. Therefore, it is necessary to measure the expression of HIF-1α from nuclear extracts of lung tissue to clarify these findings. Furthermore, HDAC2 is found up-stream of both HIF-1α and VEGF, therefore, its expression may be not be altered in by VEGF receptor blockade downstream.

5.5 CONCLUSIONS

A VEGF receptor blockade apoptotic model of pulmonary emphysema was induced in rats by a single orotracheal instillation of SU5416. CDSO3's Fe^{2+} and HIF-1α-dependent reversal of functional and morphological impairment was tested with its pulmonary administration at 60 µg/kg three times a week for two weeks after SU5416 instillation. The SU5416 instillation successfully caused functional impairment by decreasing the EE by 80.8 %, and both morphological airspace enlargement and destruction by increasing the MLI and DI values by 46.5 % and 5-fold, respectively, compared to those of healthy animals. CDSO3 at 60 µg/kg significantly reversed these functional and morphological impairments by 66.5, 74.1, and 87.0 % ($p<0.05$). However, when CDSO3 at 60 µg/kg was pre-mixed with excess Fe^{2+}, the EE, MLI, and DI all remained impaired. These results clearly suggested that CDSO3 at 60 µg/kg

administered to the lungs exerted significant *in vivo* reversal of functional and morphological impairments in an apoptotic model of *established* emphysema. However, when the lung tissue expressions of several proteins were measured in an attempt to clarify this reversal of functional and morphological impairments, the results were mixed and inconclusive. CDSO3 was found to up-regulate/normalize the expression of VEGF and cleaved caspase-3, but not HDAC2, HIF-1α, or BAX. Further studies are required to make conclusive statements about the mechanism of CDSO3's protective activities.

CHAPTER 6

SUMMARY AND GENERAL CONCLUSIONS

In this dissertation project, the therapeutic potential of sulfated dehydropolymer of caffeic acid (CDSO3) was further examined *in vitro* and *in vivo* as an oligomer drug entity for pulmonary delivery in the treatment of emphysema. Due to the polydispersity and heterogenous nature of its chemical structure, CDSO3 was tested for its batch-to-batch differences in ferrous (Fe^{2+}) chelation activity as well as its cytoprotective effect against apoptotic cell death. CDSO3's Fe^{2+} chelation and HIF-1α-dependent *in vitro* cytoprotective activity against different stimuli-induced emphysematous cell death was then assessed in three different cell lines involved in the pathogenesis of emphysema. It's ferrous chelating and cytoprotective activities were compared to those of two known chelators, DFO and EDTA. CDSO3's reversal of functional and morphological impairments, as well as stabilization/up-regulation of HIF-1α and HIF-regulating proteins were then assessed in an in vivo apoptotic model of established emphysema, while seeking correlations between exercise endurance, mean linear intercept, and alveolar destruction.

The *in vitro* assessment of ferrous (Fe^{2+}) chelating activity employed a ferrozine-chelation based competitive inhibition assay. Ferrous (Fe^{2+}) ion when bound by ferrozine, resulted in an absorbance at 562 nm, which was decreased in the presence

of a competitive chelator molecule, i.e., CDSO3. The IC_{50} and HS values were derived from non-linear regression curve-fitting. Two batches of CDSO3, i.e., $CDSO3_{BH}$ and $CDSO3_{MT}$, exhibited comparable Fe^{2+} chelation activity with IC_{50} values of 23.3±2.1 (95 % CI: 18.6, 28.0) and 17.0±1.4 (95% CI: 13.6, 20.5) µM, respectively. The HS values were 1.2±0.1 (95 % CI: 0.9, 1.4) and 1.4±0.2 (95 % CI: 1.0, 1.8), indicating an approximately 1:1 stoichiometry for CDSO3 and Fe^{2+} chelation. These IC_{50} and HS values were comparable to those of known chelators, DFO and EDTA. Furthermore, CDSO3 did not seem to exhibit ferric (Fe^{3+}) chelation activity in the concentration range of 0-50 µM, suggesting its chelation is specific for divalent ions.

The *in vitro* pro-inflammatory TNF-α release was measured using an enzyme-linked immunosorbent assay (ELISA). 1% CSE caused significant ~20-fold increase in TNF-a release compared to the vehicle control, and CDSO3 was shown to inhibit this CSE-induced TNF-α release in a concentration-dependent manner from 1-25 µM, reaching significance at 5 µM (~49 % inhibition). The trypan blue exclusion (TBE) and lactate dehydrogenase (LDH) assays were used to assess the *in vitro* cytoprotective activities using rat alveolar macrophage (NR8383), human alveolar epithelial (A549) and microvascular lung endothelial (HMVEC-L) cells. Cell death was induced with CSE, H_2O_2, HSE, TSA, and SU5416. The HIF-1α inhibitors (CAY10585 or Echinomycin) or excess Fe^{2+} ($FeSO_4$ or $FeCl_2$) or Fe^{3+} ($FeCl_3$) were added to clarify CDSO3's Fe^{2+} chelation-dependent HIF-1α up-regulatory mechanism of cytoprotection. CDSO3 at 10 µM consistently inhibited these 3-7-fold induced cell death by about 63-154 % in all three cell lines, and was shown to be more potent than both the monomer (CA) and the un-sulfated oligomer (CD), suggesting that oligomerization and sulfation play key roles

in its protection. Furthermore, the addition of both HIF-1α inhibitors and excess Fe^{2+}, regardless of the co-ion, all opposed CDSO3's cytoprotective activities; excess Fe^{3+} did not have the same effects. The chelators DFO and EDTA did not exhibit cytoprotection despite their equipotent Fe^{2+} chelation activities, due to their large size and hydrophilicity.

CDSO3's Fe^{2+}- and HIF-1α-dependent reversal of lung damages in an *in vivo* rat model of apoptotic emphysema induced by VEGF receptor blockade was tested. SU5416 induction reduced the EE by 80.8 %, and increased the airspace enlargement (MLI) and destruction (DI) by 46.5 and 5-fold, respectively. Pulmonary delivery of CDSO3 at 60 µg/kg significantly improved EE by 66.5 $ to 31.9±7.4 min, and reversed MLI and DI impairments by 74.1 and 87.0 %. However, when CDSO3 was premixed with excess Fe^{2+}, the EE, MLI, and DI all remained impaired. Furthermore, a correlation was clearly seen with impaired EE and emphysematous abnormalities of both MLI, whereas a moderate correlation was seen between DI and MLI. SC SU5416 at 20 mg/kg reduced the expression of VEGF by two-fold and increased the expression of cleaved caspase-3 by about 1.5-fold, whereas pulmonary treatment with CDSO3 at 60 µg/kg significantly normalized both of these protein. However, neither induction with SU5416 at 20 mg/kg nor treatment with CDSO3 were shown to alter the expressions of HDAC2, HIF-1α, or the pro-apoptotic marker, BAX. It is notable to mention that the expression of HIF-1α was measured from cytoplasmic extracts of lung tissue, which is rapidly degraded by HIF-PHD. It is the stabilized HIF-1α that translocates into the nucleus, where it is expected to dimerizes with HIF-1β to bind the hypoxia response element (HRE) of target genes to up-regulate VEGF, as discussed in Chapter 1.

Therefore, it is necessary to measure the expression of HIF-1α from nuclear extracts of lung tissue to clarify these findings. Furthermore, HDAC2 is found up-stream of both HIF-1α and VEGF, therefore, its expression may be not be altered in by VEGF receptor blockade downstream.

Appendix 1

Trypan Blue Exclusion Assay

1. After 18-24 h incubation, the incubation media (200 µl) was removed from the 48-well plate and transferred into labeled 1.5 ml microcentrifuge tubes (MCT #1)*.
2. The cells were washed with either 200 µl warm PBS (NR8383 and A549) or HEPES (HMVEC-L) twice; a total of 400 µl of PBS or HEPES was recovered into the microcentrifuge tubes (MCT #1).
3. 200 µl of warm trypsin-EDTA was added to each well, and the plate was allowed to sit at room temperature for 3-4 minutes to allow the cells to detach. The cells were viewed under the microscope to assure that the majority (>90%) of the cells were detached. An additional 200 µl of incubation media (NR8383 and A549) or trypsin neutralizing solution (TNS; HMVEC-L) was added to each well, and repeated pipetting was carried out to assure all the cells were detached. A total of 400 µl was transferred into labeled 1.5 ml microcentrifuge tubes (MCT #2).
4. The tubes (MCT #1 and MCT #2) were centrifuged (Eppendorf Centrifuge 5415 C) at 12,000 revolutions per minute (RPM) for 3-4 minutes and the supernatant was carefully discarded, leaving the cell pellets at the bottom of the tubes.

5. The cell pellets from MCT #1 and MCT #2 were re-suspended and combined using 100 µl of fresh incubation media.
6. Trypan blue solution, 4% (Amresco; Solon, OH) was filtered using a 5 ml syringe (Becton, Dickinson and Company, BD; Franklin Lakes, NJ) and 0.4-µm filter (Drummond Scientific Company; Broomall, PA); 100 µl was added to the re-suspended cells and allowed to sit for 4-5 minutes.
7. The tubes were centrifuged at 12,000 RPM for 3-4 minutes; the supernatant was carefully removed and discarded. The cell pellet was re-suspended with 200 µl fresh incubation media and plated into a new 48-well plate and allowed to sit for at least 2 h to allow the cells to settle.
8. Using a microscope (Omax, Kent, WA; 100x magnification) and ToupViewX (Omax, Kent, WA), at least 8-10 images were taken to allow $\geq$300 cells to be counted. Stained blue cells were considered dead and clear/white cells were considered live.
9. % cell death was calculated as:

   (total blue cells/total cells) x 100.

10. *If the LDH assay was performed, MCT #1 was centrifuged at 12,000 for 3-4 minutes after Step 1, and the supernatant was transferred into newly labeled microcentrifuge tubes and stored in -70^{o}C until ready to use for the LDH assay. Proceed to Step 2, and combined the cell pellet remaining in MCT #1 with the 400 µl of PBS or HEPES from Step 2.

Appendix 2

Treadmill running training protocol

Day 1: Place the rat in the treadmill and close the cover. Turn on the electric shock and watch the rat's movements for 5 minutes. After 5 minutes, start the treadmill at the speed of 2.0 m/min and slowly increase the speed by 1.0-m/m increments when rat learns to avoid the electric shock area. When the speed reaches 5.0 m/min, set the timer to 5 minutes. After 5 minutes, stop the treadmill, and place the rat back into its cage. Repeat the procedure 3 hours later.

Day 2: Place the rat in the treadmill and close the cover. Turn on the electric shock and start the treadmill at the speed of 3.0 m/min. Slowly increase the speed by 1.0-m/min increments when the rat learns to avoid the electric shock area. When the speed reaches 7.0 m/min, set the timer for 10 minutes. After 10 minutes, stop the treadmill, and place the rat back into its cage. Repeat the procedure three hours later.

Day 3: Place the rat in the treadmill and close the cover. Turn on the electric shock and start the treadmill at the speed of 3.0 m/min. Slowly increase the speed by 1.0-m/min increments when the rat learns to avoid the electric shock area. When the speed reaches 10 m/min, set the timer for 10 minutes. After 10 minutes, stop the treadmill and place the rat back into its cage. Repeat the procedure three hours later.

Day 4: Place the rat in the treadmill and close the cover. Turn on the electric shock and start the treadmill at the speed of 10 m/m. Set the timer for 15 minutes. After 15 minutes, stop the treadmill and place the rat back into its cage. Repeat the procedure three hours later.

Days 5-10: Place the rat in the treadmill and close the cover. Turn on the electric shock and start the treadmill at the speed of 10 m/min. Set the timer for 30 minutes. After 30 minutes, stop the treadmill and place the rat back into its cage.

Criteria for a well-trained rat: running on the treadmill without touching the electric shock for at least 3 minutes.

Treadmill Running Test

1. Turn on the treadmill and the electric shock.
2. Raise the height of the treadmill to a 5 degree angle
3. Place the rat on the treadmill and start at a speed of 10 m/min. Start the timer
4. Carefully watch the rat's running and record how many times it touches the shocks in the first 2 minutes.
5. After 2 minutes, record the time of each shock for 5 shocks total.
6. When the rat's running time is over 30 minutes, raise the treadmill angle to 10 degree. When the running time is over 40 minutes, raise the angle to 15 degree.

REFERENCES

REFERENCES

Andersson M, Stridsman C, ronmark E, Lindberg A, Emtner M. Physical activity and fatigue in chronic obstructive pulmonary disease – a population based study. *Respir Med* 2015:109:1048-1057

Arany Z, Huang LE, Eckner R. An essential role for p300/CBP in the cellular response to hypoxia. *Proc Nat Academ Sci USA* 1996; 93:12969-12973

ATCC Product Information Sheet: A549 (ATCC CCL-185), American Type Culture Collection. Available online at: http://www.atcc.org/products/all/CCL-185.aspx#documentation

ATCC Product Information Sheet: NR8383 (ATCC CRL-2192), American Type Culture Collection. Available online at: http://www.atcc.org/products/all/CRL-2192.aspx#documentation

Barnes PJ. Mediators of chronic obstructive pulmonary disease. *Pharmacol Rev* 2004; 56:515-548

Barnes PJ, Shapiro SD, Pauwels RA. Chronic obstructive pulmonary disease: molecular and cell mechanisms. *Eur Respir J* 2003; 22:672-688

Barnes PJ, Stockley RA. COPD: current therapeutic interventions and future approaches. *Eur Respir J* 2005;25:1084-1086

Barnes PJ. Histone deacetylase-2 and airway disease. Ther Adv Respir Dis 2009; 3:235-243

Bissonnette EY, Tremblay GM, Turmel V, Pirotte B, Reboud-Ravaux M. Coumarinic derivatives show anti-inflammatory effects on alveolar macrophages, but their anti-elastase activity is essential to reduce lung inflammation in vivo. *Int Immunopharmacol* 2009;9:49-54

Biswas SK, McClure D, Jiminez LA, Megson IL, Rahman I. Curcumin induces glutathione biosynthesis and inhibits NF-kappaB activation and interleukin-8 release in alveolar epithelial cells: mechanism of free radical scavenging activity. *Antioxid Redox Signal* 2005;7:32-41

Buist AS, McBurnie MA, Vollmer WM. BOLD Collaborative Research Group. International variation in the prevalence of COPD (the BOLD Study): a population-based prevalence study. *Lancet* 2007;370:741-750

Celli B, Cote C, Marin J. The body-mass index, airflow obstruction, dyspnea and exercise capacity index in chronic obstructive pulmonary disease. *N Engl J Med* 2004;350:1004-1012

Churg A, Wang RD, Tai H, Wang X, Xie C, Wright JL. Tumor necrosis factor-alpha drives 70% of cigarette smoke-induced emphysema in the mouse. Am J Respir Crit Care Med 2004; 170:492-498

de Boer WI, Alagappan VK, Sharma HS. Molecular mechanisms in chronic obstructive pulmonary disease; potential targets for therapy. *Cell Biochem Biophys* 2007; 47:131-148

Demedts IK, Demoor T, Bracke KR, Joos GF, Brusselle GG. Role of apoptosis in the pathogenesis of COPD and pulmonary emphysema. *Respir Res* 2006; 7:53

Demeo DL. The SERPINE2 gene is associated with chronic obstructive pulmonary disease. *Am J Hum Genet* 2006;78:253-264

Dinis TCP, Madeira VMC, Almeida LM. Action of phenolic derivatives (acetaminophen, salicylate, and 5-aminosalicylate) as inhibitors of membrane lipid peroxidation as peroxyl radical scavenbers. *Arc Biochem Biophys* 1994; 315:161-169

eBioscience Product Information Sheet: Mouse TNF alpha ELISA Ready-Set-Go! (88-7324). Available online at: http://www.ebioscience.com/media/pdf/tds/88/88-7324.pdf

Eidelman DH, Ghezzo H, Kim WD, Cosio MG. The destructive index and early lung destruction in smokers. *Am Rev Resp Dis* 1991;144:156-159

Ellis L, Hammers H, Pili R. Targeting tumor angiogenesis with histone deacetylase inhibitors. *Canc Let* 2009 280:145-153

Epstein J, Sanderson IR, Macdonald TT. Curcumin as a therapeutic agent: the evidence from n vitro animal and human studies. *Br J Nutri* 2010;103:1545-1557

Fallica J, Boyer L, Kim B, et al. Macrophage migration inhibitory factor is a novel determinant of cigarette smoke-indced lung damage. *Am J Respir Cell Molec Biol* 2014; 51:94-103

Fan L, Li J, Yu Z, Dang X, Wang K. The hypoxia-inducible factor pathway, prolyl hydroxylase domain protein inhibitors, and their roles in bone repair and regeneration. *Biomed Res Int* 2014; 1-11

Fischer BM, Pavlisko E, Voynow JA. Pathogenic triad in COPD: oxidative stress, protease-antiprotease imbalance, and inflammation. *Int J Chron Obstruct Pulmon Dis* 2011;6: 413-21

Ford ES, Murphy LB, Khavjou O, Giles WH, Holt JB, Croft JB: Total and state-specific medical and absenteeism costs of COPD among adults aged ≥ 18 years in the United States for 2010 and projections through 2020. *Chest* 2015;147: 31-45.

Foreman MG, DeMeo DL, Hersh CP. Polymorphic variation in surfactant protein B is associated with COPD exacerbations. *Eur Respir J* 2008;32:938-944

Gerber HP, Dixit V, Ferrara N. Vascular endothelial grwoth factor induces expression of the antiapoptotic proteins Bcl-2 and A1 in vascular endothelial cells. J Biol Chem 1998(a);273:13313-13316

Gerber HP, McMurtrey A, Kowalski J, Yan M, Keyt BA, Dixit V, Ferrara N. Vascular endothelial growth factor regulates endothelial cell survival through the phosphtaidylinositol 3'-kinase/Akt signal transduction pathway: requirement for Flk-1/KDR activation. J Biol Chem 1998(b);273:30336-30343

Giatromanolaki A, Koukourakis MI, Pezzella F, Turley H, Sivridis E, Bouros D, Bougioukas G, Harris AL, Gatter KC. Expression of prolyl hydroxylases PHD-1, 2, and 3 and of the asparagine hydroxylase FIH in non-small cell lung cancer relates to an activated HIF pathway. *Canc Let* 2008; 262:87-93

Giordano RJ, Lahdenranta J, Zhen L, Chukwueke U, Petrache I, Langley RR, Fidler IJ, Pasqualini R, Tuder RM, Arap W. Targeted induction of lung endothelial cell apoptosis causes emphysema-like changes in the mouse. *J Biol Chem* 2008;283:29447-29460

Global Initiative for Chronic Obstructive Lung Disease. Global strategy for the diagnosis, management, and prevention of chronic obstructive pulmonary disease [Updated 2016]. Available from: http://www.goldcopd.org/uploads/users/files/WatermarkedGlobal%20Strategy%202016(1).pdf. Accessed April 2016

Hanania NA, Donohue JF. Pharmacologic interventions in chronic obstructive pulmonary disease: bronchodilators. *Proc Am Thorac Soc* 2007;4:526-534

Hansel TT, Barnes PJ. New drugs for exacerbations of chronic obstructive pulmonary disease. *Lancet* 2009;374:744-755

Henry BL, Monien BH, Bock PE, Desai UR. Anovel allosteric pathway of thrombin inhibition: exosite II mediated potent inhibition of thrombin by chemo-enzymatic, sulfated dehydropolymers of 4-hydroxycinnamic acids. *J Biol Chem* 2007;282:31891-31898

Henry BL, Desai UR. Sulfated low molecular weight lignins, allosteric inhibitors of coagulation proteinases via the heparin binding site, significantly alter the active site of thrombin and factor xa compared to heparin. *Thromb Res* 2014;134:1123-1129

Henson PM, Vandivier RW, Douglas IS. Cell death, remodeling, and repair in chronic obstructive pulmonary disease? *Proc Am Thorac Soc* 2006; 3:713-717

Hersh CP, DeMeo DL, Silverman EK. National emphysema treatment trial state of the art: genetics of emphysema. Proc Am Thorac Soc 2008;5:486-493

Hioki H, Aoki N, Kawano K, Homori M, Hasumura Y, Yasumura T, Maki A, Yoshino H, Yanagisawa A, and Ishikawa K. Acute effects of cigarette smoke on platelet-dependent thrombin generation. *Eur Heart J* 2001;22:56-61

Hodge S, Hodge G, Holmes M, Reynolds PN. Increased airway epithelial and T-cell apoptosis in COPD remians despite smoking cessation. *Eur Respir J* 2005; 25:447-454

Hutchison DCS, Cook PJL, Barter CE, Harris H, Hugh-Jones P. Pulmonary emphysema and α1-antitrypsin deficiency. Brit Med J 1971; 1:689-694

Imai K, Mercer BA, Schulman LL, Sonette JR, D'Armiento JM. Correlation of lung surface area to apoptosis and proliferation in human emphysema. *Eur Respir J* 2005; 25:250-258

Ito K, Lim S, Caramori G, Chung KF, Barnes BJ, Adcock IM. Cigarette smoking reduces histone deaceytlase 2 expression, enhances cytokine expression and inhibits glucorticoid actions in alveolar macrophages. *FASEB J* 2001;15:1100-1102

Ito K, tomita T, Barnes PJ, Adcock IM. Oxidative stress reduces histone deactylase (HDAC)2 activity and enhances IL-8 gene expression:role of tyrosine nitration. Biochem Biophys Res Commun 2004;315:240-245

Ito K, Ito M, Elliott WM, Cosio B, Caramori G, Kon OM. Decreased histone deacetylase activity in chronic obstructive pulmonary disease. *N Engl J Med* 2005(a); 352:1967-1976

Ito I. Matrix metalloproteinase-9 promotor polymorphism associated with upper lung domnant emphysema. *Am J Respir Crit Care Med* 2005(b);172:1378-1382

Ivan M, Kondo K, Yang H. HIFa targeted for VHL-mediated destruction by proline hydroxylation: implications for O_2 sensing. *Science* 2001;292:468-672

Jaakkola P, Mole DR, tian YM. Targeting of HIFa to the von Hippel-Lindau ubiquitylation complex by O_2-regulated prolyl hydroxylation. *Science* 2001; 292:468-472

Karpman C, Benzo R. Gait speed as a measure of functional status in COPD patients. *Int J Chron Obstruc Pulmon Dis* 2014;9:1315-1320

Kasahara Y, Tuder RM, Taraseviciene-Stewart L, Le Cras TD, Abman S, Hirth PK, Waltenberger J, Voelkel NF. Inhibition of VEGF receptors causes lung cell apoptosis and emphysema. *J clin Invest 2000*; 106:1311-1319

Kasahara Y, Tuder RM, Cool CD, Lynch DA, Flores SC, Voelkel NF. Endothelial cell death and decreased expression of vascular endothelial growth factor and vascular endothelial growth factor receptor 2 in emphysema. *Am J Respi Crit Care Med* 2001;163:737-744

Koblizek V, Novotna B, Zbozinkova Z, Hejduk K. Diagnosing COPD: advances in training and practice – a systematic review. *Adv Med Educ Pract* 2016;7:219-231

Lee J, Hanaoka M, Kitaguchi Y, Kraskauskas D, Shapiro L, Voelkel NF, Taraseviciene-Stewart, L. Imbalance of apoptosis and cell proliferation contributes to the development and persistance of emphysema. *Lung* 2012; 190:69-82

Lonza Product Information Sheet: Clonetics Endothelial Cell System, Lonza Walkersville, Inc. Available online at: http://bio.lonza.com/uploads/tx_mwaxmarketingmaterial/Lonza_ManualsProductInstructions_Instructions__Technical_Info_-_Endothelial_Cell_Systems.pdf

Masson N, Willam C, Maxwell PH, Pugh CW, Racliffe PJ. Independent function of two destruction domains in hypoxia-inducbile factor-a chains activated by prolyl hydroxylation. *EMBO J* 2001; 20:5197-5206

Maxwell PH, Wlesener MS, Chang GW. The tumour suppressor protein VHL targets hypoxia-inducible factors for oxygen-dependent proteolysis. *Nature* 1999;399:271-275

McCauley L, Markin C, Hosmer D. An unexpected consequence of electronic cigarette use. *Chest* 2012; 141:1110-1113

McRobbie H, Bullen C, Hartmann-Boyce J, Hajek P. Electronic cigarettes for smoking cessation and reduction. Cochrane Database Syst Rev 2014;12

Messer K, Trinidad DR, Al-Delaimy WK, Pierce JP. Smoking cessation rates in the United States: a comparison of young adults and older smokers. Res Pract 2008; 98:317-322

Mie Lee Y, Kim SH, Kim HS, Jin Son M, Nakajima H, Jeong Kwon H, Kim KW. Inhibition of hypoxia-induced angiogenesis by FK228, a specific histone deacetylase inhibitor, via suppression of HIF-1alpha activity. *Biochem Biophys Res Commun* 2003 300:241-246

Mizuno S, Yasuo M, Bogaard HJ, Kraskauskas D, Natarajan R, Voelkel NF. Inhibition of histone deacetylase casues emphysema. *Am J Physiol Lung Cel Molec Physiol* 2011;300:L402-L413

Monien BH, Henry BL, Rahuraman A, Hindle M, Desai UR. Novel chemo-enzymatic oligomers of cinnamic acids as direct and indirect inhibitors of coagulation proteinases. *Bioorg Med Chem* 2006; 14: 7988-7998

Mulhall P, Criner G. Non-pharmacological treatments for COPD. *Respirology* 2016: 1-19

Murray CJ, Lopez AD. Alternative projections of mortality and disability by cause 1990-2020: global burden of disease study. *Lancet* 1996; 349:1498-1504

Nakajoh M, Fukushima T, Suzuki T, Yamaya M, Nakayama K, Sekizawa K, Sasaki H. Retinoic acid inhibits elastase-induced injury in human lung epithealial cell lines. *Am J Respir Cell Mol Biol* 2003;28:296-304

National Heart, Lung, and Blood Institute Fact Book 2012: 4. Disease Statistics [http://www.nhlbi.nih.gov/about/documents/factbook/2012/chapter4]. Last accessed January 1, 2016

Neufeld G, Coehn T, gengrinovitch S, Poltarak Z. Vascular endothelial growth factor (VEGF) and its receptors. FASEB J 1999;13:9-22

Ohh M, Park CW, Ivan M. Ubiquitination of hypoxia-inducible factor requires direct binding to the b-domain for the von Hippel-lindau protein. *Nature Cell Biol* 2000;2:423-427

Piper ME, Smith SS, Schlam TR, fiore MC, Jorenby DE, Fraser D, Baker TB. A randomized placebo-controlled clinical trial of 5 smoking cessation pharmacotherapies. *Arch Gen Psychiatry* 2009;66:1253-1262

Qian DZ, Kachlap SK, Collis SJ, Verheul HM, Carducci MA, Atadja P, Pili R. Class II histone deacetylases are associated with VHL-independent regulation of hypoxia-inducible factor 1 alpha. *Canc Res* 2006;66:8814-8821

Rahman I. Oxidative stress, transcription factors and chromatin remodeling in lung inflammation. *Biochem Pharmacol* 2002;64:935-942

Rahman I, Biswas SK, Kirkham PA. Regulation of inflammation and redox signaling by dietary polyphenols. *Biochem Pharmacol* 2006;72:1439-1452

Roche N, Marthan R, Berger P, Chambellan A, Chanez P, Aguilanieu B. Beyond corticosteroids: future prospects in the management of inflammation in COPD. *Eur Respir Rev* 2011;20:175-182

Roth M. Pathogenesis of COPD. Parth III. Inflammation in COPD. *Int J Tub Lung Dis* 2008;12:375-380.

Rycroft CE, Heyes A, Lanza L, Becker K. Epidemiology of chronic obstructive pulmonary disease: a literature review. *Int J Chron Obstruct Pulmon Dis* 2012;7:457-494

Saluja B, Li H, Desai UR, Voelkel NF, Sakagami M. Sulfated caffeic acid dehydropolymer attenuates elastase and cigarette smoke extract-induced emphysema in rats: sustained activity and a need for pulmonary delivery. *Lung* 2014; 192:481-492

Saluja B, Thakkar JN, Li H, Desai UR, Sakagami M. Novel low molecular weight lignins as potential antiemphysema agents: in vitro triple inhibitory activity against elastase, oxidation and inflammation. *Pulm Pharmacol Therap* 2013; 26:296-304

Sandford AJ, Joos L, Pare PD. Genetig risk factors for chronic obstructive pulmonary disease. *Curr Opin Pulm Med* 2002;8:87-94

Sang N, Fang J, Srinivas V, Leshchinsky I, Caro J. Carboxyl-terminal transactivation activity of hypoxia-inducible factor1a is goberned by a von Hippel-Lindau protein-independent, hydroxylation-regulated association with p300/CBP. *Mol Cel Biol* 2002;22:2984-2992

Sears JE, Hoppe G. Stimulating retinal blood vessel protection within hypoxia-inducible factor stabilization: indentification of novel small moelcule hydrazones to inhibit hypoxia-inducible factor prolyl hydroxylase (an American opthalmological society thesis). *Trans Am Opthalmol Soc* 2013;111:169-179

Siddiq A, Aminova LR, Troy CM, Suh K, Messer Z, Semanza GL, Rata RR. Selective inhibion of hypoxia-inducible factor proly-hydroxylase 1 mediates neuroprotection against normoxic oxidative death via HIF and CREB independent pathways. *J Neuro* 2009; 29:8828-8838

Sigma-Aldrich Product Information Sheet TOX7: In Vitro Toxicology Assay Kit, Lactic Dehydrogenase Based. Available online at: https://www.sigmaaldrich.com/content/dam/sigma-aldrich/docs/Sigma/Bulletin/tox7bul.pdf

Snider GL, Kleinerman J, Thurlbeck WM, Bengali ZH. The definition of emphysema. *Am Rev Respir Dis* 1985; 132:182-185

Stockley RA, Mannino D, Barnes PJ. Burden and pathogenesis of chronic obstructive pulmonary disease. *Proc Am Thorac Soc* 2009;6:524-526

Stridsman C, Lindberg A, Skar L. Fatigue in chronic obstructive pulmonary disease: a qualitative study of people's experiences. *Scand J Caring Sci* 2014;28:130-138

Suki B, Lutchen KR, Ingenito EP. On the progressive nature of emphysema. *Am J Resp Crit Care Med* 2003; 168:516-521

Sullivan SD, Ramsey SD, Lee TA. The economic burden of COPD. *Chest* 2000; 117:5S-9S

Suzuki M, Betsuyaku T, Nagai K. Decreased airway expression of vascular endothelial growth factor in cigarette smoke-induced emphysema in mice and COPD patients. Inhal Toxicol 2008; 20: 349-359

Taraseviciene-Stewart L, Voelkel NF. Molecular pathogenesis of emphysema. *J Clin Invest* 2008;118:394-402

Thompson ML. Physiochemical and structural analysis of polymers as putative drugs. Doctoral Dissertation 2015. Virginia Commonwealth University

Thurlbeck W. Internal surface area and other measurements in emphysema. *Thorax* 1967;22:483-496

Tuder RM, Petrache I. Pathogenesis of chronic obstructive pulmonary disease. *J Clin Invest* 2012; 122:2749-2755

Tuder RM, Voelkel NF: Pathobiology of emphysema. In *Chronic Obstructive Lung Diseases* (Volume 2). Edited by Voelkel NF, MacNee W. BC Decker, Inc., Ontario Canada:2008:63-75

Voelkel NF, Gomez-Arroyo J, Mizuno S: COPD/emphysema: the vascular story. *Pulm Circ* 2011;1: 320-6

Voelkel NF, Vandivier RW, Tuder RM. Vascular endothelial growth factor in the lung. *Am J Physiol Lung Cell Mol Physiol* 2006; 290: L209-L221

Wannamethee SG, Lowe GD, Shaper AG, Rumley A, Lennon L, Whincup PH. Associations between cigarette smoking, piper/cigar smoking, and smoking cessation, and haemostatic and inflammatory markers for cardiovascular disease. *Eur Heart J* 2005;26:1765-1773

Watsky EJ, Gong J, Williams KE, Reeves KR. Varnicline, an alpha4beta2 nicotinic acetylcholine receptor partial agonist, vs sustained-release buproprion and placebo for smoking cessation: a randomized controlled trial. *JAMA* 2006;296:47-55

Wise RA, Tashkin DP. Optomizing treatment of chronic obstructive pulmonary disease: an assessement of current therapy. *Am J Med* 2007;120:S4-13

Yanbaeva DG, Dentener MA, Creutzberg EC, Wesseling G, Wouters EFM. Systemic effects of smoking. *Chest* 2007;131:1557-1566

Yang IA, Seeney SL, Wolter JM. Mannose-binding lectin gene polymorphism predicts hospital admissions for COPD infections. *Genes Immun* 2003;4:269-274

Yang SR, Chida AS, Bautler MR, Shafiq N, Seweryniak K, Maggirwar SB, Kilty I, Rahman I. Cigarette smoke inducs proinflammatory cytokine release by activiation of NF-kappaB and posttranslational modifications of histone deacetylase in macrophages. *Am J Physiol Lung Cell Mol Physiol* 2006;29:L46-57

Yasuo M, Mizuno S, Kraskauskas D, Bogaard HJ, Natarajan R, Cool CD, Zamora M, Voelkel NF. Hypoxia inducible factor-1a in human emphysema lung tissue. *Eur Resp J* 2011;37:775-783

Yokohori N, Aoshiba K, Nagai A. Increased levels of cell death and proliferation in alveolar wall cells in patients with pulmonary emphysema. *Chest* 2004; 125:626-632

Yoshida T, Tuder RM. Pathobiology of cigarette smoke-induced chronic obstructive pulmonary disease. *Physiol Rev* 2007; 87:1047-1082

VITA

Tien M. Truong was born on April 16, 1986, in My-Xuyen, Vietnam. She immigrated to the United States in 1993 and is currently an American citizen. She received her Bachelor of Science in Biology at the University of Virginia (UVA), Charlottesville, Virginia, in 2008. In Fall 2009, she was admitted to the Doctor of Pharmacy (Pharm.D.) program at Virginia Commonwealth University (VCU) School of Pharmacy (SOP), Richmond, Virginia. As a Pharm.D. student, she was award the VCU Graduate/Professional Student Scholarship and the VCU SOP AD Williams Pharmacy Scholarship. She also received the Dean's Summer Research Fellowship in Summer 2010, where she started investigating CDSO3 as a novel drug entity for emphysema. That following fall, she presented her research findings at the VCU SOP Research and Career Day, where her poster received honorable mention amongst all Pharm.D. posters. In Fall 2010, she was accepted into the Pharm.D./Ph.D. combined degree program with graduate assistantship in the Department of Pharmaceutics, with Dr. Masahiro Sakagami as her advisor. During the graduate program, she has authored 6 abstracts and proceedings, and now has 2 research manuscripts in preparation. She has also made a total of 12 presentations in a podium or poster format within and outside VCU. Notably, she received the Graduate Student Award for best poster at the VCU SOP Research and Career Day in 2014. In 2014, she was 1 of 4 students in the nation to receive the Express Scripts Scholar Award from the American Association of Colleges of Pharmacy. In 2015, her poster presentation at the American Thoracic Society received the Dr. Sreedhar Nair Memorial Scholarship for Top Abstracts in Emphysema from the National Emphysema Foundation and 2 travelships from the VCU Graduate Student Travel Grant and the VCU Pharmaceutics Joseph P. Schwartz Travel Award. She has also received 2 other travelships from the VCU Graduate Student Travel Grant and the Sigma Delta Epsilon – Graduate Women in Science (SDE GWIS) Travel Grant to present her research at the American Association of Pharmaceutical Scientists (AAPS) meeting in Orland, Florida and the SDE-GWIS National Meeting in State College, Pennsylvania. Her extended abstract proceeding for Respiratory Drug Delivery (RDD) conference was selected for Posters on the Podium in 2016.

DATA SHEETS

In vitro data sheets

In vitro anti-cell death activity assessment – Trypan blue exclusion assay

NR8383 – Vehicle Control

	Stained Dead	Unstained Live	Total	% Stained Dead
n=1	5	97	102	4.90
n=2	21	389	410	5.12
n=3	40	498	538	7.43
n=4	63	425	488	12.91
n=5	54	549	603	8.96
n=6	12	137	149	8.05
n=7	30	164	194	15.46
n=8	10	313	323	3.10
n=9	22	226	248	8.87
			Mean	**8.31**
			SD	**3.92**
			SE	**1.31**

NR8383 – 3% CSE

	Stained Dead	Unstained Live	Total	% Stained Dead
n=1	14	53	67	20.90
n=2	12	51	63	19.05
n=3	16	50	66	24.24
n=4	16	29	45	35.56
			Mean	**24.94**
			SD	**7.40**
			SEM	**3.70**

NR8383 – 5% CSE

	Stained Dead	Unstained Live	Total	% Stained Dead
n=1	59	165	224	26.34
n=2	45	115	160	28.13
n=3	58	122	180	32.22
n=4	54	149	203	26.60
			Mean	**28.32**
			SD	**2.72**
			SE	**1.36**

NR8383 – 10% CSE

	Stained Dead	Unstained Live	Total	% Stained Dead
n=1	57	64	121	47.11
n=2	37	35	72	51.39
n=3	57	76	133	42.86
n=4	22	28	50	44.00
n=5	64	183	247	25.91
n=6	82	262	344	23.84
n=7	95	222	317	29.97
n=8	63	175	238	26.47
n=9	62	68	130	47.69
n=10	50	139	189	26.46
n=11	77	165	242	31.82
n=12	74	189	263	28.14
			Mean	**35.47**
			SD	**10.23**
			SE	**2.95**

NR8383 – 50% CSE

	Stained Dead	Unstained Live	Total	% Stained Dead
n=1	113	27	140	80.71
n=2	143	81	224	63.84
n=3	159	59	218	72.94
n=4	183	78	261	70.11
			Mean	**71.90**
			SD	**7.00**
			SE	**3.50**

NR8383 – 10% CSE + 1 µM CDSO3

	Stained Dead	Unstained Live	Total	% Stained Dead	% Inhibition
n=1	100	211	311	32.15	12.21
n=2	69	217	286	24.13	41.77
n=3	68	256	324	20.99	53.33
n=4	61	218	279	21.86	50.10
			Mean	**24.78**	**39.35**
			SD	**5.09**	**18.74**
			SE	**2.54**	**13.25**

NR8383 – 10% CSE + 5 µM CDSO3

	Stained Dead	Unstained Live	Total	% Stained Dead	% Inhibition
n=1	65	116	181	35.91	NA
n=2	46	217	263	17.49	66.20
n=3	47	221	268	17.54	66.03
n=4	54	182	236	22.88	46.36
			Mean	**23.46**	**59.53**
			SD	**8.68**	**11.41**
			SE	**4.34**	**6.59**

NR8383 – 10% CSE + 10 µM CDSO3

	Stained Dead	Unstained Live	Total	% Stained Dead	% Inhibition
n=1	44	203	247	17.81	65.03
n=2	31	247	278	11.15	89.55
n=3	23	274	297	7.74	102.10
n=4	31	238	269	11.52	88.19
n=5	42	222	264	15.91	72.02
n=6	58	309	367	15.80	72.43
n=7	37	276	313	11.82	87.08
n=8	41	385	426	9.62	95.18
			Mean	**12.67**	**83.95**
			SD	**3.48**	**12.81**
			SE	**1.23**	**4.53**

NR8383 – 10% CSE + 25 µM CDSO3

	Stained Dead	Unstained Live	Total	% Stained Dead	% Inhibition
n=1	38	338	376	10.11	93.39
n=2	54	380	434	12.44	84.79
n=3	68	286	354	19.21	59.88
n=4	42	296	338	12.43	84.85
			Mean	**13.55**	**80.73**
			SD	**3.93**	**14.48**
			SE	**1.97**	**7.24**

NR8383 – 10% CSE + 25 µM CD

	Stained Dead	Unstained Live	Total	% Stained Dead	% Inhibition
n=1	18	49	67	26.87	31.69
n=2	13	38	51	25.49	36.75
n=3	11	28	39	28.21	26.75
n=4	7	58	65	10.77	90.95
			Mean	**22.83**	**46.53**
			SD	**8.12**	**29.89**
			SE	**4.06**	**14.94**

A549 – Vehicle control

	Stained Dead	Unstained Live	Total	% Stained Dead
n=1	3	159	162	1.85
n=2	4	141	145	2.76
n=3	8	176	184	4.35
n=4	5	143	148	3.38
n=5	6	94	100	6.00
n=6	19	759	778	2.44
n=7	23	652	675	3.41
n=8	18	777	795	2.26
n=9	13	720	733	1.77
n=10	21	707	728	2.88
n=11	10	678	688	1.45
n=12	8	432	440	1.82
n=13	3	231	231	1.30
n=14	10	411	411	2.43
n=15	10	307	317	3.15
n=16	27	630	657	4.11
n=17	9	369	388	2.32
n=18	18	725	743	2.42
n=19	24	732	756	3.17
n=20	23	643	666	3.45
n=21	13	770	783	1.66
n=22	15	693	708	2.12
n=23	13	605	618	2.10
n=24	6	387	393	1.53
n=25	4	369	373	1.07
n=26	3	291	294	1.02
			Mean	**2.56**
			SD	**1.13**
			SE	**0.22**

A549 – CDSO3 10 µM

	Stained Dead	Unstained Live	Total	% Stained Dead
n=1	4	178	182	2.20
n=2	5	229	234	2.14
n=3	4	130	134	2.99
n=4	5	349	354	1.41
n=5	4	337	341	1.17
n=6	10	322	332	3.01
			Mean	**2.15**
			SD	**0.77**
			SE	**0.31**

A549 – 10% CSE

	Stained Dead	Unstained Live	Total	% Stained Dead
n=1	52	606	658	7.90
n=2	54	566	620	8.71
n=3	41	483	524	7.82
n=4	64	612	676	9.47
n=5	63	674	737	8.55
n=6	71	825	896	7.92
			Mean	**8.40**
			SD	**0.65**
			SE	**0.26**

A549 – 10% CSE + CDSO3 10 µM

	Stained Dead	Unstained Live	Total	% Stained Dead	% Inhibition
n=1	18	632	650	2.77	96.20
n=2	26	652	678	3.83	78.98
n=3	16	545	561	2.85	94.78
n=4	16	796	812	1.97	109.86
n=5	16	786	802	2.00	109.44
n=6	11	519	530	2.08	108.06
			Mean	**2.58**	**99.39**
			SD	**0.73**	**12.45**
			SE	**0.30**	**5.08**

A549 – 10% CSE + CDSO3 10 µM + $FeSO_4$ 50 µM

	Stained Dead	Unstained Live	Total	% Stained Dead
n=1	52	623	675	7.70
n=2	41	355	396	10.35
n=3	30	458	488	6.15
			Mean	**8.07**
			SD	**2.13**
			SE	**1.23**

A549 – 10% CSE + CDSO3 10 µM + Ech 10 µM

	Stained Dead	Unstained Live	Total	% Stained Dead
n=1	60	458	518	11.58
n=2	77	523	600	12.83
n=3	68	580	648	10.49
			Mean	**11.64**
			SD	**1.17**
			SE	**0.68**

A549 – 0.1 mM H_2O_2

	Stained Dead	Unstained Live	Total	% Stained Dead
n=1	13	113	126	10.32
n=2	8	102	110	7.27
n=3	13	169	182	7.14
n=4	20	116	136	14.71
			Mean	**9.86**
			SD	**3.55**
			SE	**1.78**

A549 – 0.1 mM H_2O_2 + CDSO3 1 µM

	Stained Dead	Unstained Live	Total	% Stained Dead	% Inhibition
n=1	11	199	210	5.24	63.20
n=2	10	221	231	4.33	75.63
n=3	5	186	191	2.62	99.03
			Mean	**4.06**	**79.29**
			SD	**1.33**	**18.19**
			SE	**0.77**	**10.50**

A549 – 0.1 mM H_2O_2 + CDSO3 10 µM

	Stained Dead	Unstained Live	Total	% Stained Dead	% Inhibition
n=1	5	215	220	2.27	103.79
n=2	4	187	191	2.09	106.25
n=3	4	147	151	2.65	98.59
			Mean	**2.34**	**102.88**
			SD	**0.28**	**3.91**
			SE	**0.16**	**2.26**

A549 – 0.1 U/ml HSE

	Stained Dead	Unstained Live	Total	% Stained Dead
n=1	7	169	176	3.98
n=2	3	108	111	2.70
n=3	6	169	175	3.43
n=4	11	94	105	10.48
n=5	15	187	187	7.43
			Mean	**5.60**
			SD	**3.28**
			SE	**1.46**

A549 – 0.1 U/ml HSE + CDSO3 1 µM

	Stained Dead	Unstained Live	Total	% Stained Dead
n=1	8	292	300	2.67
n=2	8	209	217	3.69
n=3	13	120	133	9.77
			Mean	**5.38**
			SD	**3.84**
			SE	**2.22**

A549 – 0.1 U/ml HSE + CDSO3 10 µM

	Stained Dead	Unstained Live	Total	% Stained Dead
n=1	4	232	236	1.69
n=2	2	190	192	1.04
n=3	2	119	121	1.65
			Mean	**1.46**
			SD	**0.37**
			SE	**0.21**

A549 – 1 U/ml HSE

	Stained Dead	Unstained Live	Total	% Stained Dead
n=1	22	152	174	12.64
n=2	17	124	141	12.06
n=3	36	101	137	26.28
			Mean	**16.99**
			SD	**8.05**
			SE	**4.65**

A549 – 1 U/ml HSE + CDSO3 1 µM

	Stained Dead	Unstained Live	Total	% Stained Dead	% Inhibition
n=1	6	186	192	3.13	96.00
n=2	5	147	152	3.29	94.86
n=3	11	172	183	6.01	76.02
			Mean	**4.14**	**88.96**
			SD	**1.62**	**11.22**
			SE	**0.94**	**6.48**

A549 – 1 U/ml HSE + CDSO3 10 µM

	Stained Dead	Unstained Live	Total	% Stained Dead	% Inhibition
n=1	4	206	210	1.90	104.45
n=2	8	95	103	7.77	63.86
n=3	2	125	127	1.57	106.73
			Mean	**3.75**	**91.68**
			SD	**3.48**	**24.12**
			SE	**2.01**	**13.92**

A549 – 1 µM TSA

	Stained Dead	Unstained Live	Total	% Stained Dead
n=1	41	472	513	7.99
n=2	41	552	593	6.91
n=3	46	601	647	7.11
			Mean	**7.34**
			SD	**0.57**
			SE	**0.33**

A549 – 1 µM TSA + CDSO3 1 µM

	Stained Dead	Unstained Live	Total	% Stained Dead
n=1	39	790	829	4.70
n=2	35	717	732	4.65
n=3	36	715	751	4.79
			Mean	**4.72**
			SD	**0.07**
			SE	**0.04**

A549 – 1 µM TSA + CDSO3 10 µM

	Stained Dead	Unstained Live	Total	% Stained Dead
n=1	36	795	831	4.33
n=2	22	710	732	3.01
n=3	22	539	561	3.92
			Mean	**3.75**
			SD	**0.68**
			SE	**0.39**

A549 – 2 µM TSA

	Stained Dead	Unstained Live	Total	% Stained Dead
n=1	22	219	241	9.13
n=2	42	485	485	8.66
n=3	24	276	252	8.70
n=4	27	358	385	7.01
n=5	44	430	474	9.28
n=6	34	303	337	10.09
n=7	46	439	485	9.48
n=8	45	414	459	9.80
n=9	57	580	580	8.95
			Mean	**9.01**
			SD	**0.89**
			SE	**0.30**

A549 – 2 µM TSA + CDSO3 1 µM

	Stained Dead	Unstained Live	Total	% Stained Dead
n=1	24	360	384	6.25
n=2	13	364	387	5.94
n=3	16	385	401	3.99
			Mean	**5.39**
			SD	**1.23**
			SE	**0.71**

A549 – 2 µM TSA + CDSO3 10 µM

	Stained Dead	Unstained Live	Total	% Stained Dead	% Inhibition
n=1	19	370	389	4.88	63.38
n=2	19	455	474	4.01	76.84
n=3	16	392	408	3.92	78.17
n=4	13	355	368	3.53	84.14
n=5	30	475	505	5.94	47.16
n=6	24	348	372	6.45	39.32
n=7	11	396	407	2.70	96.89
n=8	13	337	350	3.71	81.35
n=9	23	379	402	5.72	50.53
			Mean	**4.54**	**68.64**
			SD	**1.27**	**19.48**
			SE	**0.42**	**11.24**

A549 – 2 µM TSA + CDSO3 10 µM + CAY 10 µM

	Stained Dead	Unstained Live	Total	% Stained Dead
n=1	31	351	382	8.12
n=2	24	256	280	8.57
n=3	24	285	309	7.77
n=4	46	421	467	9.85
n=5	41	380	421	9.74
n=6	36	341	377	9.55
			Mean	**8.93**
			SD	**0.90**
			SE	**0.37**

A549 – 2 µM TSA + CDSO3 10 µM + Ech 10 µM

	Stained Dead	Unstained Live	Total	% Stained Dead
n=1	28	226	254	11.02
n=2	31	365	396	7.83
n=3	22	242	264	8.33
n=4	29	200	229	12.66
n=5	35	222	257	13.62
n=6	32	273	305	10.49
			Mean	**10.66**
			SD	**2.30**
			SE	**0.94**

A549 – 2 µM TSA + CDSO3 10 µM + $FeSO_4$ 50 µM

	Stained Dead	Unstained Live	Total	% Stained Dead
n=1	23	230	253	9.09
n=2	19	233	252	7.54
n=3	23	242	265	8.68
n=4	32	240	272	11.76
n=5	31	304	335	9.25
n=6	35	210	245	14.29
			Mean	**10.10**
			SD	**2.47**
			SE	**1.01**

A549 – 1 µM SU5416

	Stained Dead	Unstained Live	Total	% Stained Dead
n=1	54	735	789	6.84
n=2	52	609	661	7.87
n=3	45	717	762	5.91
			Mean	**6.87**
			SD	**0.98**
			SE	**0.57**

A549 – 5 µM SU5416

	Stained Dead	Unstained Live	Total	% Stained Dead
n=1	40	619	659	6.07
n=2	60	586	646	9.29
n=3	34	612	646	5.26
			Mean	**6.87**
			SD	**2.13**
			SE	**1.23**

A549 – 10 µM SU5416

	Stained Dead	Unstained Live	Total	% Stained Dead
n=1	64	653	717	8.93
n=2	65	556	621	10.47
n=3	60	552	612	9.80
n=4	35	275	310	11.29
n=5	34	336	370	9.19
n=6	52	284	336	15.48
			Mean	**10.86**
			SD	**2.42**
			SE	**0.99**

A549 – 25 µM SU5416

	Stained Dead	Unstained Live	Total	% Stained Dead
n=1	111	568	679	16.35
n=2	79	540	619	12.76
n=3	67	598	665	10.08
			Mean	**13.06**
			SD	**3.15**
			SE	**1.82**

A549 – 50 µM SU5416

	Stained Dead	Unstained Live	Total	% Stained Dead
n=1	128	480	608	21.05
n=2	144	517	661	21.79
n=3	165	439	604	27.32
			Mean	**23.39**
			SD	**3.43**
			SE	**1.98**

A549 – 10 µM SU5416 + CDSO3 10 µM

	Stained Dead	Unstained Live	Total	% Stained Dead	% Inhibition
n=1	18	403	421	4.28	78.76
n=2	18	339	357	5.04	69.59
n=3	15	282	297	5.05	69.49
			Mean	**4.79**	**72.61**
			SD	**0.44**	**5.32**
			SE	**0.26**	**3.07**

A549 – DFO 10 µM

	Stained Dead	Unstained Live	Total	% Stained Dead
n=1	5	370	375	1.33
n=2	2	292	294	0.68
n=3	14	302	316	4.43
			Mean	**2.15**
			SD	**2.00**
			SE	**1.16**

A549 – 10 µM SU5416 + DFO 10 µM

	Stained Dead	Unstained Live	Total	% Stained Dead
n=1	44	321	365	12.05
n=2	53	334	387	13.70
n=3	28	295	323	8.67
			Mean	**11.47**
			SD	**2.56**
			SE	**1.16**

A549 – EDTA 10 µM

	Stained Dead	Unstained Live	Total	% Stained Dead
n=1	12	401	413	2.91
n=2	6	347	353	1.70
n=3	3	305	308	0.97
			Mean	**1.86**
			SD	**0.98**
			SE	**0.56**

A549 – 10 µM SU5416 + EDTA 10 µM

	Stained Dead	Unstained Live	Total	% Stained Dead
n=1	51	375	426	11.97
n=2	50	292	342	14.62
n=3	36	310	346	10.40
			Mean	**12.33**
			SD	**2.13**
			SE	**1.23**

HMVEC-L – Vehicle control

	Stained Dead	Unstained Live	Total	% Stained Dead
n=1	18	416	434	4.15
n=2	13	303	316	4.11
n=3	9	252	261	3.45
n=4	24	360	384	6.25
n=5	28	484	512	5.47
n=6	29	404	433	6.70
n=7	28	451	479	5.85
n=8	34	453	487	6.98
n=9	28	399	427	6.56
n=10	15	289	304	4.93
n=11	12	265	277	4.33
n=12	21	299	320	6.56
n=13				2.44
n=14				3.41
n=15				2.26
			Mean	**5.45**
			SD	**1.21**
			SE	**1.89**

HMVEC-L – CDSO3 10 µM

	Stained Dead	Unstained Live	Total	% Stained Dead
n=1	12	274	286	4.20
n=2	15	313	328	4.57
n=3	10	254	264	3.79
n=4	36	467	503	7.16
n=5	20	397	417	4.80
n=6	19	254	273	6.96
n=7	11	293	304	3.62
n=8	21	306	327	6.42
n=9	15	289	304	4.93
			Mean	**5.16**
			SD	**1.35**
			SE	**0.45**

HMVEC-L – 10% CSE

	Stained Dead	Unstained Live	Total	% Stained Dead
n=1				7.90
n=2				8.71
n=3				7.82
			Mean	**8.14**
			SD	**0.62**
			SE	**0.36**

HMVEC-L + 10% CSE + CDSO3 10 µM

	Stained Dead	Unstained Live	Total	% Stained Dead	% Inhibition
n=1				2.77	165.6
n=2				3.83	132.89
n=3				2.85	163.10
			Mean	**3.15**	**153.9**
			SD	**0.59**	**18.20**
			SE	**0.34**	**10.51**

HMVEC-L – 2 µM TSA

	Stained Dead	Unstained Live	Total	% Stained Dead
n=1	38	207	245	15.51
n=2	64	209	273	23.44
n=3	78	218	296	26.35
n=4	113	270	383	29.50
n=5	152	397	549	27.69
n=6	179	455	634	28.23
			Mean	**25.12**
			SD	**5.14**
			SE	**2.10**

HMVEC-L – 2 µM TSA + CDSO3 10 µM

	Stained Dead	Unstained Live	Total	% Stained Dead	% Inhibition
n=1	24	221	245	9.80	76.24
n=2	18	197	215	8.37	83.33
n=3	28	186	214	13.08	59.89
n=4	78	489	567	13.76	56.54
n=5	85	498	583	14.58	52.45
n=6	81	480	561	14.44	53.15
			Mean	**12.34**	**63.60**
			SD	**2.39**	**13.01**
			SE	**0.97**	**5.31**

HMVEC-L – 2 µM TSA + CDSO3 10 µM + Ech 10 µM

	Stained Dead	Unstained Live	Total	% Stained Dead
n=1	143	298	441	32.43
n=2	102	304	406	25.12
n=3	56	149	205	27.32
			Mean	**28.29**
			SD	**3.75**
			SE	**2.16**

HMVEC-L – 2 µM TSA + CDSO3 10 µM + $FeSO_4$ 50 µM

	Stained Dead	Unstained Live	Total	% Stained Dead
n=1	116	287	403	28.78
n=2	119	262	381	31.23
n=3	91	184	275	33.09
			Mean	**31.04**
			SD	**2.16**
			SE	**1.25**

HMVEC-L – 10 µM SU5416

	Stained Dead	Unstained Live	Total	% Stained Dead
n=1	77	272	349	22.06
n=2	77	289	366	21.04
n=3	74	328	402	18.41
			Mean	**20.50**
			SD	**1.89**
			SE	**1.09**

HMVEC-L – 10 µM SU5416 + CDSO3 10 µM

	Stained Dead	Unstained Live	Total	% Stained Dead	% Inhibition
n=1	32	295	327	9.78	73.23
n=2	34	378	412	8.25	83.71
n=3	21	349	370	5.68	101.32
			Mean	**12.34**	**68.09**
			SD	**2.39**	**14.09**
			SE	**0.97**	**8.19**

HMVEC-L – 10 µM SU5416 + CDSO3 10 µM + CAY 10 µM

	Stained Dead	Unstained Live	Total	% Stained Dead
n=1	46	257	303	15.2
n=2	45	254	299	15.1
n=3	47	318	365	12.9
			Mean	**14.37**
			SD	**1.29**
			SE	**0.75**

HMVEC-L – 10 µM SU5416 + CDSO3 10 µM + $FeCl_2$ 50 µM

	Stained Dead	Unstained Live	Total	% Stained Dead
n=1	52	248	300	17.3
n=2	50	207	257	19.5
n=3	45	280	325	13.8
			Mean	**16.88**
			SD	**2.83**
			SE	**1.64**

HMVEC-L – 10 µM SU5416 + CDSO3 10 µM + $FeCl_3$ 50 µM

	Stained Dead	Unstained Live	Total	% Stained Dead
n=1	12	289	301	4.0
n=2	28	261	289	9.7
n=3	26	310	336	7.7
			Mean	**7.14**
			SD	**2.90**
			SE	**1.67**

HMVEC-L – 25 µM SU5416

	Stained Dead	Unstained Live	Total	% Stained Dead
n=1	166	369	535	31.03
n=2	138	314	452	30.53
n=3	125	347	472	26.48
			Mean	**29.35**
			SD	**2.49**
			SE	**1.44**

HMVEC-L – 25 µM SU5416 + CDSO3 10 µM

	Stained Dead	Unstained Live	Total	% Stained Dead	% Inhibition
n=1	67	311	378	17.72	49.52
n=2	73	317	390	18.72	45.26
n=3	57	302	359	15.88	57.36
			Mean	**17.44**	**50.71**
			SD	**1.44**	**6.14**
			SE	**0.83**	**3.54**

HMVEC-L – 25 µM SU5416 + CDSO3 10 µM + CAY 10 µM

	Stained Dead	Unstained Live	Total	% Stained Dead
n=1	100	284	384	26.04
n=2	101	238	339	29.79
n=3	95	267	362	26.24
			Mean	**27.36**
			SD	**2.11**
			SE	**1.22**

HMVEC-L – 10 µM SU5416 + CDSO3 10 µM + $FeCl_2$ 50 µM

	Stained Dead	Unstained Live	Total	% Stained Dead
n=1	119	261	380	31.3
n=2	128	204	332	38.6
n=3	119	246	365	32.6
			Mean	**34.16**
			SD	**3.86**
			SE	**2.23**

$CDSO3_{BH}$ - Ferrozine chelating assay

CDSO3		Abs					Fraction		%	
[µM]	[M]	#1	#2	#3	mean	SD	mean	SD	mean	SD
0.0	**0.0E+00**	0.606	0.696	0.579	0.627	0.061	**1.000**	**0.098**	100.00	9.77
0.1	**1.0E-07**	0.634	0.606	0.573	0.604	0.031	**0.964**	**0.049**	96.38	4.87
0.5	**5.0E-07**	0.550	0.635	0.609	0.598	0.044	**0.954**	**0.069**	95.37	6.95
1.0	**1.0E-06**	0.461	0.610	0.564	0.545	0.076	**0.869**	**0.122**	86.92	12.17
5.0	**5.0E-06**	0.554	0.539	0.530	0.541	0.012	**0.863**	**0.019**	86.28	1.93
10.0	**1.0E-05**	0.446	0.448	0.476	0.457	0.017	**0.728**	**0.027**	72.83	2.68
25.0	**2.5E-05**	0.373	0.281	0.344	0.333	0.047	**0.531**	**0.075**	53.06	7.50
50.0	**5.0E-05**	0.236	0.135	0.118	0.163	0.064	**0.260**	**0.102**	26.00	10.17
100.0	**1.0E-04**	0.111	0.058	0.029	0.066	0.042	**0.105**	**0.066**	10.53	6.63
200.0	**2.0E-04**	0.062	0.070	0.058	0.063	0.006	**0.101**	**0.010**	10.10	0.97
250.0	**2.5E-04**	0.044	0.042	0.046	0.044	0.002	**0.070**	**0.003**	7.02	0.32
500.0	**5.0E-04**	0.015	0.012	0.016	0.014	0.002	**0.023**	**0.003**	2.29	0.33
1000.0	**1.0E-03**	-0.001	0.015	0.008	0.007	0.008	**0.012**	**0.013**	1.17	1.28

$CDSO3_{MT}$ – Ferrozine chelating assay

CDSO3		Abs					Fraction		%	
[µM]	[M]	#1	#2	#3	mean	SD	mean	SD	mean	SD
0.0	**0.0E+00**	0.385	0.381	0.370	0.379	0.008	**1.000**	**0.021**	100.00	2.12
0.1	**1.0E-07**	0.376	0.373	0.374	0.374	0.002	**0.989**	**0.004**	98.86	0.42
0.5	**5.0E-07**	0.375	0.366	0.319	0.353	0.030	**0.933**	**0.082**	93.31	8.22
1.0	**1.0E-06**	0.366	0.366	0.355	0.362	0.006	**0.957**	**0.017**	95.69	1.74
5.0	**5.0E-06**	0.299	0.329	0.297	0.308	0.018	**0.814**	**0.049**	81.43	4.90
10.0	**1.0E-05**	0.262	0.266	0.242	0.257	0.013	**0.678**	**0.035**	67.78	3.51
20.0	**2.0E-05**	0.220	0.191	0.161	0.191	0.030	**0.504**	**0.081**	50.35	8.06
50.0	**5.0E-05**	0.048	0.055	0.040	0.048	0.008	**0.126**	**0.021**	12.59	2.05
100.0	**1.0E-04**	0.027	0.019	0.021	0.022	0.004	**0.059**	**0.011**	5.90	1.14

EDTA – Ferrozine chelating assay

EDTA		Abs					Fraction		%	
[µM]	[M]	#1	#2	#3	mean	SD	mean	SD	mean	SD
0.0	0.0E+0	0.534	0.524	0.571	0.543	0.025	1.000	0.046	100.00	4.56
0.1	1.0E-07	0.613	0.591	0.594	0.599	0.012	1.104	0.022	110.37	2.20
0.5	5.0E-07	0.513	----	0.553	0.533	0.028	0.982	0.052	98.16	5.21
1.0	1.0E-06	0.598	0.562	0.571	0.577	0.019	1.063	0.035	106.26	3.45
2.0	2.0E-06	0.571	0.534	0.569	0.558	0.021	1.028	0.038	102.76	3.83
5.0	5.0E-06	0.533	0.429	0.371	0.444	0.082	0.818	0.151	81.83	15.12
10.0	1.0E-05	0.435	0.371	0.391	0.399	0.033	0.735	0.060	73.48	6.03
20.0	2.0E-05	0.336	0.244	0.226	0.269	0.059	0.495	0.109	49.48	10.87
50.0	5.0E-05	0.101	0.144	----	0.123	0.030	0.226	0.056	22.56	5.60
100.0	1.0E-04	0.147	----	0.161	0.154	0.010	0.284	0.018	28.36	1.82
200.0	2.0E-04	0.118	----	0.115	0.117	0.002	0.215	0.004	21.45	0.39

Animals

Healthy control	CDSO3 [60 µg/kg]	SU5416 [20 mgkg]		
		+ Saline	+ CDSO3 [60 µg/kg]	+ CDSO3 [60 µg/kg] pre-mixed with $FeSO_4$ [10 mM]
1	TR175	TR76	TR26	TR110
2	TR176	TR77	TR101	TR111
3		TR102	TR114	TR112
4		TR103	TR163	TR113
5		TR181	TR167	
6		TR193	TR168	
7		TR195	TR171	
8		TR206	TR172	
9		TR207	TR194	
10		TR208	TR209	
11			TR210	
TR203			TR211	
TR204				
TR205				

In vivo exercise endurance (EE) data

Healthy (negative) control
PBS + PBS

Animal	**EE (min)**
1	41.25
2	46.27
3	41.475
4	61.81
5	46.27
6	41.25
7	47.35
8	42.88
9	45.93
10	41.67
11	41.8
TR203	39.23
TR204	30.32
TR205	38.70
Mean	43.30
SD	6.83

Healthy CDSO3 control
PBS + CDSO3

	EE (min)	
Animal	Pre-dosed	Post-dosed
TR175	42.75	40.98
TR176	45.73	42.28
Mean	44.24	41.63
SD	2.11	0.92

Positive control
SU5416 + PBS

	EE (min)		
Animal	Pre-induction	Post-treatment	Post-treatment
TR76	-	13.9	13.6
TR77	-	9.85	14.55
TR102	-	9.97	9.27
TR103	-	4.29	5.06
TR181	-	5.01	2.82
TR193	-	8.70	8.59
TR195	-	8.85	6.74
TR206	58.50	7.68	9.47
TR207	40.30	8.92	9.44
TR208	30.12	5.65	6.01
Mean	42.97	8.28	8.56
SD	14.38	2.82	3.63

SU5416 + CDSO3

	EE (min)		
Animal	Pre-induction	Post-induction	Post-treatment
TR26	-	12.78	41.82
TR101	-	10.40	34.62
TR114	-	15.25	32.12
TR163	-	16.26	33.61
TR167	-	12.80	40.21
TR168	-	8.11	34.83
TR171	-	11.72	32.74
TR172	-	12.01	34.74
TR194	-	13.19	35.80
TR209	37.90	10.58	22.93
TR210	54.08	8.02	19.74
TR211	33.20	7.97	19.19
Mean	41.73	11.59	31.87
SD	10.95	2.72	7.39

SU5416 + CDSO3 pre-mixed with $FeSO_4$

	EE (min)	
Animal	Post-induction	Post-treatment
TR110	5.52	15.53
TR111	6.70	6.09
TR112	9.15	8.54
TR113	8.68	7.90
Mean	7.51	9.51
SD	1.70	4.14

In vivo mean linear intercept (MLI) data
Left lung section

Healthy (negative) control
PBS + PBS

Animal	**MLI (µm)**
1	66.50
2	67.99
3	48.86
4	54.82
5	57.30
6	52.41
7	51.67
8	55.61
9	51.29
10	54.28
11	56.17
Mean	56.08
SD	6.04

Healthy CDSO3 control
PBS + CDSO3

Animal	**MLI (µm)**
TR175	46.22
TR176	52.86
Mean	49.54
SD	4.69

Positive control
SU5416 + PBS

Animal	**MLI (µm)**
TR76	84.99
TR77	79.41
TR102	82.56
TR103	81.85
Mean	82.20
SD	2.30

SU5416 + CDSO3

Animal	**MLI (µm)**
TR26	67.87
TR101	65.96
TR114	63.14
TR163	60.81
TR167	61.40
TR168	67.61
TR171	51.66
TR172	64.41
Mean	62.86
SD	5.23

In vivo destructive index (DI) data
Left lung section

Healthy (negative) control
PBS + PBS

Animal	Destroyed	Normal	Total	DI (%)
1	156	2966	3122	5.00
2	165	1845	2010	3.49
3	106	2932	3038	8.21
			Mean	5.56
			SD	2.41

Positive control
SU5416 + PBS

Animal	Destroyed	Normal	Total	DI (%)
TR77	404	1624	2028	19.92
TR102	680	1330	2010	33.83
TR103	612	1376	1988	30.78
			Mean	28.18
			SD	7.31

SU5416 + CDSO3

Animal	Destroyed	Normal	Total	DI (%)
TR26	305	2695	3000	10.17
TR101	241	2764	3005	8.02
TR171	144	1860	2004	7.19
			Mean	8.46
			SD	1.54

SU5416 + CDSO3 pre-mixed with $FeSO_4$

Animal	Destroyed	Normal	Total	DI (%)
TR110	447	1640	2087	21.42
TR111	434	1591	2025	21.43
TR112	539	1496	2035	26.49
			Mean	23.11
			SD	2.92